

© 2014 Patrick J. Mears

ILLUMINATING THE RELATIONSHIP BETWEEN FLAGELLAR ACTIVITY
AND BACTERIAL SWIMMING

BY

PATRICK J. MEARS

DISSERTATION

Submitted in partial fulfillment of the requirements
for the degree of Doctor of Philosophy in Physics
in the Graduate College of the
University of Illinois at Urbana-Champaign, 2014

Urbana, Illinois

Doctoral Committee:

Assistant Professor Thomas E. Kuhlman, Chair
Associate Professor Yann R. Chemla, Director of Research
Professor Karin A. Dahmen
Professor Klaus J. Schulten

Abstract

Bacterial swimming and chemotaxis serves as a model system for understanding information processing in living organisms. My thesis project was focused on studying the swimming behavior of *Escherchia coli* bacterial cells. These cells swim by rotating helical filaments called flagella. An individual cell can have anywhere from 1 to 10 flagella. In a process called chemotaxis, cells modulate the rotational direction of their flagella to modify their swimming behavior and move towards more favorable environments. The primary goal of this thesis was to determine how the number of flagella on a cell affects its swimming behavior.

I designed and constructed a unique instrument, combining optical tweezers and high-speed fluorescence imaging. This instrument allowed me to simultaneously measure the activity of the individual flagella on a cell, while also monitoring the swimming behavior of the cell. These results provided a large amount of data regarding the relationship between flagella number, CW bias and tumble bias. In particular, I discovered that the tumble bias of a swimming cell is robust against variations in flagellar number. Cells with 2 flagella and cells with as many as 8 flagella have the same average tumble bias. Many other results regarding this system are presented throughout this thesis. The goals and organization of the thesis are summarized in Chapter 1.

*To my parents Karen and Gerry
and my wife and best friend Amanda*

Acknowledgements

I would like to thank Ido Golding for being a fantastic advisor. Ido's enthusiasm is contagious, and his emphasis on precision and clarity taught me how to be a serious scientist. Even after moving to Houston, Ido managed to meet with me every week to guide my research and keep me on track.

I would like to thank Yann Chemla who effectively adopted me into his lab after Ido moved to Houston. I was extremely lucky to have two great advisors. Yann's skills complemented Ido's and I learned an immense amount about experimental design and technologically driven science from Yann. I learned more about science in my weekly meetings with Yann and Ido than in all of the classes I've ever taken. I will miss working for Yann and Ido.

I would like to give special thanks to Taejin Lance Min. Lance began the *E. coli* trapping project shortly before I joined the lab. He taught me how to grow and trap bacteria, how to pipette and how to produce awesome papers. Throughout graduate school, Lance and I worked together on research, summer schools, homework, grants and life. Lance was a great role model and a great friend.

I would like to thank Matt Comstock. Matt was a post-doc in the Chemla lab who basically taught me how to build scientific instruments. Matt was always generous with his time and I am grateful for his criticism which helped mold me into a better, more careful scientist.

I would like to thank Santosh Koirala who taught me how to perform molecular cloning, with great patience and generosity.

I would like to thank and offer good luck to Tanya Perlova and Roshni Bano. Tanya and Roshni have taken over the E Fleezers instrument and the bacterial swimming project. Their inquisitiveness and excitement about science was a source of inspiration which helped me polish my research and finish graduate school with enthusiasm.

I would like to thank Paul DeYoung, who was my research advisor when I was an undergraduate at Hope College. Paul taught me how to do research and how to keep a lab notebook. He instilled in me the meticulous habits that are necessary to be a successful scientist.

I would like to thank the many wonderful professors and teachers who helped me get where I am today by fostering my love for science. Especially Paul Selvin, Bob Clegg, Klaus Schulten, Taekjip Ha, Nigel Goldenfeld, Cathy Mader, Peter Gonthier, Graham Peaslee, Marty Landorf, Leslie Vaughn, Brian Kay, Heidi Leech, and many others.

I would like to thank all of the members of the Chemla and Golding labs for their scientific help and for making graduate school a great experience. In addition to those mentioned above, I

would like to thank Sam Skinner, Leonardo Sepulveda, Sukrit Suksumbot, Zhi Qi, Markita Landry, Barbara Stekas, Kevin Whitley, Kiran Girdhar, Alice Troitskaia, Isaac Li, Rustem Khavizhov, Tommy So, Lanying Zeng, Chenhang Zong, and Eli Rothenberg.

I would like to thank other friends who made graduate school a time of exploration and deep learning. I'm glad that I was able to spend the past six years learning much more about the world than just science. Thanks to my physics friends Yu Gan, Nir Friedman, Brian Mulcahy, Hannah DeBerg, Zak Yoskovits, Gus Olson, Michael Murray, Suffian Khan, Daniel Sussman, Kevin Zielnicki, Janet Sheung, and Allison Dove.

I would like to thank many other people in the Physics department at the University of Illinois who helped me throughout graduate school. Especially Sharlene Denos who started the iRise science outreach program where I learned how to conduct outreach and design and evaluate lessons for middle school students. Thanks also to Sandra Patterson and Susan Flannegin.

I would like to thank everyone who helped me finish this thesis by proof-reading chapters, feeding me and opening their homes to me while I commuted from Chicago. Especially Tanya, Santosh, Natalya, Roshni, Barbara and Alice.

I would like to thank my brother Brendan for always challenging me. He helped me develop a competitive instinct that has driven me to do my very best in everything that I do.

I would like to thank my parents. My love of science began with trips to the Science and Industry museum and playing with Duplos and Legos as a child. Since then they have supported and propelled me in everything that I attempt. Without their care and encouragement I could never have done this.

Finally, words cannot express how grateful I am for the love and support of my best friend, Amanda Mulcahy. Without her I could not have survived graduate school. She is constant source of inspiration, creativity and motivation.

I also thank the National Science Foundation for funding. My research was supported by the Center for the Physics of Living Cells, NSF Physics Frontiers Center, Grant 082265.

Table of Contents

Chapter 1. Introduction	1
1.1 Background.....	1
1.1.1 <i>E. coli</i> chemotaxis is a model system for information processing.....	1
1.1.2 Why study <i>E. coli</i> ?.....	1
1.1.3 How <i>E. coli</i> swims	2
1.1.4 Chemotaxis in <i>E. coli</i>	3
1.1.5 Swimming machinery is highly regulated in <i>E. coli</i>	4
1.1.6 Studying swimming behavior and flagella activity.....	5
1.2 Goals	6
1.2.1 Mapping the relationship from individual flagella activity to whole-cell swimming....	6
1.3 Tools.....	6
1.3.1 Optical traps.....	6
1.3.2 Fluorescence imaging	6
1.3.3 Digital image processing and analysis	7
1.3.4 Genetics	7
1.3.5 Models and simulations.....	8
1.4 Summary	8
Chapter 2. Counting Flagella	9
2.1 Background.....	9
2.2 Electron microscopy	9
2.2.1 Why use electron microscopy?	9
2.2.2 Imaging flagella in an electron microscope	10
2.2.3 Results.....	11
2.3 Fluorescence Imaging	12
2.3.1 Background	12
2.3.2 Imaging flagella on free swimming cells.....	12
2.3.3 Imaging flagella on surface-bound cells.....	13
2.3.4 Imaging flagella on optically trapped cells.....	14
2.3.5 Results.....	15
2.4 Future directions.....	15
2.5 Summary	15
Chapter 3. The E Fleezers instrument	17
3.1 Background.....	17
3.2 Instrument design	19
3.2.1 General instrument design	19
3.2.2 Acousto-optics for timesharing	21

3.2.3	High speed fluorescence imaging	23
3.3	Instrument control	23
3.3.1	Electronics control and acquisition	23
3.3.2	Controlling trap position via Acousto-optic deflection.....	24
3.3.3	Controlling fluorescence excitation timing via acousto-optic modulation.....	25
3.3.4	Quadrant photodiode detectors.....	26
3.3.5	EMCCD camera timing.....	27
3.4	New trap data	28
3.5	Future Directions.....	29
3.5.1	Quantifying CheY-YFP in trapped cells.....	29
3.5.2	Imaging Tar-YFP and other fluorescent chemotaxis proteins in the trap.....	30
3.6	Summary	31
Chapter 4.	How flagellar number affects swimming behavior.....	32
4.1	Background: Flagellar imaging and the veto model.....	32
4.2	Experimental procedure	34
4.2.1	Choosing a bacterial strain	34
4.2.2	Growing cells.....	34
4.2.3	Labeling flagella	35
4.2.4	Building the microfluidic flow chamber.....	36
4.2.5	Injecting bacteria into chamber.....	36
4.2.6	Turning on E Fleezers instrument and focus the trap beam	37
4.2.7	Trapping a cell	37
4.2.8	Recording fluorescence images and QPD data	38
4.2.9	Analyzing QPD data to extract tumble bias	39
4.3	Initial results: The veto model fails	40
4.4	Why doesn't data match the veto model?.....	40
4.4.1	Analyzing individual flagella.....	40
4.4.2	Extracting CW bias.....	43
4.4.3	The veto model stands.....	43
4.4.4	Wild-type tumbles typically involve multiple flagella.....	44
4.5	Control experiment with a CheY* mutant strain.....	45
4.6	Wild-type behavior matches a veto model with a lower effective number of flagella	46
4.7	Discussion	49
4.8	Future Directions.....	49
4.9	Summary	49
Chapter 5.	Modeling runs and tumbles	51
5.1	Mapping flagella states →run/tumble states.....	51
5.1.1	Introduction to run-tumble modeling.....	51
5.1.2	The unanimous model.....	53

5.1.3	The voting model.....	54
5.1.4	The veto model.....	55
5.1.5	The 3-state modified veto model.....	55
5.1.6	The distortion factor model.....	57
5.2	Mapping from CheY-P → motor states.....	58
5.2.1	Why is the mapping from CheY-P → motor states relevant?.....	58
5.2.2	CW bias is a function of CheY-P concentration.....	58
5.2.3	Numerical simulations of flagellar switching reproduce CheY* strain behavior.....	59
5.2.4	Modeling fluctuations in CheY-P reproduces wild-type behavior.....	60
5.2.5	Discussion of simulations.....	63
5.3	Flagellar interactions.....	65
5.4	Future Directions.....	66
5.5	Summary.....	67
Chapter 6. Detailed observations of flagella activity.....		69
6.1	Eradicating flagellar cross-linking.....	69
6.2	Flagella waveforms and transitions.....	70
6.2.1	Flagella waveforms.....	70
6.2.2	Sequences of flagella waveforms.....	71
6.2.3	Flagellar waveform transition rates.....	72
6.3	Relating flagellar number to other swimming statistics.....	74
6.3.1	Run-tumble statistics vs. flagellar number.....	74
6.3.2	Flagella and body rotation rates vs. flagellar number.....	75
6.4	Cell length.....	76
6.4.1	Cell length and flagellar number.....	76
6.4.2	Cell length vs. flagella and body rotation rates.....	77
6.4.3	Swimming speed and cell length.....	78
6.5	Qualitative observations of trapped and swimming cells.....	79
6.5.1	Runs with CW rotating flagella.....	79
6.5.2	Flagella and surface attachment.....	79
6.6	Future Directions.....	80
6.6.1	Collect additional data to verify correlations between swimming variables.....	80
6.6.2	Examine flagella length and bundle tightness.....	80
6.6.3	Investigate runs with all <i>curly-1</i> (CW) flagella.....	81
6.7	Summary.....	81
Chapter 7. Two-dimensional swimming.....		82
7.1	Background.....	82
7.2	Wild-type 2D assay results.....	83
7.2.1	General results.....	83
7.2.2	Angle change during tumbles.....	85

7.3	Chemotaxis adaptation	86
7.4	Flagella dilution experiments.....	87
7.4.1	Producing populations of cells with different numbers of flagella.....	87
7.4.2	Effect of flagella number on swimming parameters.....	89
7.5	Future Directions.....	90
7.5.1	2D dilution experiment with strain HCB1660.....	90
7.5.2	Step-down chemotaxis adaptation with CheB mutant.....	90
7.6	Summary	91
References		92
Glossary		98
Appendix A. Instrumentation.....		100
A.1	Custom mount for acousto-optic deflector	100
A.3	Optical components	102
A.4	FPGA breakout box wiring assignments.....	103
Appendix B. Protocols		104
B.1	Flagella labeling protocol	104
B.2	Bacterial trapping protocol	106
B.3	Trap fluorescence imaging protocol.....	111
B.4	Flagella imaging electron microscopy protocol	113
B.5	2D swimming protocol.....	115
B.6	2D chemotaxis adaptation protocol	117
B.7	Flagella dilution protocol (with optional labeling).....	119
B.8	Cloning a gene into a different plasmid protocol.....	121
B.9	One-step preparation and transformation of competent cells.....	124
Appendix C. Bacterial strains and plasmids		125
C.1	Strains.....	125
C.2	Plasmids.....	126
C.3	Plasmid pPM5 sequence and map	128
C.4	DNA Primers.....	131
Appendix D. Models		133
D.1:	Veto model – Analytical derivation	133
D.2:	Unanimous model – Analytical derivation	133

Chapter 1. Introduction

This chapter introduces the *Escherichia coli* swimming system which is the subject of my thesis. I begin by providing background on *E. coli* swimming and chemotaxis. I then present the specific goals of this thesis, followed by a brief introduction to the most important tools which were used to achieve these goals. I conclude by summarizing each of the remaining chapters of this thesis.

1.1 Background

1.1.1 *E. coli* chemotaxis is a model system for information processing

In order to survive, all living organisms must process and respond to information from their environment. Bacterial chemotaxis, the self-directed movement of cells towards more favorable conditions, serves as a model system for cellular information processing [4]. *E. coli* cells can sense miniscule changes in chemical concentration, temperature, pH and osmotic pressure [5-13]. Upon a change in conditions, cells respond by relaying the signal across the cell to alter their motion accordingly [14-21]. Model biological systems are studied to develop deep understanding of the precise manner which a single organism functions. It is not feasible to study every aspect of every species on Earth, but discoveries in model systems provide insight about general strategies that organisms use to solve similar problems. Knowledge about information processing in *E. coli* can be used to guide research in subjects as diverse as immunology, embryology, visual processing and homeostasis.

1.1.2 Why study *E. coli*?

For many reasons, *Escherichia coli* is one of the most studied organisms in the world [4, 22]. First, it is fairly easy to work with; cells are easily grown, stored and manipulated in laboratory settings. Second, it is a relatively simple organism. It is a single-celled bacterium with a single chromosome and a short life cycle. It is much easier to perform controlled experiments in a single-celled organism than in larger, multicellular organisms where many parameters might be difficult or impossible to control. The short life cycle also makes it easy to rapidly grow and study millions and billions of genetically identical cells in a single day. Under optimal conditions, *E. coli* can double in number every 20 minutes. Finally, *E. coli* is studied because other scientists have spent considerable time studying it. As a result, there exist robust protocols and commercially available tools for genetically altering the cells and controlling their gene expression or physiological behavior[22, 23]. Online databases document every known *E. coli* gene and variants of those genes

[24, 25]. These tools make it relatively easy to design and carry out studies that address fundamental biological questions and probe complicated and subtle aspects of cellular behavior. In summary, *E. coli* is relatively simple, when compared to other organisms, and due to the wealth of existing information *E. coli* is the perfect system in which to seek a deeper, quantitative understanding of biological information processing.

1.1.3 How *E. coli* swims

Under certain conditions, *E. coli* grow long, helical filaments called flagella [6]. The rotation of these flagella generates propulsive forces which allow cells of *E. coli* to swim and perform chemotaxis. A typical cell possesses several (~1–8) flagella which are arranged randomly on its surface [4]. Each flagellum is controlled by an independent motor which is capable of rotating both clockwise (CW) and counter-clockwise (CCW). When all of the flagella rotate CCW, they form a bundle which propels the cell in a roughly straight path defined as a run. When some of the flagella rotate CW, the bundle is disrupted, and the cell orientation is randomized in a process called a tumble (**Figure 1.1**). Each motor spends most of the time rotating CCW, so it is very rare for all of the flagella to rotate CW at the same time. Together, runs and tumbles comprise a three-dimensional random-walk [26].

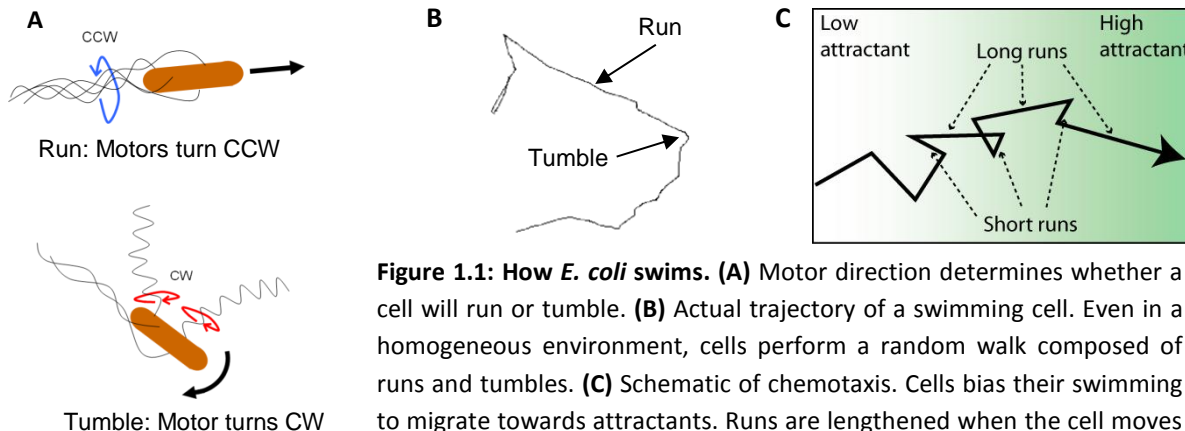


Figure 1.1: How *E. coli* swims. (A) Motor direction determines whether a cell will run or tumble. (B) Actual trajectory of a swimming cell. Even in a homogeneous environment, cells perform a random walk composed of runs and tumbles. (C) Schematic of chemotaxis. Cells bias their swimming to migrate towards attractants. Runs are lengthened when the cell moves up the concentration gradient of an attractant. Green background indicates area of higher attractant concentration.

E. coli do not always swim; they only express flagella under conditions in which it is presumed to be beneficial to explore a larger area. In order to swim, *E. coli* must first construct motors which drive the rotation of each flagellum. Rotation of the motor is driven by protons flowing across the cell membrane, through the flagellar motor [27]. The rotational speed of the motor is proportional to the proton flux [28]. After building the motor, cells must then construct the flagella themselves, which are narrow (~20 nm diameter) but commonly grow to be longer than

the cell body [29-32].

The swimming process is physically incredible because the world in which *E. coli* lives is very different from our own. Because it is a small organism, *E. coli* swimming occurs at low Reynolds number [33, 34]. The Reynolds number, $R = \rho v \ell / \eta$, is a dimensionless parameter which conveys the relative significance of viscous forces and inertia (ρ = density of fluid, v = speed, ℓ = characteristic length and η = fluid viscosity) [35]. For *E. coli*, which is roughly 1 μm in diameter and swims in water at about 30 $\mu\text{m/s}$, the Reynolds number is approximately 10^{-5} ($\rho \approx 10^3 \text{ kg/m}^3$, $\eta \approx 10^{-3} \text{ N}\cdot\text{s/m}^2$). At a low Reynolds number, viscous forces dominate over inertia. There is no momentum for swimming *E. coli*. Cells must continually propel themselves because all motion is dominated by viscous drag. As a result, the motion of a single rotating flagellum more closely resembles the motion of a corkscrew moving through a cork, than a person swimming in water.

1.1.4 Chemotaxis in *E. coli*

To achieve chemotaxis, cells continuously adjust their frequency of tumbling to move up gradients of chemicals referred to as chemoattractants (**Figure 1.1C**) [26, 36]. A complex system of intra-membrane receptors, signaling proteins, and motor switches allows cells to respond and adapt to nano-molar changes in chemoattractant concentration (**Figure 1.2**) [16, 37, 38]. The central component of this system is the response regulator protein, CheY. Information about the external environment is communicated through phosphorylation and de-phosphorylation CheY molecules. Phosphorylated CheY (CheY-P) binds to a protein on the flagellar motor, increasing the CW bias of the motor. Modulating the phosphorylation of CheY alters the tumble frequency of cells, producing the biased random walk that is chemotaxis. This is achieved through the activity of the proteins CheA and CheZ, which add and remove a single phosphate to CheY, respectively. When receptors sense an increase in the concentration of chemoattractants, they decrease the activity of CheA, decreasing the amount of active CheY-P. With less CheY-P, motors spend more time rotating CCW, and the cell tumbles less frequently. Thus, when cells move up a concentration gradient of chemoattractants, they lengthen their runs (**Figure 1.1C**). Similarly, when cells move down a chemoattractant concentration gradient, CheA activity increases, creating more CheY-P which increases the CW bias, and shortens the run length. All of this occurs on a time scale of $\sim 1-4$ seconds [37], which is necessary since bacterial swimming is significantly affected by Brownian forces and the persistence length of runs is only $\sim 10 \text{ s}$ [4].

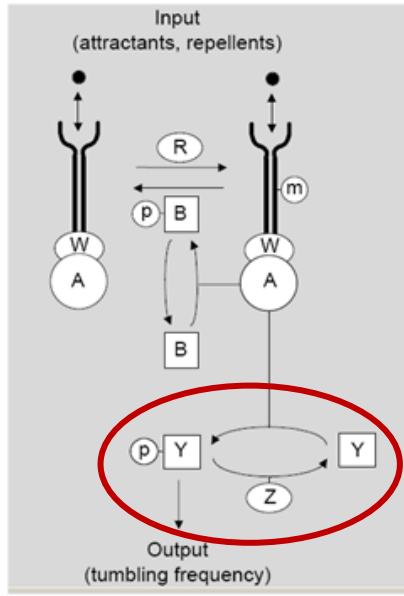


Figure 1.2: Regulatory network. A simplified schematic of the signaling network that produces chemotaxis in *E. coli*. Stimuli are sensed by receptors and processed by various protein interactions. CheY (Y) is the response regulator, which carries the signal across the cell. CheA (A) adds phosphate to CheY (Y), while CheZ (Z) removes phosphates. Finally the CheY-P protein (p-Y) stochastically binds to the flagella motor, increasing the probability of CW rotation.

Figure from Alon *et al.* [1]

The CW bias of a flagellar motor is very sensitive to the local concentration of CheY-P, and displays a sigmoidal relationship with a Hill coefficient of 10.3 [39] (**Equation 5.4, Chapter 5**). This relationship is routinely used in chemotaxis models to determine the CW bias as a function concentration of CheY-P [17, 40-44]. Recent studies regarding adaptive re-configuration of the flagellar motor have suggested that the actual dependence of an individual motor may be even steeper than previously reported [45]. These results suggest that the Hill coefficient for a single motor may be as high as 21. What's more, it has recently been established that even in a homogenous environment, the concentration of CheY-P fluctuates [46]. The source of the fluctuations is not known but may be related to cooperative activation of cluster of chemoreceptors. The extreme sensitivity of CW bias to small changes in CheY-P means that small fluctuations in the concentration of CheY-P can lead to significant changes in swimming behavior. This feature is important for understanding the relationship between flagella activity and swimming behavior.

1.1.5 Swimming machinery is highly regulated in *E. coli*

As mentioned above, *E. coli* cells only swim under certain conditions. When the environment is favorable and food is readily available, cells don't bother growing flagella and swimming [4]. All components of the swimming machinery, including receptors, motor proteins and flagellar filaments are controlled by a complex series of genetic regulatory circuits [47-49]. The production of flagellar motors and subsequently flagellar filaments is precisely timed, and includes several checkpoints to ensure that each step is completed before the next one begins [47, 49, 50]. For example, the protein FliC, which constitutes the entire main structure of the flagellum, is only expressed after a flagellar motor has been assembled [47].

The flagellar motor is composed of precise copy numbers of twenty different proteins [51, 52]. The flagellum is a hollow rod composed of thousands of copies of the FliC protein [53-55]. Flagella grow continuously by adding new FliC proteins to existing flagella. These new FliC proteins are excreted by the flagellar motor, flow through the inner core of the flagellum and eventually attach to the distal end of the flagellum [30, 54, 55].

In contrast to these highly regulated features, the number of flagella on an *E. coli* cell is highly variable [29, 31, 56, 57] (~1-8 flagella per cell, **Chapter 2**). Flagella are essential for swimming behavior, since they propel the cell and determine when it runs or tumbles. My goal was to explore how the number of flagella on a cell affects its swimming behavior.

1.1.6 Studying swimming behavior and flagella activity

Bacterial swimming and chemotaxis is a well-studied model system. Decades of work have elucidated many of the inner-workings of this system. Many different assays have been developed to study the model system of bacterial chemotaxis. Swimming cells have been tracked in three dimensions [26, 58, 59] and two dimensions [1, 36, 60, 61]. The activity of individual flagella have been monitored by measuring the rotation of a bead attached to a flagellum [39, 46, 62, 63], or by watching a cell rotate relative to a flagellum attached to a surface [64, 65]. Recently, assays have been developed to monitor the interactions of signaling proteins inside the cell [17, 66-68]. Details about the genetic network, signaling proteins and flagellar motors that generate chemotaxis in *E. coli* have been investigated for over a century. Much of this work has been summarized Howard Berg's excellent book, "*E. coli* in Motion" [4]. Nonetheless, some aspects of this system are still poorly understood. In particular, details about interactions between the flagella that propel the cell, and their rotational states are still not understood.

Previous observations of flagella on swimming cells were limited to very short times (~1s), precluding a quantitative assessment of the relationship between flagella activity and tumble behavior [31, 56]. These studies confirmed that CW rotation of a single flagellum was sufficient to cause a tumble. But they were unable to determine how the number of flagella and states of each flagellum affected long-term swimming behavior. As a part of my thesis project I developed new techniques which allowed me to address this problem. I also developed an algorithm to determine the run-tumble state of a swimming cell based on the CW-CCW state of every flagellum on a cell.

1.2 Goals

1.2.1 Mapping the relationship from individual flagella activity to whole-cell swimming

The primary goal of this thesis was to develop a quantitative relationship between the number and state of flagella on a cell and its swimming state. Since existing assays were unable to achieve this, it was necessary to develop new experimental tools which would allow me to observe flagella at high speeds while also measuring the swimming state of the cell. The specific aims of this thesis were to:

1. Construct an instrument combining optical traps and high-speed fluorescence imaging to allows observation of flagellar waveforms and swimming behavior of a single cell
2. Develop a quantitative relationship between the number of flagella on a cell and its long-term swimming behavior
3. Develop a mechanistic model to explain the relationship between number of flagella on a cell, the internal chemotaxis signaling network, and long-term swimming behavior
4. Quantify flagellar transition rates and relationships between cell length, flagella rotational rates, number of flagella and CW bias to refine existing models of bacterial chemotaxis

1.3 Tools

1.3.1 Optical traps

An optical trap is a tightly focused beam of light which can be used to apply force to microscopic objects which are located near the focal point [69, 70]. Any object with a different dielectric constant from the surrounding medium can be trapped [69, 71, 72]. The trap works by passively applying a restorative force on the trapped object whenever it moves away from the center of the trap (**Figure 1.3**). I used a pair of optical traps to hold and manipulate individual *E. coli* cells. The specific design and application of the optical tweezers instrument developed for this thesis project is described in detail in **Chapter 3**.

1.3.2 Fluorescence imaging

Fluorescent dyes are a ubiquitous tool in molecular biology and biophysics. Dyes can be attached to structures of interest, allowing visualization of objects and processes that are otherwise not visible [31, 39, 67, 68, 73-76]. Fluorescent dyes function by absorbing light of a given wavelength and later emitting light of a longer wavelength. The difference in frequency between the absorbed and emitted light is called a Stokes shift, and results from vibrational modes of the

molecule. This allows the dye to absorb a photon whose energy is higher than the difference between the relaxed and excited state of the molecule. The Stokes shift is useful because it allows the excitation light to be blocked from reaching the imaging device and facilitates imaging of very dim samples. Dyes can be attached to biomolecules, such as flagella using a variety of chemical linkers, such as NHS-esters which bind to free amine groups, and maleimides which form di-sulfide bounds with free thiol groups. In this thesis, I used maleimide functionalized dyes to label and image flagella on *E. coli* cells (**Chapter 2**).

1.3.3 Digital image processing and analysis

Images contain a large amount of information. In order to extract useful, quantitative features from an image (or a sequence of images) it often necessary to perform image processing. A large set of tools exist to automate the process of extracting useful data from a series of images. I used the Matlab (*Mathworks*) Image Processing Toolbox throughout this thesis project to facilitate image analysis. Gaussian filters and other smoothing functions reduce the appearance of noise in pixelated images, making it easier to resolve objects like fluorescently labeled flagella. To track objects over time, an intensity threshold can be applied to convert a grayscale image into a binary image. Individual, connected objects can then be identified and tracked over time. I used a wide variety of image processing techniques throughout this thesis project to facilitate data analysis.

1.3.4 Genetics

One of the reasons that *E. coli* serves well as a model organism is that there exists a large set of robust tools and methods for modifying genes in *E. coli*. In this thesis, I worked with strains that expressed different version of the FliC protein (flagellin) and the CheY signaling protein. Genes that encode for these proteins were located on the chromosome or on separate, shorter segments of DNA called plasmids. The expression level of each protein was determined by a combination of factors including the number of copies of the gene in a cell (number of plasmids), the affinity of the ribosome binding site for RNA polymerase, and the concentration of inducer chemicals which promote the production of proteins from a specific gene. Inducers are introduced to the cell by adding them to the fluid in which cells grow, which allows us to experimentally control the amount of protein produced in a given experiment. In this thesis, I performed several series of cloning experiments to create plasmids expressing different combinations of FliC and CheY variants, at specific concentrations. This allowed me to perform well-controlled experiments where I compared the behavior of bacterial strains which were genetically identical, with the exception of a single mutation in the CheY protein (**Chapter 4**).

1.3.5 Models and simulations

Mathematical models can provide clear, quantitative synopses of physical phenomena. They allow us to distill out the most significant aspects of a system in order to understand how it functions. Phenomenological models provide a heuristic synopsis of a given behavior without addressing the underlying causes of the behavior. Mechanistic models begin with fundamental, known aspects of a system to generate predictions about behavior. In this thesis, I used numerical simulations and analytical solutions to solve both types of models and approximate the behavior of swimming cells (**Chapter 5**).

1.4 Summary

My goal was to create an instrument that would facilitate high-resolution imaging of all flagella on a bacterial cell, while simultaneously measuring long-term swimming behavior. More generally, I hoped to create a flexible instrument that could be used to facilitate high-speed, high resolution imaging of a wide array of optically trapped samples. Achieving these goals required building new tools and developing new assays to observe flagella and swimming behavior over prolonged periods of time (>10 seconds). I modified and improved existing methods for labeling and imaging flagella on individual cells (**Chapter 2**). I designed and constructed a new instrument combining optical tweezers and high-speed, fluorescence imaging to trap single cells and observe their swimming behavior and flagella over time (**Chapter 3**). I used this instrument to determine the relationship between the number of flagella and tumble bias in two different bacterial strains, revealing a new level of control in the bacterial chemotaxis system (**Chapter 4**). I modified and evaluated several different models of bacterial swimming to establish a quantitative description of the relationship between fluctuating CheY-P concentrations, number of flagella, and swimming behavior (**Chapter 5**). I used movies of fluorescent flagella on trapped cells to extract waveform transition rates and other new quantitative metrics of bacterial swimming (**Chapter 6**). Finally, I used a two-dimensional swimming assay as a control experiment to corroborate and expand upon some of the discoveries from the trap assay (**Chapter 7**).

Chapter 2. Counting Flagella

The primary goal of my thesis project was to investigate how the number of flagella on a bacterial cell affects its swimming behavior. The first step was to develop a robust technique for counting flagella. In this chapter I describe various methods for imaging and counting flagella. Results from images acquired using electron microscopy and fluorescence microscopy are reported.

2.1 Background

Swimming *E. coli* grow flagella continuously. As discussed in **Chapter 1**, *E. coli* don't always swim; flagella production is promoted under certain growth conditions in which it is advantageous for cells to swim and search for superior environments. Under these conditions cells are continuously growing and dividing. As a result, the new daughter cells only have half as many flagella, on average, as the mother cell. This means that the number of flagella on a cell must double at the same rate as the population, in order to maintain a consistent density of flagella per cell. For example, if the average daughter cell has four flagella, then it must grow four new flagella to have a total of eight before it divides. A model for how bacteria such as *E. coli* and *Salmonella* might achieve this has been proposed [77].

For cells grown in this manner, the number of flagella on individual cells in a population can vary greatly. Understanding the effect that this wide distribution has on individual cells requires measuring the distribution. Previous work has been done imaging and even counting flagella [31, 36, 56, 57, 78-80]. However, none of the previous studies have gone further to investigate how the number of flagella on an individual cell affects its behavior. The first step to achieving this goal is establishing a reliable technique for counting flagella, which will also facilitate the measurement of other swimming properties on the same cell.

2.2 Electron microscopy

2.2.1 Why use electron microscopy?

For my first attempt to accurately count the number of flagella on an *E. coli* cell, I chose to use electron microscopy. Flagella on *E. coli* are only 20 nm thick [81], which makes them nearly impossible to see using traditional light microscopes. Alternatively, electron microscopy has a much higher resolution, which makes 20-nm thick flagella trivial to image (features smaller than 1 nm are routinely resolved [51, 54]).

Several previous studies have used electron microscopy to image and count flagella. However, these studies were usually not interested in the effects of flagella numbers. They also

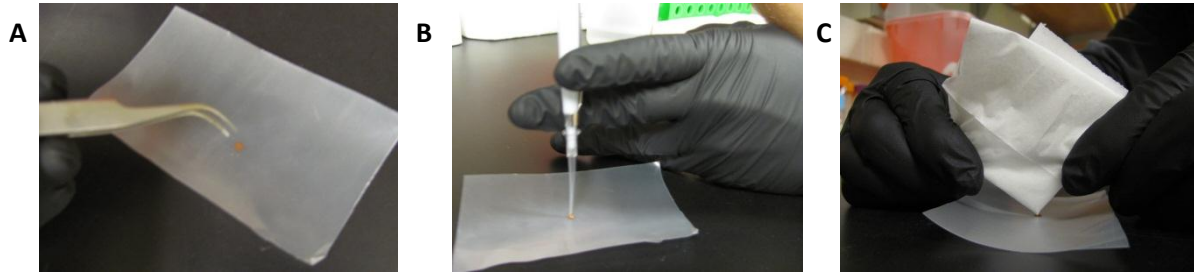


Figure 2.1: Electron microscopy sample preparation. Photos of the procedure for preparing electron microscopy samples for imaging flagella. **(A)** Use tweezers to place grid onto parafilm. **(B)** Pipetting fluid (solution with cells or water for rinsing) onto the grid. It is important to keep the pipette tip perpendicular to the surface of the grid. Otherwise, the grid will often stick to the side of the tip and lift off of the parafilm. **(C)** After incubating the grid with each fluid it must be removed by wicking away the fluid with a Kim wipe. The wipe is folded twice to form a point. The point is then careful brought into contact with the fluid, but not the grid. (See protocol in **Appendix B.4**)

provide a wide range of values for the average number of flagella; mean values range from 2-7 [36, 57, 79, 80]. Furthermore, the specific strain and growth conditions can potentially have a significant effect on the number of flagella per cell. Regulation of flagella production is controlled by a large gene regulatory network that depends on temperature, nutrients, cell density and other factors [4, 47, 82, 83]. Therefore it was necessary that I conduct independent measurements of flagellar number under my specific experimental conditions. I needed to know the number of flagella on the particular cells that I would be studying.

2.2.2 Imaging flagella in an electron microscope

I used the JEOL Cryo 2010 Transmission Electron Microscope at the MRL CMM user facility at the University of Illinois. This instrument provides up to 200 keV for imaging. The basic protocol involves depositing cells on top of a small carbon-coated copper grid (**Figure 2.1**, see **Appendix B.4** for the detailed protocol). The grid is then placed in a sample holder and loaded into the microscope which is pumped down to a low pressure vacuum prior to imaging.

The primary challenge when imaging flagella in an electron microscope is the sample preparation. Flagella can break off from cells and cells can sometimes aggregate making it impossible to count flagella on individual cells. Cell adhesion to the grid was highly sensitive to slight changes in deposition conditions. Other artifacts, such as protein crystals or damaged/burst cells, also make it difficult to count the number of flagella per cell.

I learned several lessons which should be useful for future researchers conducting similar measurements. First, do not use holey grids. These are commonly used in EM, but for imaging flagella they were a source of frustration. Cells aggregate near the holes, which causes a high cell

density and makes individual flagella hard to count. Furthermore, flagella would drape across the holes, and then break off when subjected to vacuum, which made them impossible to see. Instead use non-hole grids. Second, do not use a stain. Stains containing heavy metals are often used for EM. However, flagella are clearly visible without staining. The stain just adds an extra step, and sometimes forms clumps on the sample which make flagella harder to see. Third, fix the cells. I used glutaraldehyde. This reduced the occurrence of broken flagella, possibly because the flagella were passive instead of actively moving while the sample was dried. Finally, the specific medium and method of depositing cells had a significant effect on cell adhesion to the grid, especially salt concentration, pH, and presence of amino acids. Incubation time and the rinsing protocol also had an effect on the reliability of the sample preparation. See protocol in **Appendix B.4** for a detailed description of favorable deposition conditions.

2.2.3 Results

I performed electron microscopy imaging of flagella on several strains. First I looked at wild-type *E. coli* cells (RP437 is the standard wild-type strain for chemotaxis studies [84])(**Figure 2.2A**). **Figure 2.2B** shows the distribution of number of flagella per cell from a population of 56 cells. The mean (3.6 ± 2.8 flagella per cell) was within the range of previous studies. But significantly, the standard deviation was large. This means that cells have a wide range of flagellar number.

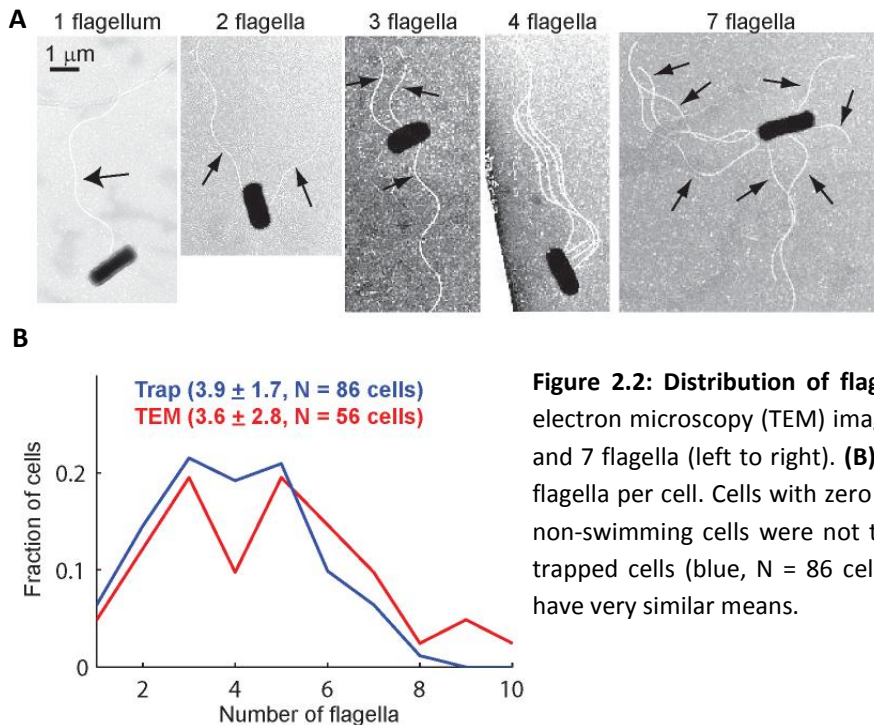


Figure 2.2: Distribution of flagella per cell. (A) Transmission electron microscopy (TEM) images of cells possessing 1, 2, 3, 4 and 7 flagella (left to right). **(B)** Distributions of the number of flagella per cell. Cells with zero flagella were excluded because non-swimming cells were not trapped. The distributions from trapped cells (blue, N = 86 cells) and TEM (red, N = 56 cells) have very similar means.

2.3 Fluorescence Imaging

2.3.1 Background

Fluorescence imaging is a recently developed alternative for counting flagella. Howard Berg's lab developed the first protocol for fluorescent labeling and imaging of flagella in 2000 [31]. A significant advantage of fluorescent imaging is that flagella can be viewed on live, swimming cells. By contrast, electron microscopy is done in a vacuum, so the cells are dead. The sample preparation for fluorescence imaging is also simpler and less time consuming.

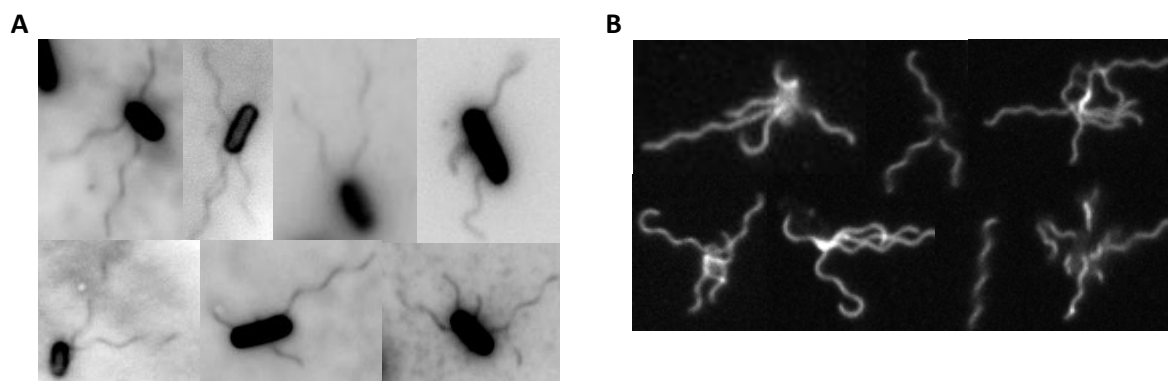


Figure 2.3: Counting fluorescent flagella. Fluorescently-labeled flagella *E. coli* cells viewed under a Nikon epi-fluorescence microscope. **(A)** Flagella labeled with NHS-ester which binds to free amine groups, including those on the cell body. Images were contrast-inverted to make flagella more visible on paper. **(B)** Flagella labeled with maleimide functionalized dyes which bind specifically to flagella.

To image flagella, fluorescent dyes must first be attached to the flagella. The simplest method is to use dyes functionalized with an NHS-ester [31, 56]. These attach non-specifically to free amine groups, so the entire surface of the bacterium and the entire length of each flagellum is tagged with dyes (**Figure 2.3A**). Unfortunately, the bright cell body makes it somewhat difficult to see flagella, especially short flagella which are overshadowed by fluorescence emission from the cell body. To avoid this problem it is preferable to specifically label the flagella. To facilitate specific labeling, the Berg lab created a mutant strain expressing $\text{FliC}^{\text{S219C}}$ (referred to as FliC^*) which replaces a Serine residue with a Cysteine (strain details in **Appendix C.1**). The mutant FliC^* protein can then be specifically labeled with a maleimide functionalized dye, which forms a di-sulfide bond with the sulfur on the Cysteine residue. Using this technique, flagella can be brightly labeled without labeling the cell body (**Figure 2.3B**).

2.3.2 Imaging flagella on free swimming cells

As mentioned above, an advantage of fluorescence imaging is that flagella can be observed

on live, swimming cells. I used epi-fluorescence microscopy to record movies of swimming cells with labeled flagella (**Figure 2.4**). High-speed imaging is required to resolve individual flagella. Since flagella rotate at a rate of ~ 100 Hz, images must be recorded with an exposure time of much shorter than 10 ms. Longer exposures generate blurred images in which individual flagella cannot be seen easily.

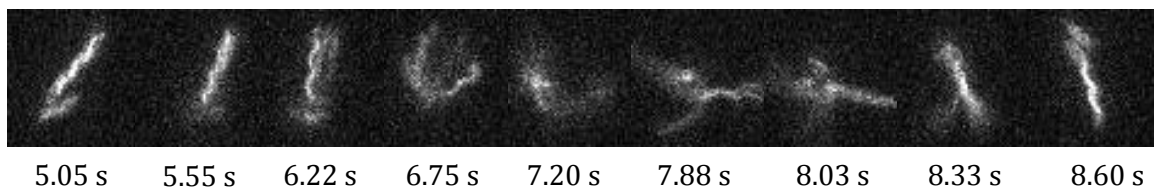


Figure 2.4: Fluorescent flagella on a freely swimming cell. A sequence of images from a movie of a swimming *E. coli* cell with fluorescently-labeled flagella, recorded using a Nikon epi-fluorescence microscope. At the beginning, the cell is running downwards and to the left. The cell then tumbles, with several flagella breaking from the bundle. Eventually the flagella coalesce into a bundle and the cell resumes running up and slightly to the left. Flagella were labeled with Alex-Fluor 532-C5-maleimide which binds specifically to flagella, using mutant strain HCB1660.

While the movies are great for understanding how cells run and tumble, it is very difficult to count flagella by watching a movie. Resolving individual flagella requires a high level of magnification, which means that the field of view must be relatively small ($\sim 30 \times 30 \mu\text{m}^2$). Therefore, an individual cell can only be viewed for a short period of time (~ 1 second) before it swims out of the field of view. Furthermore, cells spend most of the time running. When cells run, the flagella are bundled together, which makes it nearly impossible to resolve individual flagella. When cells tumble the flagella separate, which makes them easier to distinguish from one another. But the flagella often move out of the focal plane and become defocused or invisible. As a result, it is seldom possible to accurately count the number of flagella on a free swimming cell. It requires the good luck of a cell tumbling just as it passes through the field of view, and all of the flagella remaining in the focal plane.

2.3.3 Imaging flagella on surface-bound cells

An easier method for counting fluorescently labeled flagella involves attaching cells to the surface of a coverslip so they do not move. I built very shallow chambers (for holding the bacteria) by sandwiching cells between two coverslips. The volume of liquid used ($\sim 2 \mu\text{l}$) ensured that the chamber was only a few microns deep. Cells and their flagella were stuck on the surface of the coverslip. As a result, all of the flagella were motionless and in a single focal plane (**Figure 2.3.**) Using this method, we counted flagella on wild-type cells (Mean = 3.3 ± 3.3 , $N = 90$ cells, strain

RP437). The biggest disadvantage of this method is that flagella are often broken off of cells. This makes counting somewhat unreliable, but gives a lower limit on the average number of flagella per cell. Also, the cell swimming dynamics cannot be analyzed because the cells are immobilized on the chamber surface.

2.3.4 Imaging flagella on optically trapped cells

To overcome the disadvantages of other fluorescent imaging methods, we developed a new method of optically trapping cells with fluorescently labeled flagella and recording movies of the cells swimming in the trap. Using a pair of optical traps, a bacterial cell was held in place, away from the chamber surfaces, with the body length oriented in the focal plane (trapping details in **Chapter 3**). This method prevented shearing of flagella which occurs when cells are bound to the chamber surface. Since the cell was trapped, it could not leave the field of view. This allowed me to view the flagella on live cells for longer times than in the previous assay with freely swimming cells, which quickly swam out of the field of view.

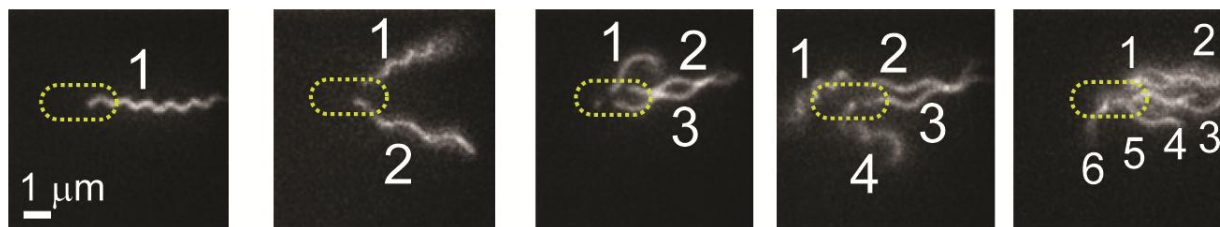


Figure 2.5: Counting fluorescent flagella on trapped cells. Fluorescently-labeled flagella on trapped *E. coli* cells. Images show cells with 1, 2, 3, 4 and 6 flagella (left to right). Dashed yellow ellipsoid indicates the approximate position of the cell body. The image contrast was adjusted to make flagella more visible.

Despite the clear advantages of imaging flagella on trapped cells over the previously discussed methods, there are still some limitations. As mentioned above, flagella rotate at a rate of ~ 100 Hz, so short exposure times are required to resolve individual flagella ($\ll 10$ ms). Additionally, the fluorophores bleach over time, which limits the duration over which flagella can be imaged. As more fluorophores enter a dark state in which they no longer fluoresce, the flagella become dimmer and eventually cannot be seen. I addressed both of these problems by using stroboscopic illumination (details in **Chapter 3**). Each image was recorded with a 20- μ s pulse of excitation light, which was timed to coincide with the camera exposure time. Since the excitation light was off while the camera was not exposing, photobleaching was minimized and longer fluorescent movies could be captured.

Flagella on each trapped cell were imaged for hundreds of frames, over the course of tens of seconds. Flagella were counted manually, by examining sequential images to identify each

flagellum on a cell. Flagella were easiest to count during tumbles, when they broke from the bundle and were separated from each other. **Figure 2.5** shows example snapshots of trapped cells with various numbers of labeled flagella.

2.3.5 Results

Figure 2.2B shows the distribution of flagella from trapped wild-type cells. This distribution is similar to data obtained from the electron microscope. The mean number of flagella per cell, on trapped cells with fluorescent flagella, was 3.9 ± 1.7 (mean \pm SD).

2.4 Future directions

Accurately counting appendages such as flagella can be useful for a diversity of studies. Most bacteria swim and many microorganisms grow flagella or other appendages. The number and length of flagella on a cell are typically regulated by an interconnected system of genes and proteins which is affected by temperature, viscosity, chemical environment, and many other factors [6]. The genes that regulate this activity are an active area of interest [48, 50, 85, 86], and imaging all of the flagella on a swimming cell can be very useful when exploring how these genetic circuits operate. For example, I used electron microscopy to count flagella on different *Salmonella* mutant strains, to help characterize the effects of several genes involved in the regulation of flagella production [85].

Similar flagella imaging studies could be done on a wide range of microorganisms, to provide better understanding of the range of regulatory strategies that have evolved in nature. The combined optical-trap/imaging assay is the most robust method available for imaging flagella. Other methods suffer from the fact that flagella must be imaged on cells on or near a surface, often on fixed cells, which leads to flagella shearing and other adverse effects that make it difficult to accurately count flagella. In the future, flagella from a wide range of microorganisms could be imaged in the optical trap. I have successfully trapped *Salmonella* and *B. subtilis* cells, and it should be feasible to trap almost any microorganism which is of a similar size. Flagella could be labeled using whichever fluorescence labeling schemes are most convenient for the specific organism.

2.5 Summary

The primary aim of my thesis was to investigate the ways in which the number of flagella on a cell affects its swimming behavior. The first step towards that goal was developing a robust method of counting flagella in a setting that would allow additional analysis of swimming behavior. In this chapter I introduced several methods for counting flagella and discussed their advantages and limitations. Distributions of flagella number were obtained using electron microscopy and

fluorescence imaging in the trap. Rough, quantitative agreement between the distributions acquired using different methods suggests that the measurements were reliable. Most importantly, imaging of fluorescent flagella in the trap allowed me to count flagella in a context where I could perform additional behavioral measurements on the same cells. The next chapter will describe the design of the E Fleezers optical trap instrument which facilitates simultaneous imaging of flagella along with measurements of swimming behavior.

Chapter 3. The E Fleezers instrument

New technologies often drive scientific discovery. In the previous chapter, I discussed several methods for imaging and counting flagella on bacterial cells. However, previous methods of counting flagella were limited in their ability to provide long-term data about other aspects of bacterial swimming. In this chapter, I describe the design of a unique instrument that solves this problem. To facilitate simultaneous imaging of flagella, while also monitoring the long-term swimming behavior of a bacterial cell, I built an instrument combining high-speed, epi-fluorescence imaging and optical traps. I describe how the instrument works and present some representative data.

3.1 Background

As described in the **Introduction**, an optical trap is a focused laser beam which is used to apply a force to a trapped object. When the laser beam is focused into a diffraction limited spot, a bacterial cell can be held in place by the optical trap. When any other forces push the bacterium away from the center of the trap, the laser light applies a restorative force which pushes the bacterium back towards the center of the trap. To first order, the trap can be modeled as a three-dimensional Hookean spring.

Since their inception, optical traps have been used to study bacteria. The first recorded instance of optically trapped bacteria appears to have occurred by chance. While trying to trap Tobacco Mosaic Viruses, Ashkin and Dziedzic apparently failed to maintain sterile working conditions and accidentally cultured bacterial samples.

“In most of our experiments with silica colloids or TMV in water, we noticed the appearance of some strange new particles in diluted samples that had been kept around for several days. They were quite large compared to Rayleigh particles, on the basis of their scattering of light, and were apparently self-propelled. They were clearly observed moving through the distribution of smaller slowly diffusing Rayleigh-sized colloidal particles at speeds as high as hundreds of micrometers per second. They could stop, start up again, and frequently reversed their direction of motion at the boundaries of the trapping beam, when they encountered a dark region, indicating some sort of attraction toward light. Their numbers increased rapidly as time went by. When examined under 800X magnification in an optical microscope, they were clearly identifiable as rod-like motile bacteria, propelled by rotating tails.” [87]

Shortly thereafter, Steve Block and Howard Berg used an optical trap to measure the torsional compliance of bacterial flagella [88]. They used the trap to rotate a cell which was tethered by a flagellum to the surface of a glass slide. This revealed that, *“flagella behaved as linear torsion springs for roughly half a revolution, but became much more rigid when turned beyond this point in either direction.” [88]*

More recently, optical traps have been used to study bacterial swimming and propulsion. Richard Berry's lab used an optical trap to study the rotation of *Vibrio alginolyticus*, a bacterium propelled by a single polar flagellum which can rotate at rates higher than 1000 Hz. They showed that, "cells rotated more rapidly in media containing higher concentrations of Na^+ , and photodamage caused by the trap was considerably less when the suspending medium did not contain oxygen." [89] Another group trapped *E. coli* and measured their displacement and rotational frequencies, while subjecting them to fluid flow at various speeds, to derive the propulsion matrix relating torque, rotational rates and propulsive force in swimming *E. coli* [90]. However, these experiments were limited to short times (a few seconds) because cells were damaged in the trap and stopped swimming.

In order to study swimming behavior over longer periods of time we had to overcome the problem of light induced, oxidative damage. As established by previous studies, a combination of near infra-red laser light and molecular Oxygen leads to damage which causes cells to stop swimming [91, 92]. To ameliorate these effects, we employed an Oxygen scavenging system to remove Oxygen from the medium in which cells were trapped (gloxy, see *Min et al.*) [2, 15]. This allowed us to observe the swimming behavior of individual cells for tens of minutes [2, 15].

Our earlier work trapping *E. coli* focused on measurements that could be done purely with the trap (without fluorescence imaging). Similar to *Chattopadhyay et al.*, [90] we observed prominent oscillations at $\sim 10\text{Hz}$ and $\sim 100\text{Hz}$, corresponding to the rotation of the cell body and the flagellar motors, respectively (Figure 3.1C). We showed that run duration distributions were not purely exponential, but exhibited a heavy tail [2], characteristic of levy-flights which have been proposed to enhance foraging efficiency [93]. In a second paper, we measured chemotactic adaptation in trapped cells which were exposed to step-wise changes in the concentration of a chemoattractant [15]. I was involved in those studies, but they were primarily the Thesis work of Taejin Lance Min, so I do not discuss them in further detail in this thesis. See Taejin's thesis for more details.

One significant advantage of the trap assay over previous methods is that it measures the run/tumble swimming behavior of a single cell over long periods of time, whereas other methods often measure an intermediate readout, such as CheA activity [20, 67], or rotation of a single flagella [94, 95]. Other assays look at populations of cells or are limited in the duration over which a single cell can be monitored, because it swims out of the field of view of the microscope. Since the trapped cell is immobilized, it can be monitored indefinitely. Furthermore, it is easier to perform fluorescence imaging on a stationary target than a moving one.

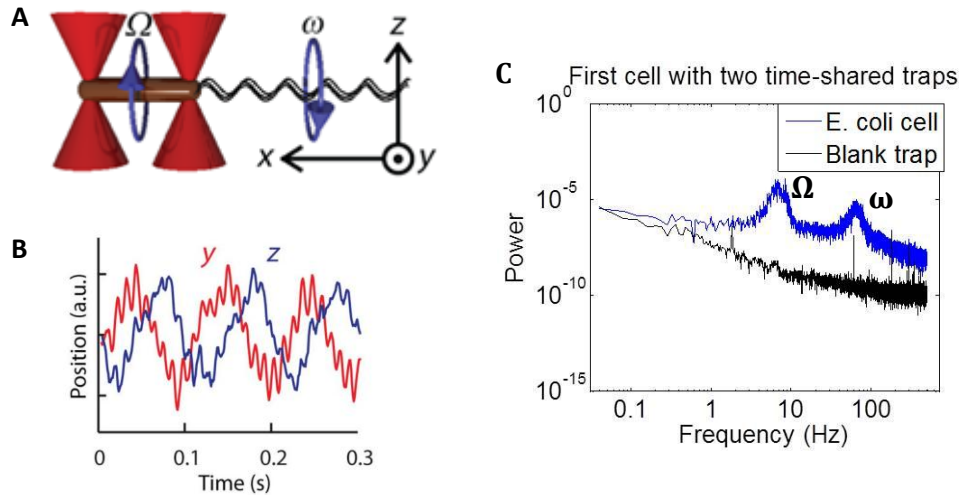


Figure 3.1: Trapped cell and signal. (A) Schematic showing optical traps (red cones) and a trapped cell. (B) Typical trap signal of a swimming cell along the y (red) and z (blue) axes. High and low frequency oscillations correspond to flagellar bundle and body rotation, respectively. (C) Power spectrum from the first live cell trapped in the E Fleezers instrument (blue) on July 1, 2010. Note the $\sim 10\text{Hz}$ (Ω) and $\sim 80\text{Hz}$ (ω) peaks in the signal from the trapped cell, corresponding to body and bundle rotation, respectively. The power spectrum of the trap signal when a cell is not present does not include either peak (black).

Following our previous studies, we wanted to expand the single-cell trapping method to incorporate fluorescence imaging which would allow us to visualize individual flagella. This is more challenging than it sounds. As discussed in Chapter 2, flagella on *E. coli* typically rotate at a rate of $\sim 100\text{ Hz}$. In order to produce a clear image of flagella on a swimming cell, the duration during which the flagella are imaged must be much significantly shorter than the duration of a full rotation. For example, a camera exposure lasting 1 ms would produce a blurry image during which the flagellum rotates through about 30 degrees. An additional challenge is that the rate at which fluorescent dyes bleach is enhanced in the presence of infra-red laser light [96]. As a result, under continuous illumination, fluorescence images can only be recorded for a short period of time (~ 1 second) before flagella become too dim to see clearly. The E Fleezers instrument was designed specifically to solve both of these problems.

3.2 Instrument design

3.2.1 General instrument design

I named this new instrument the E Fleezers, short for Epi-Flourescence optical tweezers (and also to reference the *E. coli* it was designed to trap). The detailed instrument schematic is shown in **Figure 3.2**. The general design of the instrument was derived from the Fleezers instrument developed by Matt Comstock with Yann Chemla and Taekjip Ha [3]. The instrument involves a single, near infra-red

laser which was used to generate multiple optical traps. A microscope objective was used to focus the laser beam and form the traps. A second objective was used to collimate light that has passed through the sample, and that light was directed onto a quadrant photodiode which measured the deflection of the laser beam which has passed through the trapped object (bacterium). This method, known as back-focal-plane interferometry was used to quantify the movement of the trapped object [97]. Additionally, a visible laser was used to illuminate the sample and excite fluorescent dyes which were used to image flagella or other labeled objects.

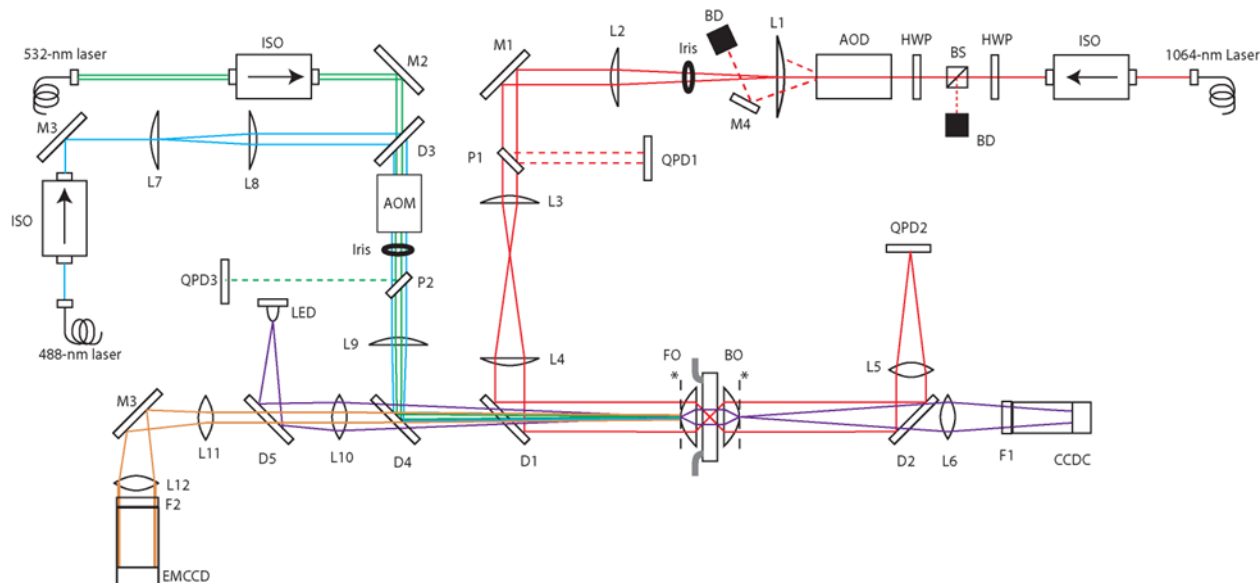


Figure 3.2: Instrument layout. A schematic of all optical components of the E Fleezers instrument. Light paths are indicated by red (1064-nm), green (532-nm), blue (488-nm), purple (white light from LED), and orange (fluorescence emission) lines. Other components are labeled; EMCCD - Electron Multiplying CCD camera, AOM - Acousto-Optic Modulator, M – Mirror, L – Lens, CCDC - Charge-Coupled Device Camera, QPD - Quadrant Photodiode Detector, BO - Back Objective, FO - Front Objective, D - Dichroic Mirror, P - Pickoff mirror, F - Filter, AOD - 2-axis Acousto-Optic Deflector, BS - Polarized Beam Splitter, BD - Beam Dump, HWP - Half-wave Plate, ISO - Optical Isolator. See **Appendix A.3** for a detailed description of all components.

There were many choices that went into the instrument design. Some were tightly constrained, others were decided based on convenience or cost. The first significant choice was which laser frequency to use for the trapping light. We wanted to use an infrared laser, because a visible laser would limit our options for fluorescence imaging. We chose to use a 1064-nm laser, largely because all of the other optical components (lenses, mirrors, acousto-optics crystals and beam splitters) were readily available. The other traps in the Chemla lab use 1064-nm lasers, so this would allow optical components to be shared. We considered using a frequency at which oxidative damage is lower (e.g. 830 nm or 970 nm [91]), but those frequencies do not sufficiently mitigate oxidative damage. Cells would still have been damaged after tens of seconds, so we still would have needed to use our Oxygen scavenger system

in order to trap cells and measure swimming for tens of minutes.

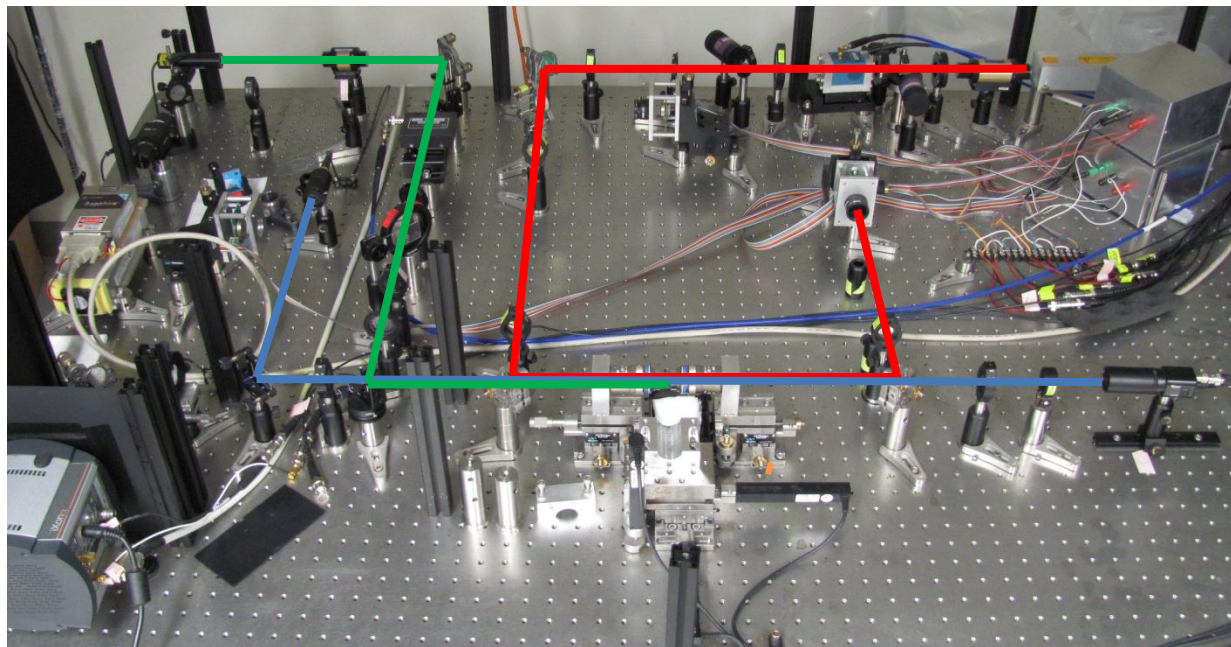


Figure 3.3: Photo of E Fleezers instrument. Approximate light paths are indicated by red (1064-nm), green (532-nm) and blue (white light from LED). See **Appendix A.3** for a detailed description of all components.

3.2.2 Acousto-optics for timesharing

Various strategies have been used to create optical tweezers that utilize multiple traps. The most obvious method would be to use a separate laser for each trap. However, this is very expensive, requires significantly more space and hardware, and also provides less accuracy in both position control and the quantitative measurement of trapped objects. This is because the two laser beams may drift relative to one another, introducing a significant source of noise to the data. A superior method is to use a single laser which is split into multiple, parallel beams which can use a shared set of optics. Such an instrument was previously designed by splitting the laser beam into 2 separate beams (separated with a polarizing beam splitter) to perform ultra-high resolution measurements on Angstrom length scales [98]. The trick to attaining such high accuracy is in measuring the differential displacement of the two traps relative to one another. Most sources of uncertainty in measuring the position of the trapped samples arise from very small movements in either the initial laser beam or the optical components such as lenses and mirrors with which the beam interacts. However, in the case of dual traps generated from a single laser, and passing through (mostly) the same beam path, all of these motions are common to both traps. Movement of any of these components does not contribute to the difference in position between the two beams.

An alternative method for splitting the beam is to use an acousto-optic crystal to precisely deflect the laser beam at a well-defined angle. Different traps are generated via timesharing, by rapidly switching the angle of deflection (see **Figure 3.4**). When switched at rates of approximately 50 KHz, each deflected beam behaves as effectively continuous in time. The key requirement is that the trapped object cannot move far during the time in between. In the E Fleezers instrument, interlacing was configured with a cycle of three time periods, each lasting 20 μs . During the first time period, the beam was deflected at an angle to create a trap at location 1 (**Figure 3.4**). During the second time period, the beam was deflected at a slightly different angle to generate a trap at location 2. During the third and finally time period, the beam was not deflected and did not reach the sample plane. As a result, there was no trap formed during the third time period. The net effect was that two traps were formed, which

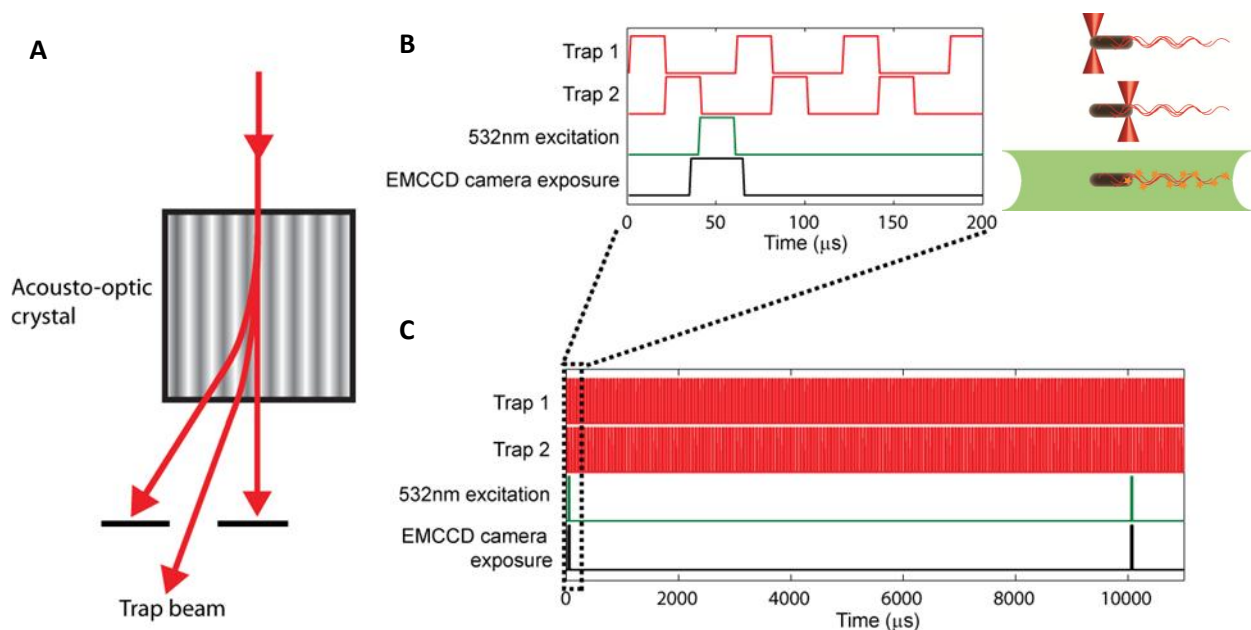


Figure 3.4: Acousto-optic deflection and time-sharing. (A) Schematic of the deflection of a laser beam via acousto-optic deflection. This process is used in the 2-axis AOD to control the timing and location of both optical traps. It is also used in the AOM to control the timing of the fluorescence excitation laser (532-nm). As the beam passes through the crystal, phonons interact with the photons and cause some of them to deflect, generating a diffraction pattern. (B) Schematic of the temporal interlacing of the trapping laser (red), excitation laser (green) and camera exposure (black). The 1064-nm trapping laser alternates with the 532-nm fluorescence excitation laser, such that they are never on at the same time. The camera exposure (30- μs exposure) is synchronized with the fluorescence excitation laser for stroboscopic imaging. To the right are cartoons showing what the sample looks like during each time period. (C) Same as (B) over a longer time scale. The fluorescence excitation pulse and camera exposure occur once every 10-ms to create movies at 100 fps.

were moved by changing the angle of deflection for either trap 1 or trap 2. The third time period was reserved for fluorescence excitation.

3.2.3 High speed fluorescence imaging

The novel aspect of the E Fleezers is that it combines epi-fluorescence imaging with high-resolution optical tweezers. Epi-fluorescence imaging of trapped cells was achieved by excitation with a 532-nm laser (*TECGL-30, World Star Tech, Toronto, Canada*) and collecting backwards emitted photons with an EMCCD camera (*iXon3 860 EMCCD, Andor, Belfast, Ireland*). The beam size at the sample plane was approximately 20 microns in diameter. I used timesharing to overcome rapid photobleaching of the fluorescent dyes, which is induced by simultaneous exposure to the fluorescence excitation light and the infra-red trapping light. Fluorescent dyes were excited during the third time cycle while there was no infra-red light at the sample plane (see **Figure 3.4**). This interlacing method has been shown to significantly enhance fluorescent dye lifetimes [96, 99], and allowed me to record much longer movies of fluorescent flagella (>10 s).

As discussed above, each image must be captured during a short time window (<1 ms) to produce clear images of rapidly rotating flagella. The fluorescence excitation beam was controlled by an acousto-optic modulator (a second acousto-optic device, separate from the one used to control the infra-red laser beam, see **Figure 3.4**.) During the third time cycle (lasting 20 μ s) the beam was occasionally deflected for 18 μ s to illuminate the sample. Usually there was nothing directed at the sample during the third time cycle. The excitation beam was only directed towards the sample once per EMCCD exposure, which occurred on a much longer timescale (2-10 ms) (**Figure 3.4B**). The EMCCD camera recorded 128 x 128-pixel images ($\sim 10 \times 10 \mu$ m) with a short, 30- μ s exposure, synchronized with each excitation pulse. This stroboscopic imaging was performed intermittently, depending on the frame rate desired. To produce movies at 400 frames per second, the sample was illuminated with a single 18- μ s excitation pulse, once every 2.5 ms. To produce movies at 100 frames per second, the sample was illuminated once every 10 ms.

This configuration allows the user to easily record images at different frame rates. It also has the advantage of only illuminating the sample while an image is being acquired. This maximizes the duration of the fluorescence movie, because dyes are not photobleaching in between camera exposures. The specific EMCCD camera settings used to acquire videos of fluorescence flagella are shown in **Appendix B.3**.

3.3 Instrument control

3.3.1 Electronics control and acquisition

The most complicated aspect of the instrument is the electronic interface between the trap

components and the user. A schematic of the information flow throughout the instrument is shown in **Figure 3.5**. With the exception of the EMCCD camera, all systems control and data acquisition is handled through custom LabVIEW code. The user controls all components, including the trap positions, sample location and timing regarding when to acquire data and when to illuminate the sample with various excitation lasers, through a LabVIEW program called “E coli Trap Control (host) - Host 2.0.vi”. The Host program runs several sub-functions (called sub-VI’s in LabVIEW) which control individual components. The initial LabVIEW code was written by Matt Comstock for the UHR Fleezers instrument [3]. However, the current design has diverged significantly, as various components and capabilities were added and removed.

The most significant subVI is the FPGA code, “E coli Trap Control (fpga) – 1.7.vi”. Most of the electronic inputs and outputs (I/O) from the computer run through a single DAQ card (Data Acquisition card) which contains a Field Programmable Gate Array (FPGA). The FPGA code configures the FPGA so

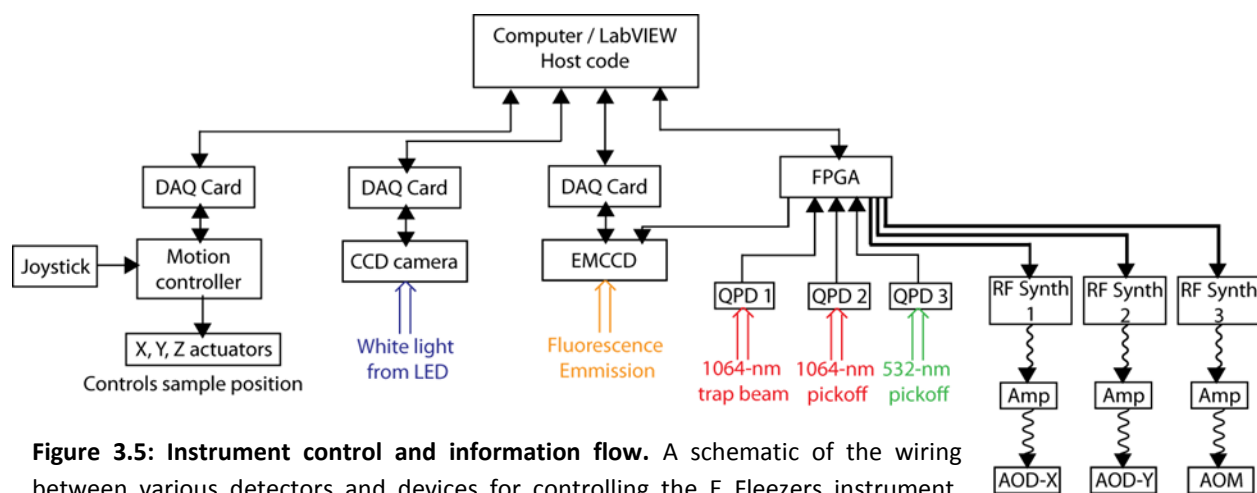


Figure 3.5: Instrument control and information flow. A schematic of the wiring between various detectors and devices for controlling the E Fleezers instrument. Arrows indicate the direction of information flow. In many cases, data flows in both directions. Colored double-arrows indicate light beams on the instrument that impinge upon detectors or cameras. Wavy lines indicate RF signals.

that it correctly handles all of these I/O’s. These signals propagate to and from the DAQ card via two breakout boxes, which contain dozens of electronic screw terminals, each of which can be connected to a wire. Each signal is assigned a specific channel number within the FPGA code. That channel number corresponds to a specific screw terminal in one of the breakout boxes. **Appendix A.4** lists every input and output signal that passes through one of the breakout boxes.

3.3.2 Controlling trap position via Acousto-optic deflection

The position of each optical trap was controlled using an acoutso-optic crystal to precisely

deflect the 1064-nm laser beam by a specific angle. Acousto-optic deflection was achieved through the interaction of the laser photons with vibrating phonons within the crystal lattice (**Figure 3.4**). The angle of deflection is determined by the frequency of the phonons, which is controlled by a piezo-electric transducer attached to the side of the crystal. When a high frequency electrical signal (usually Radio-Frequency (RF), ~30 MHz) passes through the piezoelectric transducer it vibrates at the same frequency, generating phonons in the acousto-optic crystal. In the E Fleezers instrument, a 2-axis acousto-optic deflector (AOD) was used to control the trap position in the orthogonal X and Y axes, independently. There are two crystals, each with its own piezoelectric transducer, which control deflection along one of the axes.

In the current configuration, trap 1 has a fixed position and the user controlled the position of trap 2 in real time using a computer mouse. Alternatively, the user could specify the precise location of the trap by typing frequencies into the LabVIEW Host code, to be used for deflecting either of the traps in X or Y. When the mouse was used, the LabVIEW code continually changed the RF frequencies based on the mouse location. In either case, the new frequency value was sent from the computer, via the FPGA card, through the breakout box to one of two RF synthesizer boards. The RF synthesizer boards generated the RF signals which passed through an RF amplifier and were then connected to the piezoelectric transducers in the 2-axis AOD. The specific signal sent from the computer to the RF synthesizer was somewhat complicated, because the RF synthesizer takes a series of input values to encode the RF frequency, power, and the timing for when it should switch to a new value. All of these output signals are listed by channel in **Appendix A.4**.

As discussed earlier, the two different traps were created via timesharing (**Figure 3.4**). Recall that there were 3 time periods during which trap 1 exists, then trap 2 exists, and finally no trap is formed (the third period was reserved for the fluorescence excitation laser). This interlacing was achieved by rapidly switching the RF signals between values defining the position of trap 1, then trap 2, and then 0 (no trap).

3.3.3 Controlling fluorescence excitation timing via acousto-optic modulation

A second acousto-optic device was used to fine tune the timing of the fluorescence excitation laser beam. To achieve temporal interlacing between the trap beam and the fluorescence excitation beam at speeds of 50 KHz, I used an acousto-optic modulator (AOM, see **Figures 3.2** and **3.4**) This AOM has a single acousto-optic crystal which operates in the same manner as the acousto-optic device described in the previous section. Here, the input RF signal was switched between two values (0 and 80

MHz) which caused the laser to be deflected or undeflected. When deflected, the beam passed through an iris and reached the sample plane to illuminate the trapped bacterium. When undeflected, the beam was blocked by the iris. As a result, the excitation was effectively turned on and off by the RF signal which was controlled by the LabVIEW code. The timing of this signal was synchronized with the exposure of the EMCCD camera so that fluorophores in the sample were only excited while the EMCCD camera was acquiring an image. Additionally, the timing of the signal was fine-tuned so the excitation laser was only on while the trap laser was off (**Figure 3.4**).

To ensure that all of this timing was accurate, signals for monitoring the trap laser, excitation laser, and EMCCD exposure time were all sent to an oscilloscope (these signals are explained in the next section on **Quadrant photodiodes**). Within the LabVIEW code, any of the repeating signals could be phase shifted relative to the others. At the beginning of each experiment, the relative timing of these 3 signals was fine-tuned by adjusting the phase shift of the EMCCD exposure and the fluorescence excitation laser.

3.3.4 Quadrant photodiode detectors

To detect various signals from the lasers, we used quadrant photodiodes. These position sensitive detectors were used to collect spatial and temporal information from the 1064-nm trapping laser beam and the 532-nm fluorescence excitation laser beam. The detectors measured photon intensity on 4 different quadrants, and produced 3 electrical signals based on the total photon intensity (SUM) the difference between the top and bottom halves (Y) and the difference between the left and right halves (X). These analog signals were then sent to the computer, via the breakout boxes (see analog inputs in **Appendix A.4**).

Three QPDs were included in the instrument design (**Figure 3.2**). QPD1 was used to detect motion of the trapped bacterium, using the back-focal plane detection method described earlier. As the trapped bacterium moved, the 1064-nm trapping light was deflected at different angles. This angle was mapped into a change in position of the 1064-nm beam that impinged upon the QPD. As a result, the X and Y signals from the QPD represent the movement of the bacterium within the trap. An example signal from a swimming cell is shown in **Figure 3.1B**. The power spectrum from this QPD signal was used to identify the $\sim 10\text{Hz}$ and $\sim 100\text{Hz}$ frequencies shown in **Figure 3.1C**.

A second QPD was used as part of a feedback loop to maintain constant trap power. When the trap position was changed (by altering the RF signal to the AOD, see previous sections) the power of the deflected beam varied. This is a feature of the acousto-optic deflection. To compensate for this

variation, the power of the RF signal which controls the deflection of light through the AOD was increased or decreased using an automated PID feedback loop. As shown in the trap layout (**Figure 3.2**) a small fraction ($\sim 1\%$) of the trap beam was reflected using a small pickoff mirror, and sent to QPD 2. The SUM signal from this QPD was proportional to the total trap power. This QPD2-SUM signal was used to change the power of the RF signal controlling the AOD, such that the power of the trap beam did not vary significantly. For more details on this feedback loop see *Comstock et al.* [3].

The third QPD was used to monitor the timing of the 532-nm fluorescence excitation laser beam, after it passes through the AOM. (A less expensive detector, without position sensitivity, would suffice. I only used the QPD because we already had it in the lab.) A small fraction of the fluorescence excitation beam was reflected towards QPD3 using a microscope slide (a cheap kludge that worked surprising well!) The QPD3-SUM signal was used to monitor the timing of the 532-nm excitation beam. When fine-tuning the relative position of the 532-nm excitation beam, the 1064-nm trapping beam and the EMCCD exposure, the QPD1-SUM signal and QPD3-SUM signals were both sent to an oscilloscope.

3.3.5 EMCCD camera timing

I originally tried controlling the EMCCD from LabVIEW. But for some reason (bad drivers/user error?) I could not achieve frame rates faster than ~ 300 fps. Therefore, most of the EMCCD camera settings were controlled using Andor Solis software (for specific settings see **Appendix B.4.**) However, the exact timing of the camera exposure was controlled using a signal generated by the LabVIEW Host code. The camera was set to External Trigger mode, whereby a single frame was acquired each time the camera received an external TTL-logic signal ($\sim +5V$). A digital output signal was sent from the computer, via the breakout box (**Appendix A.4**) to the “Trigger” input on the camera. Controlling the exposure timing in LabVIEW allowed for precise control of the trap, excitation and exposure signals relative to one another, to achieve consistent interlacing (**Figure 3.4**). When monitoring this timing, the “Fire” signal from the camera was sent to an oscilloscope and compared to the QPD1-SUM and QPD3-SUM signals as described in the previous section.

It is important to note that the EMCCD camera does not record and image instantaneously, and cannot acquire a new image immediately after acquiring the previous one. There is a dark period after the acquisition of each image, during which a new image cannot be acquired. This places an upper limit on the frame rate of the camera. When acquiring fast movies, the safest way to ensure that the camera records each frame as expected is to allow a small, extra window of time after each frame. When the camera settings are selected in Andor Solis software, the software reports an expected frame rate.

However, in external triggering mode, the actual frame rate will be determined by the frequency of the TTL signal generated by the LabVIEW code. To ensure that no frames were lost, I always set the TTL signal to a slightly slower rate than the Andor Solis reported rate.



Figure 3.6: High-speed images of fluorescent flagella on a trapped cell. A sequence of images from a trapped cell with fluorescently labeled flagella. At the beginning, one flagellum is rotating CCW in the *normal* waveform. The other two are rotating CW, one is *semi-coiled*, the other is *curly-1*. Over time the *normal* flagella switches to CW rotating and moves out of the focal plane. The *semi-coiled* flagellum switches to CCW rotating and eventually returns to the *normal* waveform. The *curly-1* flagellum remains in that waveform throughout the sequence. Images were recorded at 400 fps.

3.4 New trap data

As shown in **Figure 3.1C**, we were able to measure the power spectrum of a trapped cell, and identify peaks corresponding to flagellar and body rotation at ~ 100 and 10Hz, respectively. I labeled flagella and visualized the flagella using the stroboscopic imaging methods described above. A sequence of images from an example cell illustrates the high quality images we were able to record with this new instrument (**Figure 3.6**).

Additionally, we tested the sensitivity of instrument's imaging capability by visualizing single fluorescent dyes (**Figure 3.7**). We used the DNA construct from *Comstock et al.* [3] along with short DNA oligo's (sequence AACCAAGTCCTAA) which were tagged with a single fluorophore. The DNA was stretched between two beads, which were held in the two traps. We continuously recorded images while oligos bound and unbound from the trapped DNA construct. To produce a bright enough signal, we turned up the EM Gain, camera exposure and excitation laser power. We were able to see several single fluorophore spots. However, the spots appeared only for a single frame. The dyes either photobleached or detached from the DNA construct within a single camera exposure. This proof-of-concept experiment shows that the instrument is capable of imaging single molecules, but probably not for prolonged periods of time.

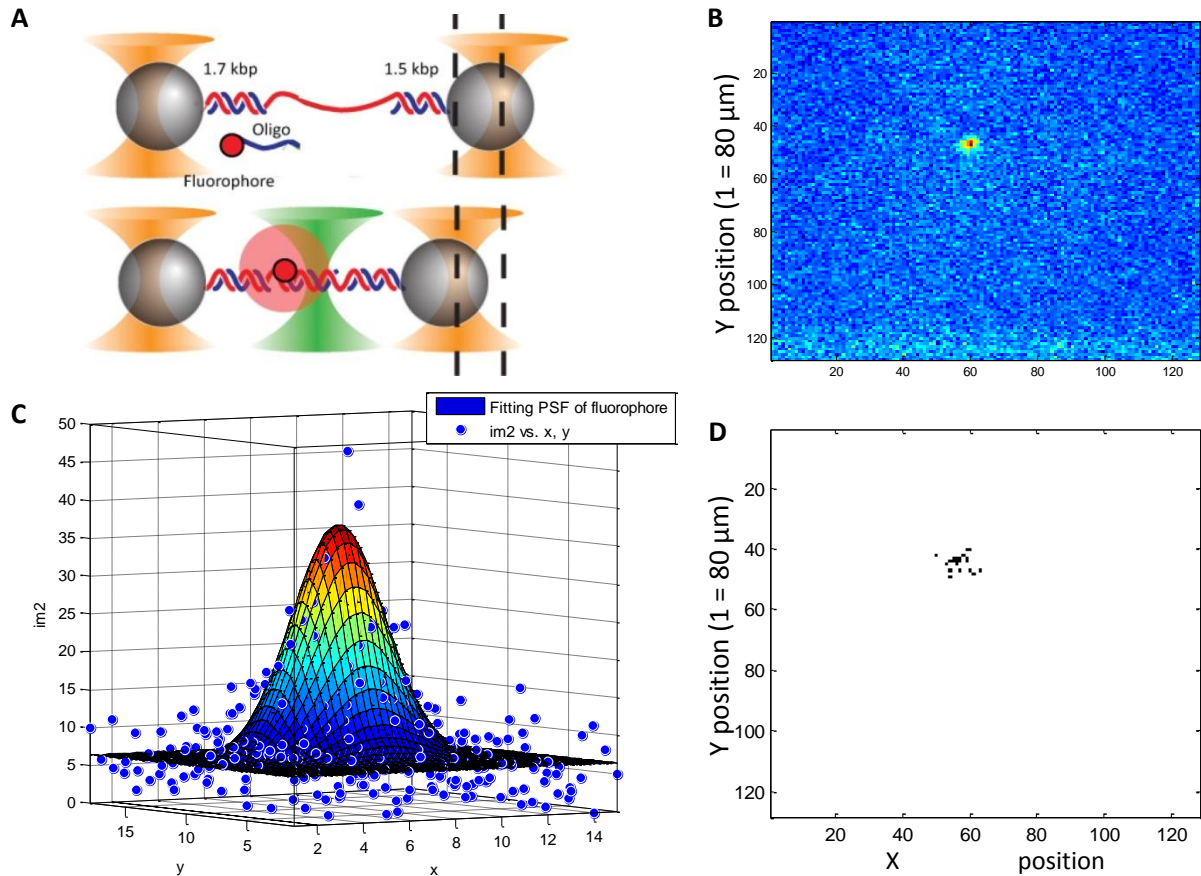


Figure 3.7: Single-molecule imaging in the E Fleezers. (A) Schematic of the experiment. A long (~3kbp) dsDNA is stretched between two beads which are held in two separate traps. In the middle of the dsDNA is a short segment of single stranded DNA which is complementary to a Cy3-labeled ssDNA oligo. When the Cy3-labeled oligo binds to the tethered DNA construct, it remains in the field of view and fluoresces. (Samples provided by Kevin Whitley, Image adapted from *Comstock et al.* [3]) **(B)** Image of a single Cy3 fluorophore in the E Fleezers. Axes labels indicate pixel number on the EMCCD camera; each pixel images an area measuring $80 \times 80 \mu\text{m}^2$. **(C)** 2D-gaussian fit to determine the location of a single oligo-bound Cy3 dye. **(D)** Scatter plot showing the location of 22 different Cy3-oligo's each bound to the same DNA construct, as determined in panel (C). Location of the dyes had a standard deviation of $300 \mu\text{m}$.

3.5 Future Directions

3.5.1 Quantifying CheY-YFP in trapped cells

As demonstrated in the previous section, the E Fleezers instrument has a wide range of potential applications. Within the field of bacterial chemotaxis, there are several other questions that could be addressed using this instrument. The relationship between CheY-P concentration and CW bias for an individual motor was established by performing fluorescence correlation spectroscopy on cells expressing mutant CheY-GFP proteins, while also measuring the rotation of a bead attached to a single flagellar motor [39]. In the trap it is possible to quantify the concentration of fluorescence proteins such

as CheY-YFP while also measuring the tumble bias of the same cell. The 488-nm laser on the E Fleezers instrument is capable of exciting YFP and GFP.

I created a plasmid expressing CheY-YFP, which can be induced to express at a wide range of concentrations (pPM9, **Appendix C.2**), and could be used to create a similar map between CheY-YFP concentrations and tumble bias to be created. Additionally, it should be possible to simultaneously measure swimming behavior and CheY-YFP concentration while imaging flagella. Based on the known relationship between CheY-P and CW bias (**Equation 5.4**), and the relationship between flagellar number and tumble bias (**Equation 4.1**), the predicted relationship is given by **Equation 3.1** and **Figure 3.8**.

$$TB = 1 - \left(1 - \frac{1}{\left(\frac{k_D}{[CheY-P]} + 1\right)^{10}}\right)^{N_{flag}} \quad (3.1)$$

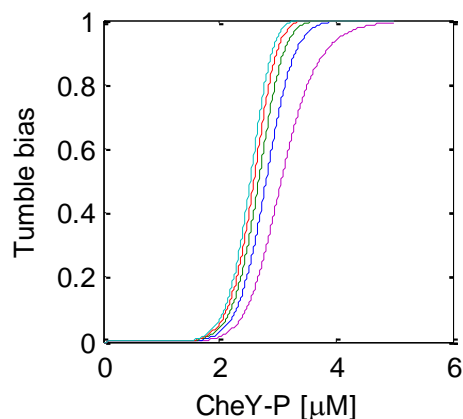


Figure 3.8: Predicted relationship between tumble bias, CheY-P and number of flagella. Each line represents the predicted trend for cells with a specific number of flagella ($N_{flag} = 1$ (purple), 2 (blue), 3 (green), 4 (red), and 5 (cyan)), Curves were derived by combining **Equations 4.1** and **5.4**. The curves for cells with more than 2 flagella are quite close and might be difficult to resolve given the typical levels of uncertainty in our current experiments.

I designed the plasmids for labelable flagella (pPM5) and CheY-YFP (pPM9) to be compatible, so both proteins can be expressed in the same cell, and controlled independently (**Appendix C.2**). Alternatively, a chromosomal insertion of the labelable *flic** gene now exists [30]. Flagella would need to be labeled with dyes of a different wavelength to avoid spectral overlap the the YFP emission and absorption. I have successfully labeled flagella on strain HCB1660 using the fluorescent dye AlexaFluor 633 C₅ maleimide (*A-20342*, *Life Technologies*). Flagella labeled with this dye can be imaged by excitation with a red laser which does not excite YFP. Fortunately, the design of the E Fleezers allows for easy integration of additional laser lines. The AOM, which is used to control the timing of the excitation light, is capable of deflecting visible light with wavelengths in the range of 400-700 nm. The stroboscopic illumination modality of the E Fleezers would make it easy to separate the images from the two different fluorescence reporters.

3.5.2 Imaging Tar-YFP and other fluorescent chemotaxis proteins in the trap

In addition to CheY, fluorescent protein fusions exist for every chemotaxis gene in *E. coli* [66,

100]. Many aspects of chemotaxis are still being investigated, and the ability to image components while measuring the behavioral output of the system will aid future investigations. For example, recent studies suggested that receptor proteins might dynamically rearrange in response to large chemotactic stimuli [101]. I used a strain expressing Tar-YFP (PM41, **Appendix C.1**) to observe receptor clusters on cells exposed to abrupt stimulus (using the trap-based chemotaxis adaptation protocol which I helped develop in *Min et al.* [15]) in the E Fleezers and under agar pads in an epi-fluorescence microscope. I found that receptors clusters did not change in response to a large 1 mM stimulus of aspartate. Future experiments could explore the dynamics of other chemotaxis proteins in trapped cells, while monitoring swimming behavior, chemotaxis response, and fluorescent flagella.

3.6 Summary

This chapter described the design, construction and control of the new E Fleezers instrument. The purpose of this instrument was to facilitate simultaneous quantification of multiple aspects of bacterial swimming in a single cell. With this instrument I was able to trap individual bacterial cells, record high-speed movies of fluorescent flagella and separately image single molecules. In the next chapter I use the E Fleezers to address the primary goal of this thesis: Quantifying the effect of flagellar number of bacterial swimming behavior.

Chapter 4. How flagellar number affects swimming behavior

In the previous chapter, I described the construction of a unique instrument combining optical traps and high-speed, fluorescence imaging. The primary purpose of this instrument was to investigate how the number of flagella on a bacterial cell affects its swimming behavior. In this chapter I describe experiments with *E. coli* cells in which fluorescently labeled flagella were imaged and the run-tumble swimming behavior was measured simultaneously for a single cell. To my surprise, I found that the tumble bias of wild-type cells does not significantly increase with number of flagella. Control experiments with a mutant strain in which run-tumble behavior was decoupled from the chemotaxis network support the conclusion that fluctuations in the concentration of the CheY-P signaling molecule explain the behavior of wild-type cells. These fluctuations lead wild-type cells to exhibit a tumble bias that is robust against variations in flagellar number.

4.1 Background: Flagellar imaging and the veto model

As described in **Chapter 1**, bacterial swimming is generally characterized as a two-state random walk composed of runs and tumbles. Whether a cell runs or tumbles is determined by the collective state of the flagella on the cell. Each flagellum is driven by a rotatory motor which is capable of switching between CW and CCW rotation. Most of the time, all of the flagella rotate CCW, which causes them to bundle together and propel the cell forward in a run. Occasionally, some of the flagella switch direction and rotate CW. This disrupts the bundle and causes the cell to tumble. The probability of a given flagellar motor rotating CW depends on the concentration of CheY-P inside the cell, but motors switch directions independently of one another [102]. Different flagella on a single cell can be in different states.

To quantify swimming behavior I calculated the tumble bias (TB), which is defined as the fraction of time that a cell spends tumbling. My goal was to determine how the number of flagella on a cell would affect its tumble bias. Prior to this work, the only direct measurements of flagellar dynamics in swimming cells have been limited to short periods of time (~ 1 s) [31, 56]. The absence of long-term observations has precluded the development of a detailed mapping between flagellar state and cell swimming behavior. Specifically, previous experimental observations were too short to determine the tumble bias. Due to the limited amount of experimental information, existing models of bacterial chemotaxis make different assumptions regarding the transition from single-motor to whole-cell swimming. For example, many models ignore the issue and assume that cells have only one flagellum [18, 93, 103-105]. Others assume a 'voting' model, in which cells only tumble if a majority of flagella

rotate CW and thereby ‘vote’ to tumble [42, 44, 104]. Several different models will be explored in detail in **Chapter 5**, but first we must examine the experimental data that will be used to judge these models.

By observing fluorescently labeled flagella during individual tumbles, *Turner et al.* established that CW rotation of a single flagellum is sufficient to cause a tumble [31]. The simplest model incorporating this observation is the ‘veto’ model. The veto model posits that a cell tumbles whenever any of its flagella are rotating CW (**Figure 4.1**). Thus, the probability that a cell runs is equal to the probability that all of its flagella remain CCW. As a consequence, cells with more flagella are expected to tumble more, since there is a higher chance that at least one flagellum will deviate from the consensus and “veto” the run. These predictions can be stated mathematically, under the assumption that the rotational directions of all flagella are independent of each other. In a cell with N_{flag} flagella, the average tumble bias TB —the fraction of time a cell spends tumbling—will be given by

$$TB = 1 - (1 - CB)^{N_{flag}}, \quad (4.1)$$

where CB is the average clockwise bias—the fraction of time the cell’s flagella rotate CW (for derivation see **Appendix D.1**).

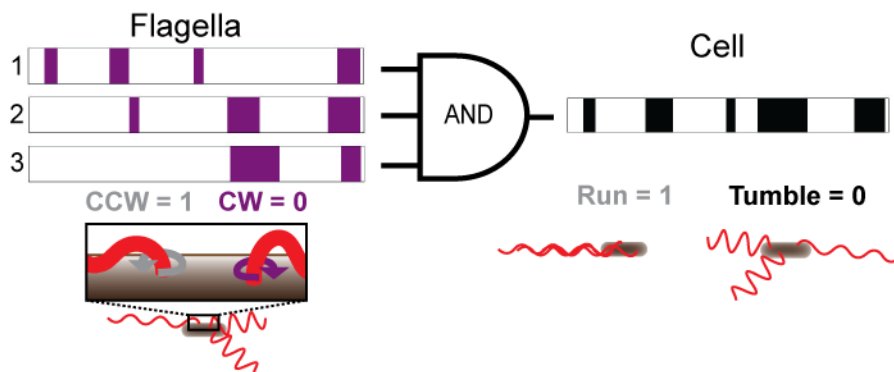


Figure 4.1: The veto model. The mapping which relates the run/tumble state of the cell to the CCW/CW state of its flagella, according to the veto model. Schematic time trace from a cell with 3 flagella, showing CW (purple) and CCW (white) intervals for each flagellar motor and the resulting tumbles (black) and runs (white) of the cell. The veto model corresponds to an AND gate, by which runs only occur when all flagella rotate CCW (where $CCW = 1$, $CW = 0$, $run = 1$, and $tumble = 0$).

To test this prediction, I quantified the swimming behavior of individual *E. coli* cells, wild-type for chemotaxis (strain HCB1660 [106], see **Appendix C.1**) using the E Fleezers instrument described in **Chapter 3**. The instrument allowed me to count flagella and measure the tumble bias of a single bacterium simultaneously.

4.2 Experimental procedure

4.2.1 Choosing a bacterial strain

Experiments were performed using two *E. coli* strains (**Appendix C.1**). The strain referred to as “wild-type” is HCB1660 [[106], gift of Howard Berg]. In this strain the *fliC* gene, which encodes for the flagellin protein which makes up the entire flagellum, has been deleted (denoted $\Delta fliC$.) As a replacement, this strain expresses a mutant version of the protein, $FliC^{S219C}$, from a plasmid under the control of arabinose. (The nomenclature $FliC^{S219C}$ indicates that the gene *fliC*, which expresses the protein FliC, has been mutated such that the 219th amino acid in the protein chain has been changed from Serine (S) to Cysteine (C)). The mutant protein $FliC^{S219C}$ was designed to contain a site that could be specifically labeled with a maleimide-functionalized fluorescent dye [106]. As discussed in **Chapter 2**, it is necessary to specifically label the flagella so that they can be clearly imaged. Non-specific fluorescent labeling methods lead to very bright cell bodies which make it difficult to see flagella clearly.

The strain referred to as “CheY*” is PM87, $\Delta fliC \Delta cheBYZ$ expressing $FliC^{S219C}$ and $CheY^{D13K}$ from separate plasmids under the control of arabinose and IPTG, respectively (**Appendix C.1**). The mutant protein $CheY^{D13K}$ is constitutively active [36], such that the CW bias of the flagellar motors was determined by the concentration of $CheY^{D13K}$, decoupled from the chemotaxis network.

4.2.2 Growing cells

For each experiment, cells were picked from a single colony on an agar plate and grown overnight in 1 ml tryptone broth [1% (wt/vol) Bacto tryptone and 0.8% (wt/vol) NaCl] [2, 48] shaking at 265 RPM at 30 °C with appropriate antibiotics. The plasmids which express mutant proteins described in the previous section confer antibiotic resistance to their host cells, so antibiotics were included to ensure that only cells containing the correct plasmids survived. The overnight culture was diluted 100-fold into

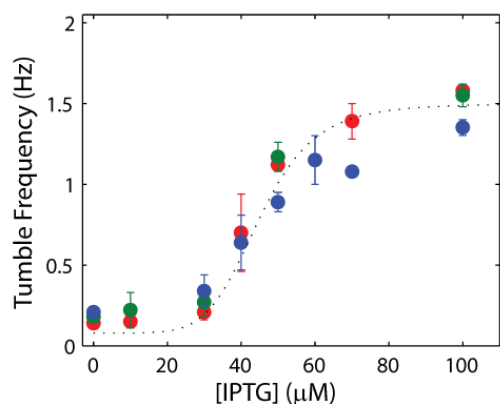


Figure 4.2: IPTG titration. Tumble frequency vs. concentration of IPTG. IPTG was added to growth medium to induce production of the CheY* protein which controls how frequently a flagella rotate CW. Three different strains expressing the protein from the same plasmid were characterized and displayed similar induction curves (PS2001, PM6, PM87; see **Appendix C** for strain and plasmid details). Dotted line is a guide to the eye. All trap data using the CheY* strain (PM87) was collected after inducing cells with 50 μM IPTG, which creates a population of cells with an intermediate tumble frequency (and tumble bias).

12-ml tryptone broth and grown, shaking at 265 RPM at 30 °C for 4.5 h (to $OD_{600} \sim 0.5$) with appropriate inducers (500 μ M arabinose for either strain and 50 μ M IPTG for strain PM87). The specific concentration of each inducer was selected by titrating through a range of concentrations and testing the behavior of each strain. The arabinose concentration was selected to be high enough to induce growth of long flagella, but not so high that it appeared to affect the tumble bias in either strain. In strain PM87, IPTG controls the concentration of CheY*, which in turn controls the average tumble bias (**Figure 4.2**). The specific concentration of IPTG was selected such that the average tumble bias matched that of the wild-type strain

4.2.3 Labeling flagella

To facilitate visualization of flagella, we used a fluorescence labeling protocol developed by *Turner et al.* [106]. The over-day culture was harvested, washed by slow centrifugation (1300g, 10 min) and gently resuspended in 1 ml motility buffer (MB) [56] (10 mM KPO_4 (pH 7.0), 70 mM NaCl and 0.1 mM EDTA). They were centrifuged a second time and then resuspended in 0.5 ml MB. Slow spinning and gentle centrifugation are necessary to prevent shearing of flagella (see **Chapter 2**). Flagella were specifically labeled using Alexa Fluor 532 C₅ Maleimide (A-10255, *Life Technologies, Carlsbad, California*). 1 mg of dry dye was dissolved in 300 μ l H₂O by vortexing for 1 min. Aliquots containing 50 μ l of dissolved dye were stored at -20 °C. Cells in 500 μ l MB were gently mixed with 5 μ l of the dissolved dye and then incubated with slow rotation (~ 10 RPM) at room temperature in the dark for 90 min. The labeled culture was washed and gently resuspended in 1 ml MB. Finally, cells were diluted 20-fold into 1 ml trap motility buffer (TMB) [70 mM NaCl, 100 mM Tris-Cl, 2% (wt/vol) glucose, and an oxygen-scavenging system (80 μ g ml⁻¹ glucose oxidase and 13 μ g ml⁻¹ catalase)] [2] and injected into the flow chamber for trapping.

At all stages, resuspension by pipetting was avoided to prevent shearing of the flagella [31]. To resuspend cells after centrifugation the supernatant was decanted and the resuspension medium, MB, was added by holding the round bottom tube at a 45 degree angle from vertical and pipetting slowly onto the inner side of the tube. This allowed the MB to slowly drop to the bottom of the tube without disturbing the pellet. The tube was then rotated by hand at an angle of about 45 degrees at a rate of a couple rotations per second. In this manner, the pellet usually dissolved in about 5-10 minutes.

It is also important to note that the maleimide dye does not readily dissolve in water. Previous protocols using this dye call for dissolving in DMSO. However, DMSO is harmful to cells, and I found that DMSO had adverse effects on cell swimming. Fortunately, I found that the majority of the dye could be dissolved in water by vortexing for several minutes. Unfortunately, this meant that the exact

concentration of dissolved dye was different for each lot of dot. Therefore, the specific concentration that was added to the cells for labeling was determined by trial and error for each new lot of dye.

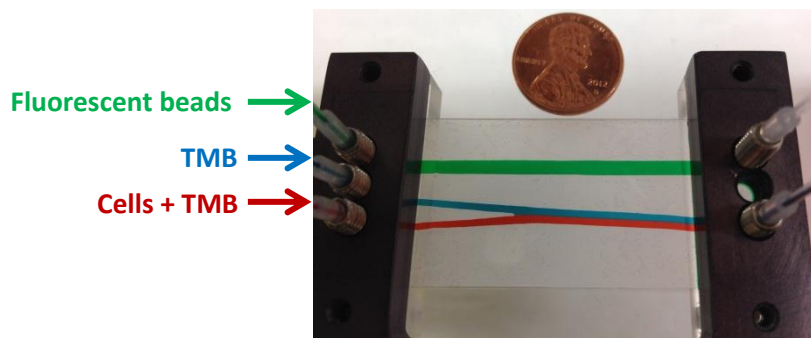


Figure 4.3: Microfluidic chamber. A photograph of the flow chamber. Food dyes were continuously flowed through the chamber while the picture was taken to illustrate the separation between channels, which is caused by laminar flow. The bottom channel (red) contains cells which are trapped and move to the middle channel (blue) which contains the same TMB buffer without any cells. The top channel (green) is used to trap and image fluorescent beads in order to fine tune the focal plane of the fluorescence imaging optics. A penny is included in the picture as a scale bar.

4.2.4 Building the microfluidic flow chamber

Trap experiments were performed in a custom-built microfluidic chamber (**Figure 4.3**). A detailed protocol for making this type of chamber is in *Min et al.* [15]. Briefly, the flow channel pattern was cut out from Nescofilm using a laser engraver and placed between two coverslips, one of which had custom-drilled holes for inlets and outlets. The Nescofilm flow channel pattern was bonded to coverslips by melting on a hot plate for 4 min. The completed flow chamber was inserted into a custom metal frame where inlet and outlet tubing were screwed on for a tight seal.

4.2.5 Injecting bacteria into chamber

Experiments were performed while cells and medium continuously flowed through the microfluidic chamber. Prior to the experiment, I filled the chamber with water. Since trapped cells are damaged by the presence of Oxygen in the surrounding medium (see **Chapter 3**) [2, 91], it was extremely important to ensure that there were no air bubbles in the trap chamber or tubing. In many cases, this required repeatedly filling the chamber with water followed by flushing the chamber out with air, until the chamber was entirely free of air bubbles. Bubbles often accumulated on the edges of the Nescofilm within the chamber. Small bubbles were removed by repeatedly pulsing the pressure on the syringe used to inject water into the chamber, at a rate of about 1 pulse per second.

Next, trapped cells and blank trapping medium (TMB) were loaded into glass syringes. Each

syringe was then attached to the inlet for the appropriate channel in the chamber (**Figure 4.3**). Throughout the experiment, the two connected channels of the flow chamber were continuously injected with appropriate buffers using a syringe pump (*PHD2000, Harvard Apparatus, Holliston, Massachusetts*) at a linear speed of 30 $\mu\text{m/s}$, which is approximately equal to the swimming speed of a healthy cell. The upper channel was injected with TMB, while the bottom channel contained cells in TMB.

4.2.6 Turning on E Fleezers instrument and focus the trap beam

Prior to each experiment, it was necessary to turn on all of the relevant electronic devices involved in the operation of the E Fleezers instrument (for startup protocol see **Appendix B.2**). The LabVIEW code and various system components were described in detail in **Chapter 3** and **Appendix A**. Once the 1064-nm optical traps were formed, it was necessary to fine tune the location of the objective which focused the beam into a tight spot. The position of the first objective was set so that the trap was formed within the middle of the microfluidic chamber, and so that the defocused light emitted from the second, back objective was collimated. It was important to precisely set the location of the first objective to ensure that the trap signal measured by the QPD detector would accurately depict the motion of the trapped cell (details of QPD detection in **Chapter 3**).

4.2.7 Trapping a cell

During the experiments, swimming cells were observed in the brightfield image of the trap chamber. The trap was invisible, but its location was easily determined once the first cell was trapped. The location of the chamber was controlled in three dimensions using three orthogonal stepper motors, controlled by a motion controller [*ESP301, Newport*]. A joystick was used to move the chamber, resulting in the movement of the cells within the chamber relative to the trap. In this way, the chamber was manipulated so that a single cell was captured by one of the two traps. Upon being trapped, the cell aligned with the long axis of its body parallel to the direction of the trapping beam (perpendicular to the imaging plane.) The cell was then immediately moved into the upper channel, which did not contain other cells. It was important to move out of the bottom channel quickly to prevent additional cells from swimming into the trap.

Once in the upper channel, away from other freely swimming cells, the trapped cell was aligned parallel to the imaging plane by maneuvering the second trap to hold the two ends of the cell apart from each other. In some instances, the cell quickly aligned in the two traps, and remained aligned indefinitely. However, in many cases the cell failed to stay aligned between the two traps. Many cells

would dissociate from one trap and align along the axis of the other trap, perpendicular to the imaging plane. If the cell could be successfully be realigned for a sufficient duration, it was used for recording data. However, if the cell failed to remain aligned between the two traps for a long enough period, it was released and a new cell was found.

4.2.8 Recording fluorescence images and QPD data

The E Fleezers instrument produced two sets of data which were used in this experiment: 1. A group of signals indicating the motion of each end of the cell in three-dimensions (referred to as the trap signal or QPD signal) 2. A sequence of fluorescence images showing flagella. For the purposes of this experiment, the QPD signal was used to determine the tumble bias of the trapped cell, and the fluorescence images were used to count the number of flagella.

In the initial experiments, I recorded 300 seconds of QPD data prior to recording the fluorescence images. This was primarily due to the fact that fluorescence excitation often caused flagella to cross-link (a more detailed description of this phenomenon is provide in **Chapter 6**). Cross-linked flagella were unable to rotate and this phenomenon prevented cells from swimming properly. Once the cross-linking problem was solved (**Chapter 6**), I changed the protocol and refrained from recording QPD data prior to fluorescence imaging. Instead, I recorded QPD during and sometimes after the fluorescence imaging, to avoid recording a large amount of data that would later be discarded due to flagella cross-linking. This strategy allowed me to study more cells in a single day and increased throughput. With the latter protocol I was usually able to acquire good data from 5-10 cells per day.

Epi-fluorescence imaging of trapped cells was achieved as described in **Chapter 3** by excitation with a 532-nm laser and collection of backwards emitted photons with the EMCCD camera. Stroboscopic

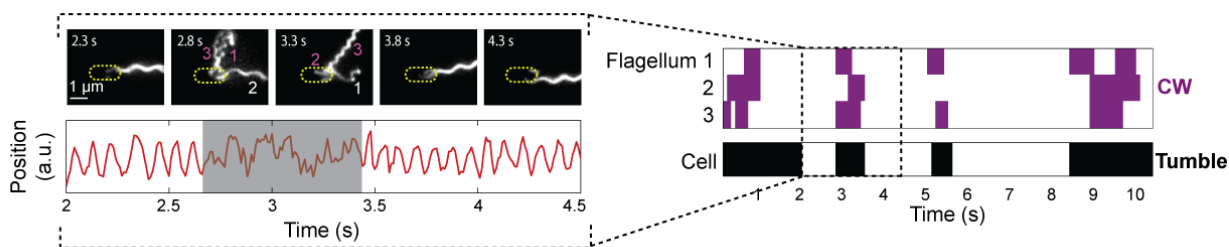


Figure 4.4: Typical data. Representative data from a trapped cell with three flagella. Left, top: Still images of fluorescently labeled flagella at 0.5-s intervals. The approximate location of the unlabeled cell body is indicated by a dashed yellow line. Flagella rotating CW (purple) and CCW (white) are numbered in frames in which they appear distinct. Corresponding cell body rotation signal for the same cell (red line, bottom) as detected from deflections of the trapping laser. Tumbles (shaded area) were determined from the erratic cell-body rotation signal. Right, long-term time trace of CCW/CW flagellar rotation state and run/tumble cell swimming state. CW intervals (purple, top) for each flagellum were determined from the fluorescence images. Tumbles (black, bottom) were determined from the cell-body rotation signal.

illumination was achieved by intermittently deflecting the 532-nm laser beam with an acousto-optic modulator, so as to generate short-duration excitation pulses (18 μ s). The EMCCD recorded 128 x 128-pixel images ($\sim 10 \times 10 \mu$ m) synchronized with each excitation pulse. Additionally, I pulsed the IR trapping laser out of phase with the fluorescence excitation at a rate of 16 kHz, a technique which has been shown to significantly reduce photo-bleaching, with minimal consequence to the trapping [3, 99]. The results were high speed movies showing sharp images of all the flagella for many seconds (typically > 10 s), along with synchronous signal traces from the optical traps (**Figure 4.4**).

4.2.9 Analyzing QPD data to extract tumble bias

For each trapped cell the tumble bias was determined by analyzing the trap QPD signal, which measured the motion of each end of the cell. As established by *Min et al.* [2], the signal from a running cell exhibits regular oscillations with a frequency of about 10 Hz, corresponding to the rotation of the cell body. During tumbles, the oscillations disappear, and the QPD signal appears erratic. For our analysis, we used the Y-differential signal, which is the difference between the QPD-Y signals from the two traps. This signal represents the difference between the vertical positions of the two ends of the trapped cell. The Y-differential is used because it provides a more accurate measurement, which is less sensitive to common sources of noise, such as vibrations in optical components or fluctuations in the trapping laser [2, 98] (**Chapter 3**).

Using a Matlab program to apply a wavelet signal analysis algorithm to the QPD data, we extracted the peak frequency of the trap signal over time (the algorithm is described in detail in *Min et al.* [2]). A frequency threshold was determined for each cell (usually ~ 4 Hz) by looking for the local minimum between the two peaks in the distribution of peak frequencies from an entire trace (**Figure 4.5**). The analysis identified runs whenever the peak frequency exceeded the threshold and tumbles whenever it was below the threshold (**Figure 4.5**). Finally, the tumble bias was calculated by dividing the time spent tumbling by the total duration of the data trace.

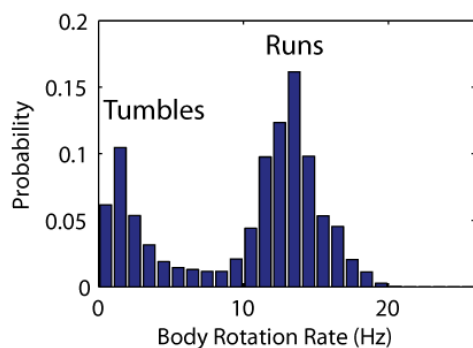


Figure 4.5: Body roll frequency distribution. The peak rotational frequency of the rotating bacterium was identified during each 10 ms time period. This distribution is from a single cell which was trapped and monitored for 20 minutes. Two clear peaks are observed in the distribution, and are used to identify tumbles (~ 2 Hz) and runs (~ 13 Hz).

4.3 Initial results: The veto model fails

As reported in **Chapter 2**, the distribution of number of flagella per cell in wild-type *E. coli* cells is wide. In the trap assay I observed cells with as few as 1 and as many as 8 flagella per cell. To test the veto model I calculated the average tumble bias for cells with a given number of flagella. I then plotted the average tumble bias vs. the number of flagella per cell (**Figure 4.6**). To my surprise, the tumble bias did not monotonically increase as a function of flagella per cell. There was a clear increase from 1 to 2 flagella, but beyond that the tumble bias was surprisingly constant.

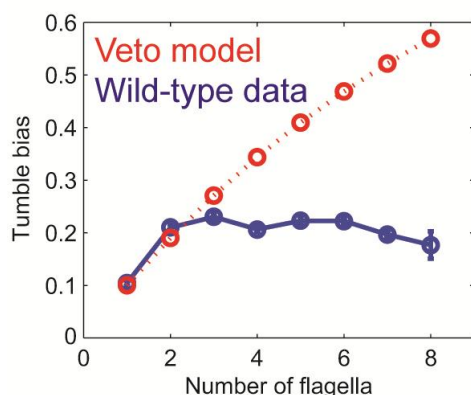


Figure 4.6: Data disagrees with veto model. Tumble bias vs. number of flagella. Tumble bias determined by averaging the tumble bias of all wild-type cells with the same number of flagella (blue), compared to the predictions of the veto model (orange). Tumble bias of individual cells was determined by analyzing the QPD trap signal from 300-second traces of swimming cells.

For a long time I tried to think of an explanation for this result. It seemed unlikely that the basic premise of the veto model was incorrect, since *Turner et al.* had clearly observed that tumbles could be caused by a single flagellum rotating CW [31]. Observations from other studies suggest that there might be additional factors at play. For example, *Turner et al.* had also observed that cells sometimes resumed running before all of the flagella returned to CCW rotation, provided the CW rotating flagella were in the more quiescent *curly-1* state [31]. Other studies showed that the switching rate of the motor is sensitive to the torque and rotational rate of the motor [63, 107]. Could any of these effects explain the discrepancy between our data and the veto model? Eventually we realized that the only way to solve the riddle would be to look more closely at the behavior of the individual flagella.

4.4 Why doesn't data match the veto model?

4.4.1 Analyzing individual flagella

I wanted to determine why the wild-type data disagreed with the veto model. In the previous

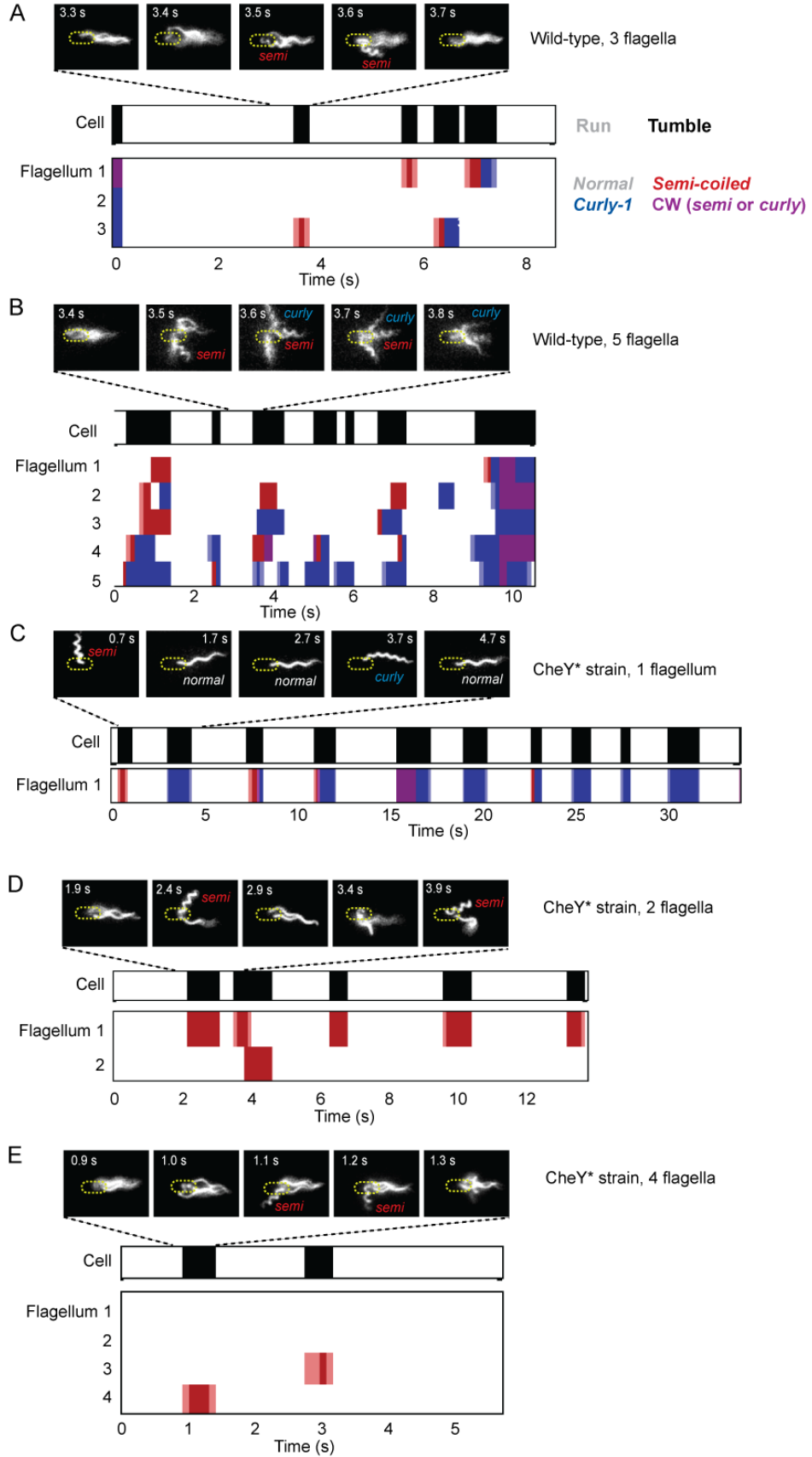
section I only counted flagella. The videos of fluorescently labeled flagella contain much more information about the state of each flagellum over time. Since the trapped cell remained in the field of view for a prolonged period, flagella were observed through multiple runs and tumbles (typically ~5 events), limited by photobleaching, which eventually made flagella become too dim to discern (~8-40 s). As shown by *Darnton et al.* [56], flagella may take on different helical waveforms which are related to the rotation state of the motor. These waveforms, termed “*normal*”, “*semi-coiled*”, “*curly-1*”, and “*curly-2*”, can be visually identified based on their pitch and wavelength (**Figure 4.7**). CCW rotating flagella are always in the “*normal*” waveform, but CW rotating flagella are observed in any of the other waveforms.

To characterize the behavior of the individual flagella, I manually examined each movie in slow motion, and recorded the shape (waveform) of each flagellum over time, during 100-ms time windows (100 ms was chosen because it is approximately the period of a single revolution of the cell body). This was very tedious work. In many cases, one or more flagella would leave the field of view. If the flagellum appeared at some point within the 100-ms time window, I recorded its shape. If not, the state was recorded as ‘unknown’. However, in many cases the flagellum would return to the field of view in the subsequent time window. If the flagellum was still in the same state, the ‘unknown’ shape would be assumed to be that of the surrounding time windows. Keeping track of individual flagella was trivial for cells with only one or two flagella, but more difficult for cells with several flagella. I distinguished different flagella on a cell by their length, location along the cell body, and location relative to other flagella around the cell body. On cells with more than five flagella, it became nearly impossible to reliably track each flagellum, so the analysis was not performed.

Figure 4.7: Sample data from representative cells. Typical data from trapped cells with different numbers of flagella. A few still images (out of hundreds for each sample) of the fluorescently labeled flagella at different time points are shown. In the panels below, colors indicate the swimming state as runs/tumbles (white/black) and flagella waveforms as “*normal*”/“*semi-coiled*”/“*curly-1*”/“*semi-coiled* or *curly-1*” (white/red/blue/purple). Light colors indicate periods when the flagellum was transitioning between two different waveforms. Light blue indicates a transition between *normal* and *semi-coiled*, light red indicates a transition between *normal* and *curly-1*. A and B are wild-type cells, C-E are CheY* cells.

(Figure is on the next page)

Figure 4.7



4.4.2 Extracting CW bias

The sequences of flagellar waveforms contain rich information from which several parameters were extracted. To test the veto model, I calculated a new variable, the CW bias (CB) of each cell, using the flagellar waveform data. Flagella in the *normal* waveform were designated as CCW rotating flagella, because it has been shown that only CCW adopt the *normal* waveform [56]. CW rotating flagella were identified by their *curly-1* or *semi-coiled* shape. From the identification of CCW and CW intervals, the cell's mean CW bias was determined by averaging the fraction of time that all the flagella on the cell spent rotating CW. In other words, the CW bias for the cell was defined as the average CW bias of all of its flagella.

This analysis allowed us to determine all the parameters in **Equation 4.1** directly. For each cell, we measured the tumble bias (using the optical trap), flagellar number N_{flag} , and CW bias (using fluorescence imaging). We used these values to compare our experimental data to the prediction of the veto model. Reorganizing **Equation 4.1**, we define the parameter η :

$$\eta \equiv \frac{\log(1-TB)}{\log(1-CB)} - N_{flag}, \quad (4.2)$$

which quantifies the deviation of the data from the veto model. Comparing **Equations 4.2** and **4.1**, η may also be interpreted as the difference between two terms: the number of flagella on the cell as determined by counting directly, and the number of flagella estimated from the veto model based on the cell's swimming behavior. **Figure 4.8** (black circles) shows η versus N_{flag} . η was calculated for each individual cell and then averaged over all cells with the same number of flagella. Similar to my previous results (**Figure 4.6**), I found that wild-type cells with multiple flagella systematically deviated from the predicted behavior. Specifically, η was consistently negative for cells with $N_{flag} > 1$ (35/48 cells), indicating that cells with multiple flagella tumbled less than expected from the model. In the context of the veto model, the cells behaved as if they had a smaller number of flagella than what they actually had.

4.4.3 The veto model stands

Before developing an entirely new model, I verified the basic premise of the veto model. To investigate the discrepancy between our data and the veto model, I examined individual tumble events in greater detail. In agreement with the original observation of *Turner et al.* [31], I found that CW rotation of a single flagellum was indeed sufficient to cause a tumble in multi-flagellated cells (**Figure 4.7A, D and E**). This result was not surprising, but I had to confirm it before exploring more complicated solutions for this puzzle.

Since the basic assumption of the veto model was supported by the data, I next considered the possibility that a more sophisticated version of the veto model might explain the observed behavior and reconcile this discrepancy. Several alternative models are explored in detail in **Chapter 5**, but none of these models prove capable of explaining my data.

4.4.4 Wild-type tumbles typically involve multiple flagella

Our data confirmed that the premise of the veto model is correct: Cells tumble when a single flagellum rotates CW. So something else must explain the discrepancy between the veto model and our data. Upon further inspection, I observed that more than half of tumbles in multi-flagellated cells (56%, 117/210 events) involved multiple CW flagella. The high fraction of CW flagella during tumbles is in qualitative agreement with previous measurements in which it was observed that a majority of tumbles involved multiple flagella leaving the bundle [31] (see Figure 12 in that paper). **Figure 4.9A** shows a representative trace from a wild-type cell with three flagella. There are times during each tumble in this trace where all three flagella are in a CW state. As shown in **Figure 4.9C**, the number of CW flagella “participating” in a tumble (black circles) was significantly larger than would be expected if flagella were independently switching (gray dashed line, obtained from simulations of a cell with independent flagella; see **Chapter 5**). Our results thus suggest that, while a single CW flagellum is sufficient to induce a tumble (in agreement with a simple veto model), flagella are coupled and may thus switch in groups, in a correlated fashion. Further evidence for inter-flagella coupling was obtained by calculating the cross-correlation between pairs of flagella on a given cell. We found a significant correlation between the rotational directions of pairs of flagella on the same cell (**Figure 4.9D**), black data points). This correlation persisted for ~ 1 s, the average duration of a tumble. Our findings are consistent with previous observations by *Terasawa et al.* on surface-immobilized cells [108]. In that study, correlations between individual motors on the same cell were detected by monitoring beads attached to flagellar

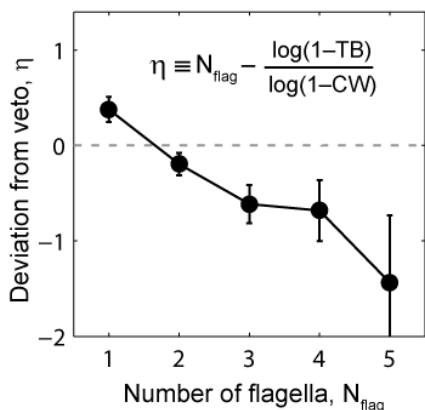


Figure 4.8: Deviation from veto model.

Mean deviation, η , from the veto model vs. number of flagella per cell. Wild-type cells with multiple flagella deviate significantly from the model ($p = 0.0003$, $N = 69$ cells). Error bars denote SEM.

stubs, as opposed to complete flagella on swimming cells in my work. This discovery provided an important clue to explaining the discrepancy between my data and the veto model.

4.5 Control experiment with a CheY* mutant strain

From the results in the previous section, we hypothesized that correlations between the rotational states of flagella on a single cell might help explain the deviation of our data from the predictions of the veto model. However, the source of inter-flagellar correlation remained under debate. *Terasawa et al.* observed that mutant cells, in which the concentration of CheY-P was decoupled from the chemotaxis network, displayed no flagellar correlations [108]. This led us to likewise investigate the behavior of a strain, PM87, expressing a constitutively-active CheY [CheY^{D13K} [36], denoted CheY*, see **Appendix C.1**]. The protein was exogenously expressed from a DNA plasmid. I used an expression level that resulted in a tumble bias which matched that of the wild-type cells (**Figure 4.2**). A representative trace from a CheY* cell with three flagella is shown in **Figure 4.9B**. Upon inspection, flagellar switching appears far less correlated than in wild-type cells (**Figure 4.9D**, compare black and gray data points). Comparing 54 wild-type and 24 CheY* cells with the same mean CW biases (0.11 ± 0.07 vs. 0.11 ± 0.07 , mean \pm SD) I found that, on average, fewer CW rotating flagella participated in tumbles in the CheY* strain (**Figure 4.9C**), open circles). Moreover, the number of participating flagella in the CheY* strain closely matched the expectation for cells with independently switching flagella (**Figure 4.9C**, dashed line). (This number deviates from unity and trends upwards with number of flagella simply because of the finite probability that two tumbles overlap by chance.) Our results indicate that when the signal for flagellar motors to switch their rotational state is decoupled from the chemotaxis network, the motors switch independently. Based on our interpretation of the wild-type data, we thus expect CheY* cells to adhere to the simple veto model. As shown in the plot of η in **Figure 4.10** (open circles), CheY* cells indeed match the veto model closely ($\eta = -0.08 \pm 0.15$, mean \pm SEM). The only difference between these strains is the CheY-P protein whose concentration can only fluctuate in the wild-type cells. The existence CheY-P fluctuations which lead to correlations between flagellar states in cells may thus explain why wild-type cells with multiple flagella deviate from the veto model.

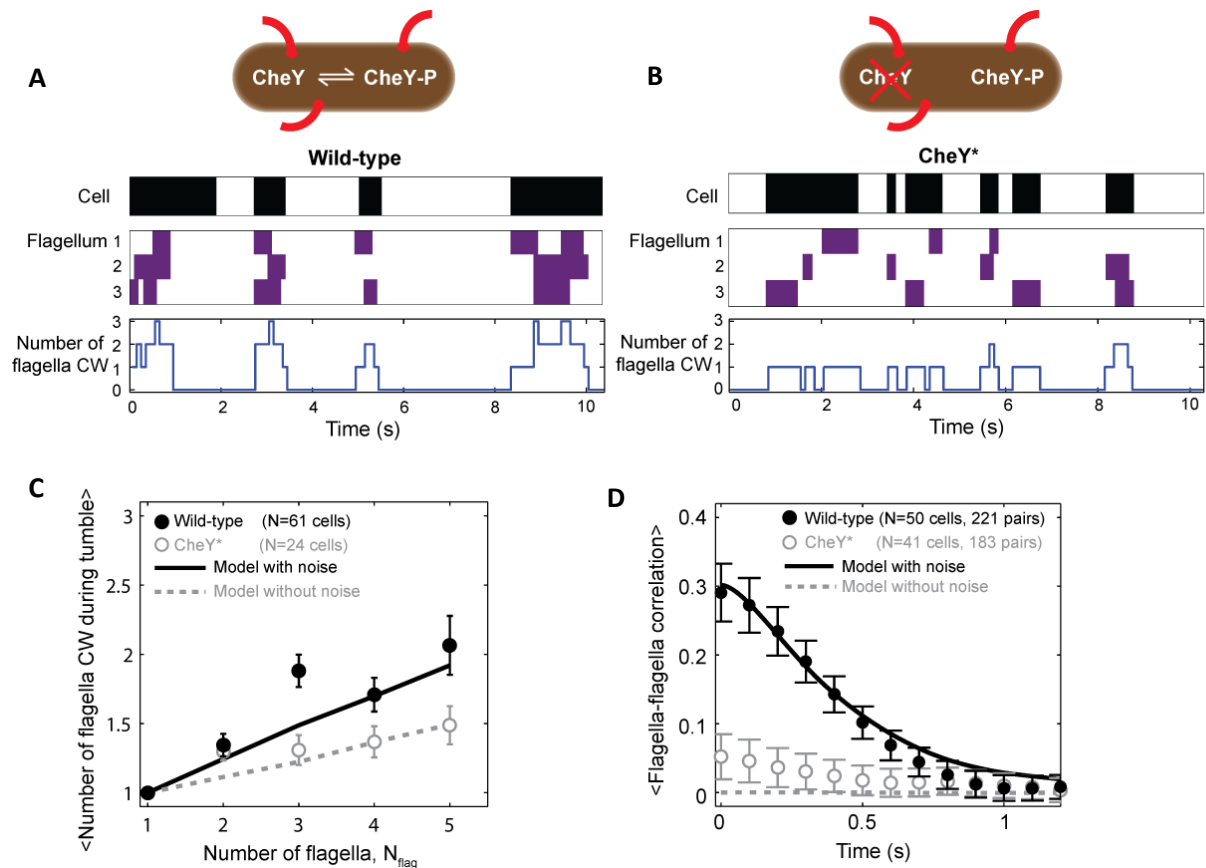


Figure 4.9: Tumbles in wild-type cells involve multiple CW flagella. (A) A typical time trace from a wild-type cell with 3 flagella. Colors indicate runs/tumbles (white/black, top) and CCW/CW (white/purple, middle). The blue line (bottom) shows the corresponding number of CW flagella at each time point. **(B)** Same as (A) for a typical CheY* cell with 3 flagella. **(C)** Mean of the maximum number of CW flagella during a tumble vs. number of flagella per cell. Consistently more flagella are CW during tumbles in the wild-type (black circles; $N = 61$ cells) compared to the CheY* strain (open gray circles; $N = 24$ cells). Simulations incorporating fluctuations in CheY-P (black line) and without fluctuations (gray dashed lines) reproduce the observed trends (simulation details in **Chapter 5**). **(D)** Cross-correlation between flagella pairs, averaged over all pairs and all cells. Wild-type (black circles) match simulations with fluctuations in CheY-P (black line). CheY* strain (open gray circles) matches simulations without fluctuations in CheY-P (gray dashed line), which exhibit almost no correlation. Error bars denote SEM. For simulation details, see **Chapter 5**.

4.6 Wild-type behavior matches a veto model with a lower effective number of flagella

Our results so far suggest that, while wild-type cells obey the fundamental premise of the veto model—i.e., a single CW flagellum is sufficient to induce a tumble—the presence of inter-flagellar correlations leads to the failure of **Equation 4.1** in relating the observed CW bias and tumble bias. To describe the relation between single flagellar state and whole-cell behavior successfully, this expression must then be modified to account for flagellar correlations. To this end, we examined the relation

between CW bias and tumble bias in all individual cells having a given flagellar number (**Figure 4.11A-B**).

Equation 4.1 defines a single curve, along which the CW bias and tumble bias of all cells with N_{flag}

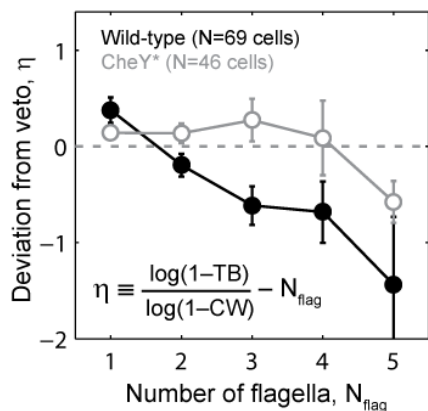


Figure 4.10: CheY* mutant cells match veto model

Mean deviation, η , from the veto model vs. number of flagella per cell. Wild-type cells (solid black circles) with multiple flagella deviate significantly from the model ($p = 0.0003$, $N = 69$ cells). CheY* cells (open gray circles) match the model ($p = 0.77$, $N = 46$ cells). Error bars denote SEM.

flagella should lie (dashed line in **Figures 4.11A-B**). As expected, the CheY* cells follow these predicted curves closely for all N_{flag} values (**Figure 4.11B**) ($R^2 = 0.89$). In contrast, wild-type cells with multiple flagella consistently fall below the predicted curves (**Figure 4.11A**) (35/48 cells).

Based on our observation that wild-type cells exhibited η values consistent with cells with a lower number of flagella than the actual value, we hypothesized that wild-type behavior may be described within the framework of the veto model by allowing the parameter N_{flag} in **Equation 4.1** to deviate from the actual flagellar number. As shown in **Figure 4.11A** (solid lines), using the flagellar number as a fitting parameter (now denoted N_{eff}) indeed allows for a good match for the wild-type data ($R^2 = 0.85$). In this revised equation, N_{eff} can be thought of as the “effective” number of independent flagella on a cell, which captures the fact that flagella in wild-type cells switch in a correlated manner. Consistent with this picture, the effective number of flagella N_{eff} is consistently smaller than the actual flagellar number N_{flag} (**Figure 4.11C**), black circles). As a control, estimating N_{eff} for CheY* cells produces values very close to the original flagellar number N_{flag} (**Figure 4.11B**), solid line and **Figure 4.11C** (open circles). The introduction of the parameter N_{eff} allows us to formulate a generalized veto model, which describes the mapping between the CW bias and tumble bias for both wild-type and CheY* cells. The generalized model now defines a universal curve,

$$1 - TB = (1 - CB)^{N_{eff}} \quad (4.3)$$

along which all individual cells of both genotypes should lie (using $N_{eff} = N_{flag}$ for CheY* strain and the best fit value of N_{eff} for wild-type). As seen in **Figure 4.11D**, this expression successfully collapses all single-cell data from both strains and all flagellar numbers.

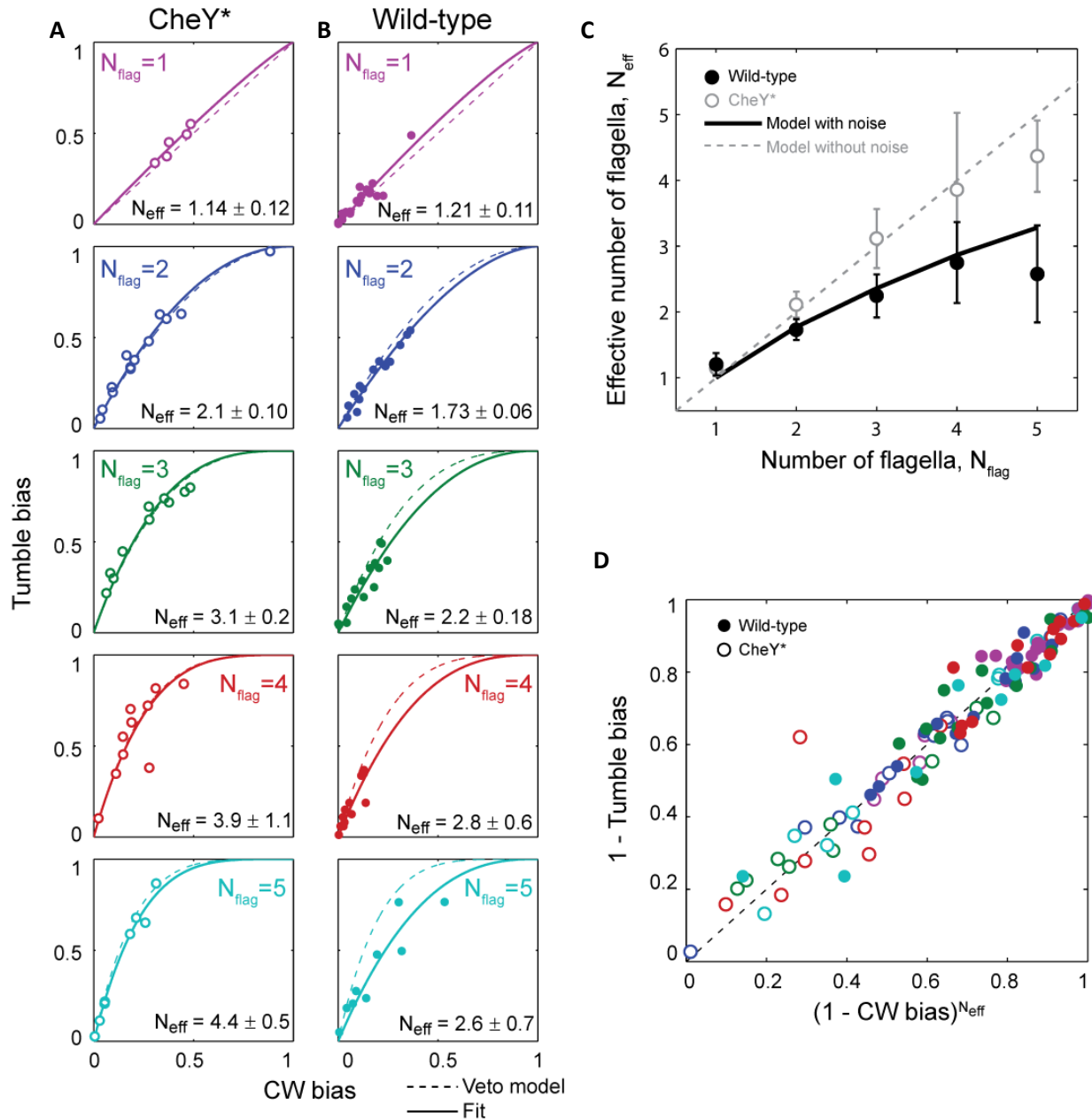


Figure 4.11: Wild-type behavior matches the veto model for cells with a lower effective number of flagella. (A) Tumble bias vs. CW bias for individual CheY* cells ($N = 46$), plotted separately for different numbers of flagella per cell ($N_{\text{flag}} = 1$, purple; 2, blue; 3, green; 4, red; 5, cyan). The prediction from the veto model in Equation 4.1 (dashed lines) matches the data well ($R^2 = 0.91, 0.97, 0.93, 0.67, 0.98$ for $N_{\text{flag}} = 1, 2, 3, 4, 5$). Additionally, the data were fit (solid lines) to Equation 4.1, while allowing the number of flagella to be used as a fitting parameter, N_{eff} . Error bars denote SD. (B) Same as (A) for wild-type cells (same color code as (A); $N = 69$ cells). The veto model prediction (dashed lines) does not match the data for cells with multiple flagella ($R^2 = 0.88, 0.60, 0.41, 0.39$ for $N_{\text{flag}} = 2, 3, 4, 5$). (C) Fitted N_{eff} values vs. number of flagella per cell for wild-type (black circles) and CheY* (open gray circles) cells. Simulations (described in the text) reproduce the observed trends. (D) Data points from individual wild-type (solid circles) and CheY* (open circles) cells all collapse onto a single line when using N_{eff} from fits to wild-type data in (A) and the actual flagellar number N_{flag} for CheY* cells in (B). Error bars denote SEM.

4.7 Discussion

The observation that multi-flagellated wild-type cells tumble significantly less than expected implies that the cell's swimming behavior (and presumably its chemotactic response) is robust against variations in the number of flagella (**Figure 4.6**). We hypothesize that this phenomenon may confer evolutionary advantages, in light of the large fluctuations in flagellar numbers within a cell population (**Chapter 2**). If cells with many flagella did not behave like cells with fewer flagella, then they would spend the majority of their time tumbling, a behavior that would inhibit chemotaxis. *E. coli* thus appears to have developed a mechanism to achieve similar tumble biases with a wide range of flagellar number.

4.8 Future Directions

Bacterial swimming is studied largely to understand how chemotaxis occurs. A recent study showed that chemotactic efficiency in *E. coli* could be doubled by incorporating the fact that cells re-orient to a larger degree during tumbles that involve a high fraction of CW rotating flagella [109]. It would be possible to count the number of flagella rotating CW as a function of time after a chemotaxis stimulus, using the trap assay. In this chapter, I measured the number of CW flagella during tumbles (**Figure 4.9**). In previous experiments, we measured the chemotactic adaptation response of trapped cells to sudden increases and sudden decreases in the concentration of aspartate [15]. Combining these approaches would allow us to determine how the number of CW flagella is affected by chemotactic stimuli. For example, we would expect that all of the flagella would rotate CW for a period of time following a large negative stimulus. On the other end, we would expect that all of the flagella would rotate CCW for a long time on cells adapting to a large positive stimulus. As a cell adapts to the new environment the first few tumbles would only involve a single CW rotating flagellum, since the CW bias is still very low.

We have performed some preliminary experiments to demonstrate the feasibility of this measurement. We exposed cells to a large step-down stimulus. Contrary to our expectations, we observed some CCW rotating flagella within a few seconds of the negative stimulus. Further studies could reveal how significant the fraction of CW rotating flagella is for overall chemotaxis efficiency.

4.9 Summary

The goal of this chapter was to quantify the effect that the number of flagella on a swimming cell has on its behavior. Using the E Fleezers instrument described in **Chapter 3**, we discovered that the tumble bias of swimming cells does not dramatically increase with the number of flagella. This was in

disagreement with the simple veto model (**Figures 4.6** and **4.8**), which relates the collective activity of individual flagella to the run-tumble state of the swimming cell. It turns out that the problem with the veto model was an implicit assumption that the rotational state of each flagellum is completely independent. Once this assumption was removed, we were able to construct a phenomenological model (**Equation 4.3**) which accurately reproduced the trends in our data (**Figure 4.11**). Using this model, all of the data from both strains collapsed onto a single curve (**Figure 4.11D**). The next chapter will examine more detailed models and simulations, including models which specifically include fluctuations in the concentration of CheY-P, to explore the physical mechanisms underlying the observations in this chapter.

Chapter 5. Modeling runs and tumbles

The overarching goal of all research into bacterial chemotaxis is to develop a complete end-to-end understanding of the entire process. Several models have been developed towards this purpose [17, 40, 43, 103-105]. An unresolved step in this process is the manner in which the states of individual flagella determine the run/tumble swimming state of the entire cell. In the previous chapter I showed that wild-type *E. coli* cells satisfied the basic assumption of the veto model: A single flagellum rotating CW is sufficient to cause a tumble. However, the tumble bias of wild-type cells did not match the predictions of the veto model. Instead, cells with a wide range of flagella per cell had very similar tumble biases. Using a mutant strain which decoupled CheY-P concentration from the chemotaxis network provided data that was in agreement with the veto model. This supported the idea that fluctuations in the concentration of CheY-P in wild-type cells causes tumble bias to be independent of flagellar number.

In this chapter I explore several models which map the collective state of multiple flagella to whole-cell run/tumble behavior. I show that a modified veto model does the best job of explaining all of the available data. I then use a model which incorporates fluctuations in the concentration of CheY-P to reproduce all of the experimental trends from wild-type data in the previous chapter. Comparisons between models with and without fluctuations in CheY-P provide strong evidence that those fluctuations are responsible for the difference in behavior between the two strains used in the previous chapter. All together, these models support the conclusion that fluctuations in the concentration of CheY-P in wild-type cells makes their swimming behavior robust against variations in flagellar number. Finally, the model is used to estimate the time-scale and amplitude of CheY-P fluctuations in wild-type cells required to reproduce our experimental data.

5.1 Mapping flagella states → run/tumble states

5.1.1 Introduction to run-tumble modeling

The mapping from single-flagellum state to whole-cell swimming behavior has been a missing link to developing an end-to-end picture of bacterial chemotaxis. In the 1970's it was shown that CCW rotation of flagella was related to running behavior in swimming cells, and CW rotation was related to tumbles [95]. However, cells were known to possess multiple flagella, and it was not clear how the different flagella collectively gave rise to coordinated running and tumbling. Many chemotaxis models simply ignore the issue and treat cells as if they have only 1 flagellum [18, 93, 103-105]. Over time, various models were proposed to explain whether a cell would run or tumble, given a specific set of flagella states. The first and simplest model suggested was a unanimous model, in which it was imagined

that all flagella might switch direction simultaneously [88]. But no evidence supported that model. The first model with experimental support was the voting model, in which the rotational direction of the majority of the flagella on a cell determine whether it runs or tumbles [102]. As experimental techniques have advanced, models have improved to reflect new findings.

Table 5.1 – Schematic of common models

Flagella			Models			
1	2	3	<i>Coordinated unanimous</i>	<i>Unanimous</i>	<i>Voting</i>	<i>Veto</i>
CCW	CCW	CCW	Run	Run	Run	Run
CCW	CCW	CW	DNE	Run	Run	Tumble
CCW	CW	CW	DNE	Run	Tumble	Tumble
CW	CW	CW	Tumble	Tumble	Tumble	Tumble

Note: DNE ≡ Does not exist

Schematic of common models which map flagella states to run-tumble state of the swimming cell, for four different scenarios. Each of the four rows represents a different situation. Left, the state of each of the three flagella on the cell. Right, the run-tumble state of the cell, as determined by different models. For example, when all three flagella rotate CCW, the cell is predicted to run by all of the models.

Each model makes unique predictions which can be compared to experimental data. The basic predictions of the three most common models are shown in **Table 5.1**. The run/tumble state of the cell depends on the rotational state of each flagellum on the cell. Each model has a different set of rules to determine whether a cell runs or tumbles, given a set of flagella states. This leads to distinctly different expectations for the duration and frequency of tumbles as a function of the number of flagella per cell. As shown in **Chapter 4**, tumble bias is a useful quantitative metric for assessing the validity of a model. To compare each model with the experimental data, numerical simulations were performed modeling the state of each flagellum and applying the rules of a given model to determine the run-tumble state of the simulated cell (**Table 5.1**). The tumble bias from simulated cells was compared to the tumble bias measured from trapped cells with the same number of flagella in **Chapter 4**. For the unanimous and veto model, it was easy to derive an analytical expression which relates the tumble bias to the CW bias and number of flagella per cell. For both models, the analytical predictions for tumble bias as a function of flagellar number matched the results from numerical simulations, as expected. Additionally, direct observations of flagella during runs and tumbles allowed assessment of the underlying assumptions of each model. The specific assumptions and predictions of each model are compared to experimental data in the sections below.

5.1.2 The unanimous model

There are two distinct versions of the unanimous model. The first version, which was disproven in the early 1980s, suggested that all flagella on a cell rotated in the same direction at the same time. This is the “coordinated unanimous model” in **Table 5.1**. In this model, either all flagella are rotating CCW and the cell runs, or all flagella rotate CW and the cell tumbles. *Ishihara et al.* disproved this model by observing asynchronous rotation of beads attached to different flagellar motors on a single cell [102]. In that experiment, they found that different motors on a single cell could rotate in opposite directions, and that the rotational directions did not appear correlated (recent studies have refuted the latter finding [108], but the observation of asynchronous switching has been confirmed by all subsequent studies).

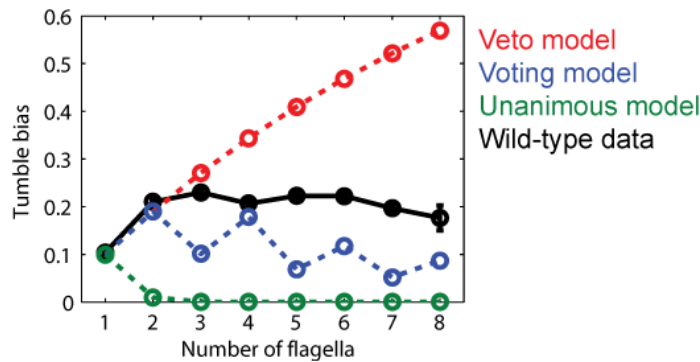


Figure 5.1: Model predictions. Tumble bias vs. N_{flag} . Predictions from the unanimous model (green), voting model (blue) and veto model (red) are compared to the experimental results from **Chapter 4**. All models were evaluated with a CW bias of 0.1. Changing the CW bias produced different curves, but the trends for each model were unaffected. None of these models were able to reproduce the experimental results at any CW bias.

The second version of the unanimous model posits that the cell only tumbles when all flagella rotate CW. The basic idea is that a single CCW rotating flagellum might be able to propel the cell forward in a run, regardless of the activity of the other flagella. This model is expressed analytically by **Equation 5.1** (derivation in **Appendix D.2**). The average CW bias (CB) for a flagellar motor in an unstimulated wild-type cell is known to be around 0.1 (flagellar motors spend $\sim 10\%$ of the time rotating CW) [36]. Given $CB = 0.1$, the unanimous model predicts that cells with several flagella would almost never tumble (**Figure 5.1**). This is in clear disagreement with our experimental data from **Chapter 4** (**Figure 5.1**). Furthermore, the premise of the model contradicts direct observations of tumbles by *Turner et al.*, *Darnton et al.*, and myself [31, 56]. Cells with 3 or more flagella were never observed to run when only one flagellum was rotating CCW. Instead, runs occurred only when the majority of flagella were rotating CCW. The

unanimous model is clearly wrong.

$$TB = CB^{N_{flag}} \quad (5.1)$$

5.1.3 The voting model

The voting model was first proposed by *Ishihara et al.* [102] and has since been used in a wide range of chemotaxis models [42, 44, 104, 110]. In the voting model, a cell runs when the majority of flagella rotate CCW and tumbles when a majority rotate CW. (In my implementation of the voting model, if half of the flagella rotate CCW and the other half rotate CW, then the cell tumbles. But different iterations of the voting model have dealt with this differently.) The voting model provides the closest match to the experimental data in **Figure 5.1**. Early support for the voting model was based on the observation that flagella switch asynchronously [102]. However, the same study found that the voting model was incapable of explaining discrepancies between the predicted distributions of tumble and CW durations. Specifically they found that flagella would have to rotate CW frequently and, “the observed tumble times are too short to be accommodated by the voting hypothesis, given the measured values for mean rotational times” [102]. Furthermore, observations of fluorescently labeled flagella on freely swimming cells [31, 56], and our own results from **Chapter 4**, refute the basic assumption of the voting model that a majority of flagella must rotate CW to cause a tumble. In experiments observing cells with several flagella, CW rotation of a single flagellum was sufficient to produce a tumble. This directly invalidates the voting model, which requires that multiple flagella must rotate CW to occur in cells with 3 or more flagella.

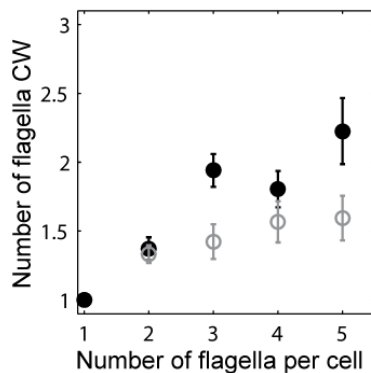


Figure 5.2: Number flagella CW during tumbles. The average number of flagella which rotated CW during tumbles vs. the number of flagella per cell. Both strains, wild-type (black) and CheY* (grey), had tumbles that involved less than half of the flagella rotating CW. This result invalidates both the unanimous and voting models.

5.1.4 The veto model

The basic assumption of the veto model is that a cell tumbles whenever any flagellum is rotating CW. This can be expressed analytically using **Equation 5.2** (derivation in **Appendix D.1**). As shown in **Figure 5.1** the veto model predicts that cells with more flagella will spend more time tumbling. This occurs because each additional flagellum increases the probability that at any given time, at least one flagellum will be rotating CW.

$$TB = 1 - (1 - CB)^{N_{flag}} \quad (5.2)$$

Unlike the unanimous and voting models, the original assumption of the veto model is supported by observations of flagella during tumbles. However, as shown in **Chapter 4** and **Figure 5.1**, wild-type cells do not reproduce the prediction of the veto model for tumble bias as a function of N_{flag} . Rather than increasing, the tumble bias was roughly constant regardless of the number of flagella per cell (**Figure 5.1**). This discrepancy indicated that something else is affecting the tumble bias, so next I explored models that are effectively extensions of the veto model.

5.1.5 The 3-state modified veto model

The previous models treated flagella as having 2-states: CW or CCW rotation. However, CW rotating flagella can adopt multiple, distinct waveforms, which can have different effects on swimming behavior. In my experiments flagella were observed in three different states: *normal* (CCW), *semi-coiled* (CW) and *curly-1* (CW) (see images in **Chapter 4** and **Figure 6.1**). Previous observations of flagella during tumbles indicated that the specific waveform of the CW rotating flagella affects whether or not a cell tumbles [56]. In some cases, it was observed that a cell began running while some of the flagella were in the *curly-1* waveform, provided the other flagella were all rotating CCW[56]. Physically this appears feasible because the *curly-1* waveform is much more flexible than the *semi-coiled* waveform, and by eye does not appear to exert as much force on the cell body.

Following these observations a 3-state model was developed in which cells could run when some of the flagella were rotating CW, provided those flagella were in the *curly-1* waveform [111]. Specifically, the Sneddon model states that a cell with a minimum of X CCW flagella will run rather than tumble, provided the remaining $(N_{flag} - X)$ CW flagella are in the *curly-1* conformation only (X is a parameter in the model, with possible values in the range $[1, N_{flag} - 1]$). Thus, the veto model in previous section corresponds to $X = N_{flag}$, and the least perturbative refinement to the veto model corresponds to $X = N_{flag} - 1$, in which a cell with a single *curly-1* flagellum still runs. However, the frequency at which this phenomenon occurred was unknown because statistics of flagella states during

tumbles were not provided.

To test the effect of runs involving *curly-1* flagella, I augmented the simulations following the approach of *Sneddon et al.* [111]. For each simulated flagellum, the binary CCW/CW trace was converted into a 3-state (*normal*, *semi-coiled*, *curly-1*) trace, using $\lambda^{-1} = 0.68 \text{ s}^{-1}$ as the transition rate from *semi-coiled* to *curly-1* (see **Table 5.2** for parameter values). Transition rates are determined experimentally in **Chapter 6**. There were two other parameters in the 3-state Sneddon model which had not previously been constrained; X (the number of flagella that must be *normal* for a run to occur) and the probability of a run occurring when $N_{\text{flag}} - X$ flagella were in the *curly-1* waveform. Fortunately, my experimental observations provide both of these numbers. I found that cells almost never ran with more than one flagellum in the *curly-1* state. In cells with a single CW flagellum in the *curly-1* state ($X = N_{\text{flag}} - 1$) runs only occurred 18% of the time (observed from 44 seconds of cumulative time in which one flagellum was in the *curly-1* state; **Figure 5.3**). Using these values I ran numerical simulations of cells with various numbers of flagella and extracted the tumble bias. As shown in **Figure 5.3**, this effect was not sufficient to reproduce the trend observed in our experimental data.

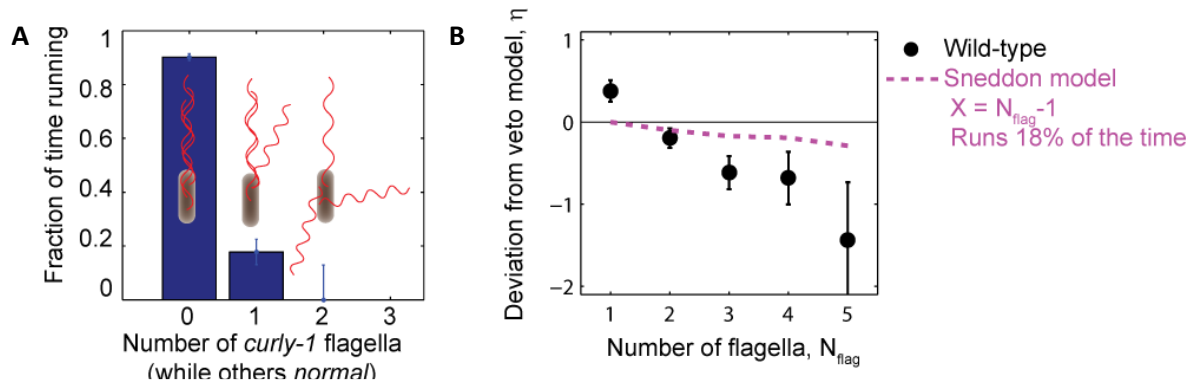


Figure 5.3: Sneddon 3-state model. Cells with flagella in the *curly-1* state rarely run. **(A)** Experimental data showing the fraction of time that cells spent running vs. the number of flagella that were in the *curly-1* waveform (while all other flagella were in the *normal* waveform). When all flagella were in the *normal* waveform, cells ran 91% of the time. When the waveform of a single flagellum was *curly-1*, and the rest were *normal*, cells ran 18% of the time. **(B)** Mean deviation from veto model, η , vs. number of flagella per cell (black circles, experimental data). The theoretical model with the probability of running = 0.18 when the waveform of a single flagellum is *curly-1* (magenta, model), fails to reproduce the experimental data. Error bars denote SEM.

5.1.6 The distortion factor model

Vladimirov *et al.* developed a detailed model for mapping flagella states to run-tumble states [109], based on previous observations of flagella during tumbles [31, 56]. The primary motivation for this model is the observation that the degree of angular change in direction during a tumble is dependent on the number of flagella that rotate CW during the tumble [31]. When a larger number of flagella rotate CW and break from the bundle, the average change in cell swimming direction is larger. Surprisingly, they show that when this effect is incorporated into a theoretical model of bacterial chemotaxis, the chemotactic drift is nearly doubled (compared to a baseline model that does not include this effect) [109]. While this feature is not relevant to the present investigation, the model they created has a unique construction for mapping individual flagella to the run/tumble state.

They developed a model in which runs and tumbles are determined by the duration that flagella have been rotating CW, rather than the number of flagella that are CW. This model is built around a distortion factor d_{cw} ,

$$d_{cw} = t_{cw}, \quad (5.3)$$

which is equal to the time that a motor has been rotating CW (**Equation 5.3**). In the model, the cell tumbles when total distortion factor D_{cw} (defined as the sum of distortion factors d_{cw} from all flagella on the cell) exceeds a threshold value. This idea stems from the fact that when a flagellar motor switches direction, it takes some time for the flexible flagellar hook that attaches the flagellum to the motor to untwist and retwist in the opposite direction. After the hook has twisted, the new waveform (usually *semi-coiled* in a transition from CCW to CW rotation) propagates along the length of the flagellum, in a process that can take up to hundreds of milliseconds. Finally, the model specifies that a CW rotating flagellum only generates a tumble for 0.2 seconds. After that the cell resumes running, unless another

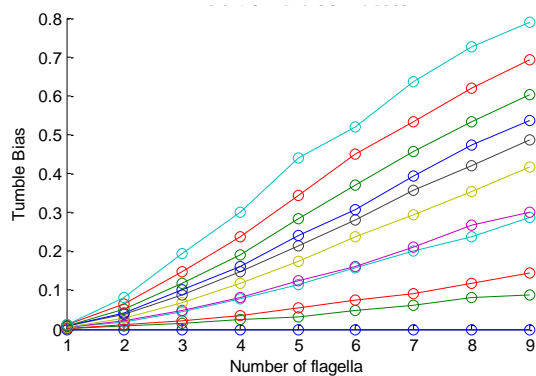


Figure 5.4: Distortion factor model. Tumble bias vs. N_{flag} , as modeled by the Vladimirov model using a distortion factor to determine when the cell tumbles. Different lines represent the same model evaluated with different CW biases. The model was unable to reproduce the experimental results.

flagella has switched to CW rotation. One result of this model is that cells do not immediately tumble when a flagellum switches to CW rotation, and very short CW intervals do not generate tumbles. On the other hand, the model is still effectively quite similar to the veto model, in that a single CW-rotating flagellum is sufficient to cause a tumble, and having more flagella increases the probability of tumbling (**Figure 5.4**). As seen in the figure, this model also fails to reproduce the trend observed in wild-type cells.

5.2 Mapping from CheY-P → motor states

5.2.1 Why is the mapping from CheY-P → motor states relevant?

Despite many attempts, using increasingly sophisticated models of the mapping from individual flagella to whole-cell run-tumble behavior, none of the models in the previous section were in complete agreement with the experimental data. My results in **Chapter 4** show that *E. coli* cells adhere to a phenomenological, modified veto model, and that inter-flagellar correlations lead to a renormalization of the effective number of flagella. In a previous study, *Terasawa et al.* proposed that fluctuations in CheY-P levels may provide a mechanism by which the CW biases of multiple flagella on a cell can be coupled to each other [108]. To test whether such a mechanism could account for the different features of bacterial swimming observed in **Chapter 4**, I performed simulations of whole-cell swimming driven by the chemotaxis network. In the sections below, I explored models in which the concentration of CheY-P controls flagella activity, in order to reproduce the behavior of both wild-type cells and the mutant strain. In order to evaluate this hypothesis I first compared simulations with a fixed CheY-P concentration to results from a mutant strain with constant CheY-P [2, 46]. I then performed simulations which included fluctuations in the concentration of CheY-P over time, and found that they were able to reproduce all of the observed trends in wild-type cells.

5.2.2 CW bias is a function of CheY-P concentration

As discussed in **Chapter 1**, chemotaxis is the self-directed motion towards more favorable chemical environments. At the heart of *E. coli* chemotaxis is the signaling molecule CheY. Phosphorylation of CheY is the signal used to convey information about the changing external environment to the flagellar motors. When the environment is becoming less favorable, the concentration of CheY-P increases, which raises the probability of CW motor rotation, and consequently raises the probability of tumbling. In the opposite scenario, when the environment is improving, the concentration of CheY-P decreases, motors are more likely to rotate CCW, and the cell runs for a longer

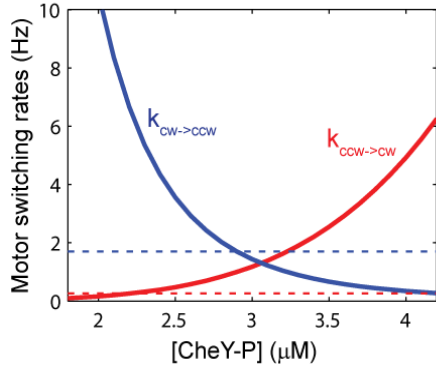


Figure 5.5: Motor switching rates. The switching rate of flagellar motors as a function of CheY-P concentration. At high concentrations, the CW bias is elevated because the switching rate from CCW→CW (red) is increased and the opposite rate from CW→CCW (blue) is lowered. Solid lines show the rates used in the model (Equation 5.5). Dashed lines show the rates observed in experiments (see Chapter 6 and Table 5.2).

period of time. The CW bias of a flagellar motor is governed by the local concentration of CheY-P following the experimentally established Hill function in Equation 5.4 [39].

$$CB = \frac{1}{1 + \left(\frac{3.1}{CheY-P}\right)^{10.3}} \quad (5.4)$$

5.2.3 Numerical simulations of flagellar switching reproduce CheY* strain behavior

I performed stochastic simulations of flagellar motor activity and then applied the two-state veto rule. The results of an example simulation are presented in Figure 5.6A (see Table 5.2 for parameter values). The temporal resolution of all simulations was one data point per millisecond ($dt = 0.001$ s). Simulations were performed with a given concentration of CheY-P. CW bias was calculated from CheY-P using Equation 5.4 [39]. From that, rotational state of each flagellar motor was determined stochastically, using Equation 5.5 (equation from *Sneddon et al.* [111]). This was done by generating a random number for each flagellum at each time point and comparing it to a threshold value (given by multiplying $dt * k_{\pm}$ from Equation 5.5) to determine whether the motor continued rotating in the same direction or switched directions (Figure 5.5).

$$k_{\pm} = \omega \times e^{\left\{ \pm \left[\frac{g_0 - g_1}{4} \left(\frac{Y_p(t)}{V_p(t) + K_D} \right) \right] \right\}} \quad (5.5)$$

Runs and tumbles were determined using the veto model: whenever any flagellum was rotating CW the cell tumbled, when all flagella were rotating CCW the cell ran. Finally, the simulated data was analyzed in the exact same manner as the experimental data from Chapter 4, to extract the mean number of flagella participating in tumbles (Figure 5.7 A), flagella cross-correlation (Figure 5.7 C) the effective number of flagella (N_{eff} , Figure 5.7 B) and the deviation from veto model η , Figure 5.7 D). The dashed line in each panel shows the results of these simulations. Note that these simulations successfully reproduce the behavior of the CheY* mutant cells.

Table 5.2 – Values of parameters used in simulations

Parameter	Description	Value	Source
$k_{CCW \rightarrow CW}$	Motor switching rate from CCW→CW	0.26 s^{-1}	Our data
$k_{CW \rightarrow CCW}$	Motor switching rate from CW→CCW	1.7 s^{-1}	Our data
CB	Average clock-wise bias of wild-type motors	0.13	Our data
$\langle Y \rangle$	Mean concentration of CheY-P	$2.59 \text{ } \mu\text{M}$	Fit to data
ω	Characteristic motor switching time	0.5 s	Our data
λ^{-1}	Transition rate from <i>semi-coiled</i> to <i>curly-1</i> state	0.68 s^{-1}	Our data
x	From the model in <i>Sneddon et al.</i> ; number of flagella that must be <i>normal</i> for a run to occur (while other flagella are <i>curly-1</i>) [111]	N_{flag} (variable in Figure 5.3)	Our data
σ^2	Variance in [CheY-P]	$1.0 \text{ } \mu\text{M}^2$	Fit to data
τ	Characteristic time-scale of fluctuations in [CheY-P]	0.2 s	Fit to data
K_d	Midpoint of CW bias vs. CheY-P response curve	$3.1 \text{ } \mu\text{M}$	[39]
H	Hill coefficient for CW bias vs. CheY-P response curve	10.3	[39]
dt	Simulation time steps	0.001 s	-
$g0 = g1$	Free energy factor in motor switching equation.	$40 \text{ k}_B\text{T}$	[111]

Note: $\omega \equiv \frac{CB}{k_{CCW \rightarrow CW}}$

5.2.4 Modeling fluctuations in CheY-P reproduces wild-type behavior

In wild-type cells, CheY-P levels are subject to phosphorylation and de-phosphorylation reactions by chemotaxis network components and are believed to fluctuate in time [46, 111]. Stochastic simulations were performed to model the effects of fluctuations in CheY-P concentration over time, using a method similar to *Sneddon et al.* [111]. An example of one of these simulations is illustrated in **Figure 5.6B**. CheY-P fluctuations were generated using **Equation 5.6** below (see **Table 5.2** for parameter values), where Y is the instantaneous concentration of CheY-P, τ is the characteristic timescale of fluctuations in [CheY-P], σ^2 is the variance in [CheY-P], and ξ are normally distributed random numbers with unit variance (**Table 5.2**).

$$Y(t+dt) = Y(t) - \frac{(Y(t) - \langle Y \rangle)}{\tau} dt + \sigma \sqrt{\frac{2dt}{\tau}} \xi \quad (5.6)$$

As before, the CW bias was calculated from [CheY-P] using **Equation 5.4** [39]. After generating the CheY-P time trace, the mean CW bias of that trace was checked, to ensure that the bias was within the same range as the data mean (0.13-0.145). Since the concentration of CheY-P cannot be negative in

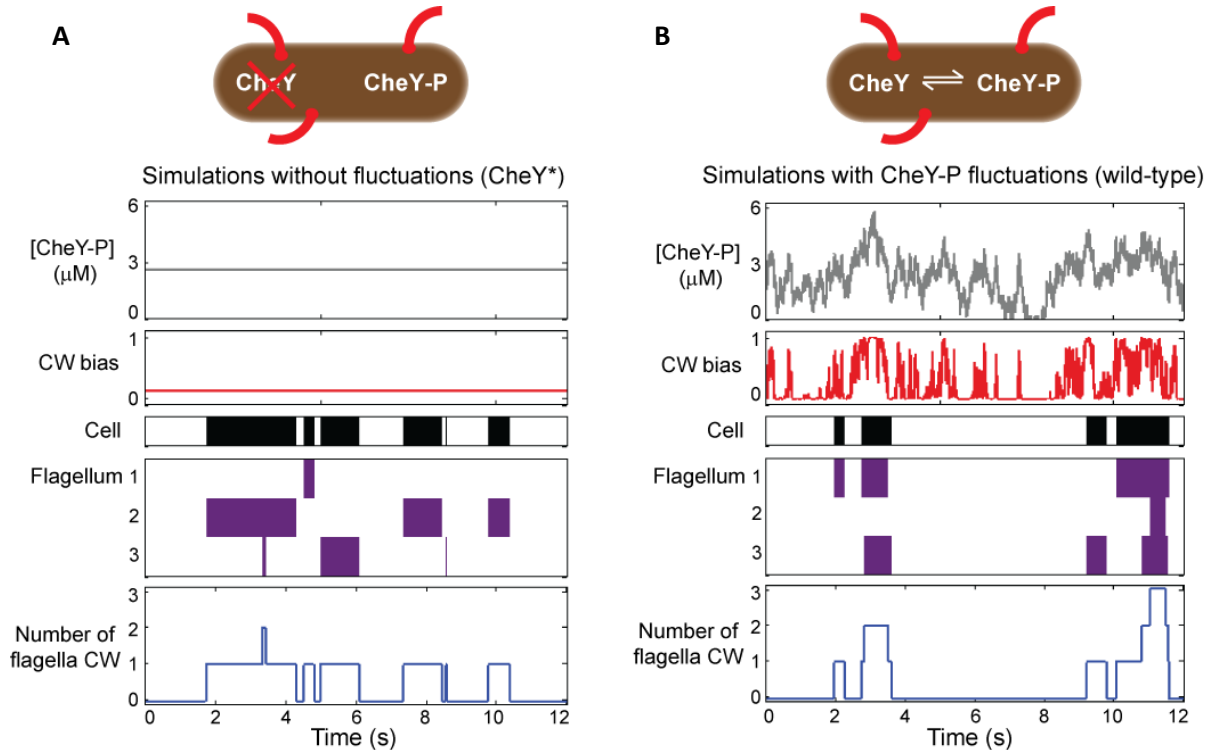


Figure 5.6: A theoretical model incorporating CheY-P fluctuations reproduces wild-type data. (A) Simulated time trace for a wild-type cell. Representative simulated time trace of CheY-P concentration (gray line, top), CW bias (red), run/tumble state (white/black), CCW/CW flagellar rotational direction (white/purple) and number of CW flagella (blue line, bottom) for a cell with 3 flagella. CheY-P simulation parameters are described in the text and in Table 5.2. **(B)** Same as (A) from a simulated CheY* cell, in which CheY-P concentration (gray line) does not fluctuate.

reality, the model was constrained so that Y was not allowed to drop below zero. As a result, in simulations with large fluctuations, the mean value of the simulated CheY-P concentration was not necessarily equal to the input mean $\langle Y \rangle$ value. If the tumble bias was outside the specified range, the input mean $\langle Y \rangle$ was shifted and the simulation was re-run, until the tumble bias was within the specified range.

After generating the CheY-P concentration time series, the rest of the simulation proceeded in the same manner as the previous simulations without fluctuations: The rotational state of each flagellar motor was determined stochastically, using **Equation 5.5**. (The specific form of **Equation 5.5** is based on data from Figure 4B in *Bai et al.* [112] and different equations can have a large effect on simulation results.) Runs and tumbles were determined using the veto rule. Finally, the simulated data was analyzed in the exact same manner as the experimental data. Results from the simulations are shown by black-solid lines in **Figure 5.7**. Remarkably, the simulations were in good agreement with all of the experimental data from **Chapter 4**. This is the first model which successfully reproduces all of the data.

Only by combining fluctuations in CheY-P concentration and the veto model was I able to reproduce all of our observations.

Most of the values used in these simulations were provided by previous studies or extracted directly from my data (**Table 5.2**). The only significant free parameters were σ and τ , which denote the amplitude and timescale of simulated CheY-P fluctuations. The values of σ and τ were determined by scanning through a range of values, and minimizing the global, reduced- χ^2 [113] from comparisons of simulations to data (**Figures 5.8 and 5.9**). The minimum, global, reduced χ^2 value indicates that all of the

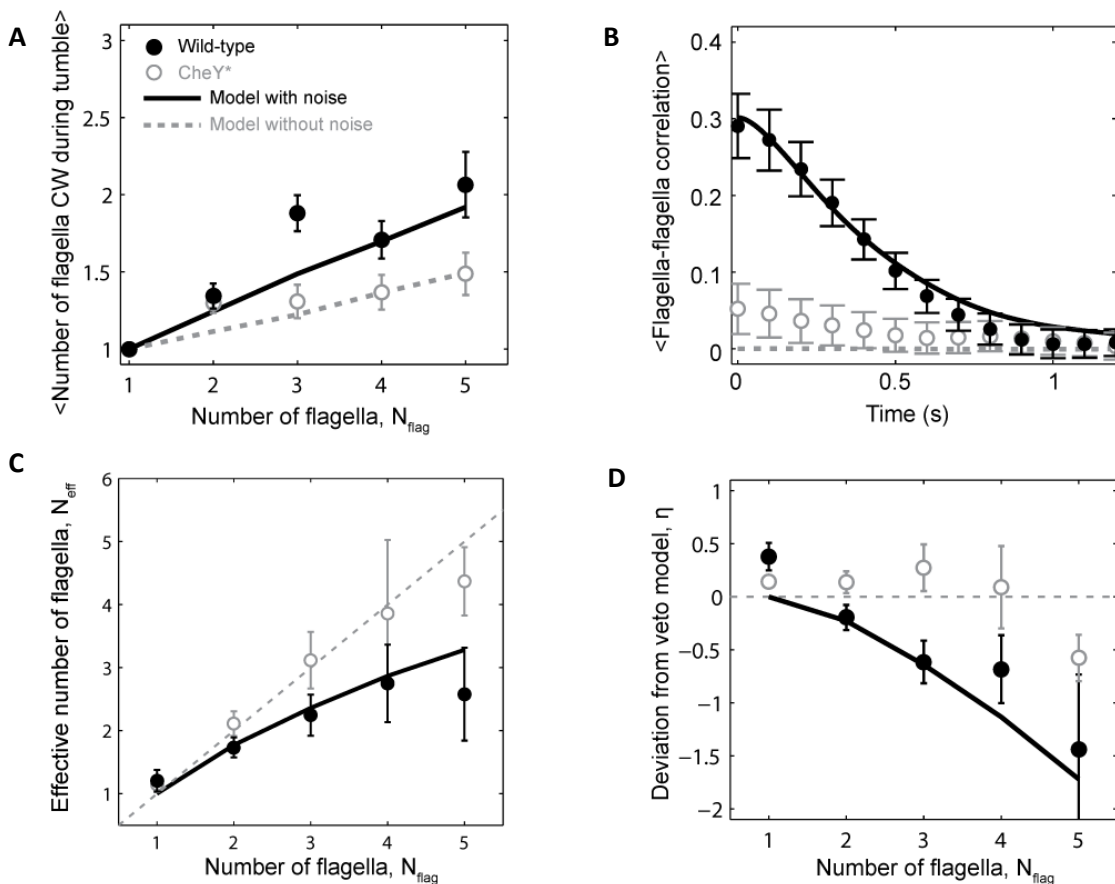


Figure 5.7: Simulations with and without fluctuations match wild-type and CheY* data, respectively.

Black circles show wild-type data, grey open circles show CheY* data, solid black line shows results from model with fluctuations in CheY-P concentration, and dashed grey lines show results from the model without fluctuations. Error bars denote SEM. **(A)** Mean of the maximum number of CW flagella during a tumble vs. number of flagella per cell. Consistently more flagella are CW during tumbles in the wild-type compared to the CheY* strain. **(B)** Cross-correlation between the rotational directions of flagella pairs, averaged over all pairs and all cells. Flagella on wild-type cells exhibited significant correlation, while CheY* cells exhibited almost no correlation. **(C)** Fitted N_{eff} values vs. number of flagella per cell. The number of effective flagella was extracted from data and simulations as in Chapter 4. **(D)** Deviation from veto model. For all four measurements, the theoretical model that included CheY-P concentration fluctuations (black line) reproduced the wild-type data (black circles). A simple veto model with constant CheY-P concentration (gray dashed line) reproduced the CheY* data (open gray circles).

experimental data is best reproduced by simulations in which $\sigma = 1.0 \mu\text{M}^2$ and $\tau = 0.2 \text{ s}^{-1}$. The global reduced χ^2 was calculated by summing the individual reduced χ^2 values from fits to data in **Figure 5.7A, B & D**.

5.2.5 Discussion of simulations

Experimental results from the CheY* strain in **Chapter 4** provided an important piece of evidence linking inter-flagellar coupling to the chemotaxis network. We propose that fluctuations in the concentration of CheY-P are at the heart of wild-type *E. coli* behavior. In the preceding simulations, the existence of temporal fluctuations in CheY-P concentration was sufficient to explain all of the data. Stochastic simulations with and without CheY-P fluctuations (representing wild-type and CheY* cells, respectively) reproduced all of the observed differences between our two strains (**Figure 5.7**). **Figure 5.6** illustrates how CheY-P fluctuations could lead to correlated flagellar switching.

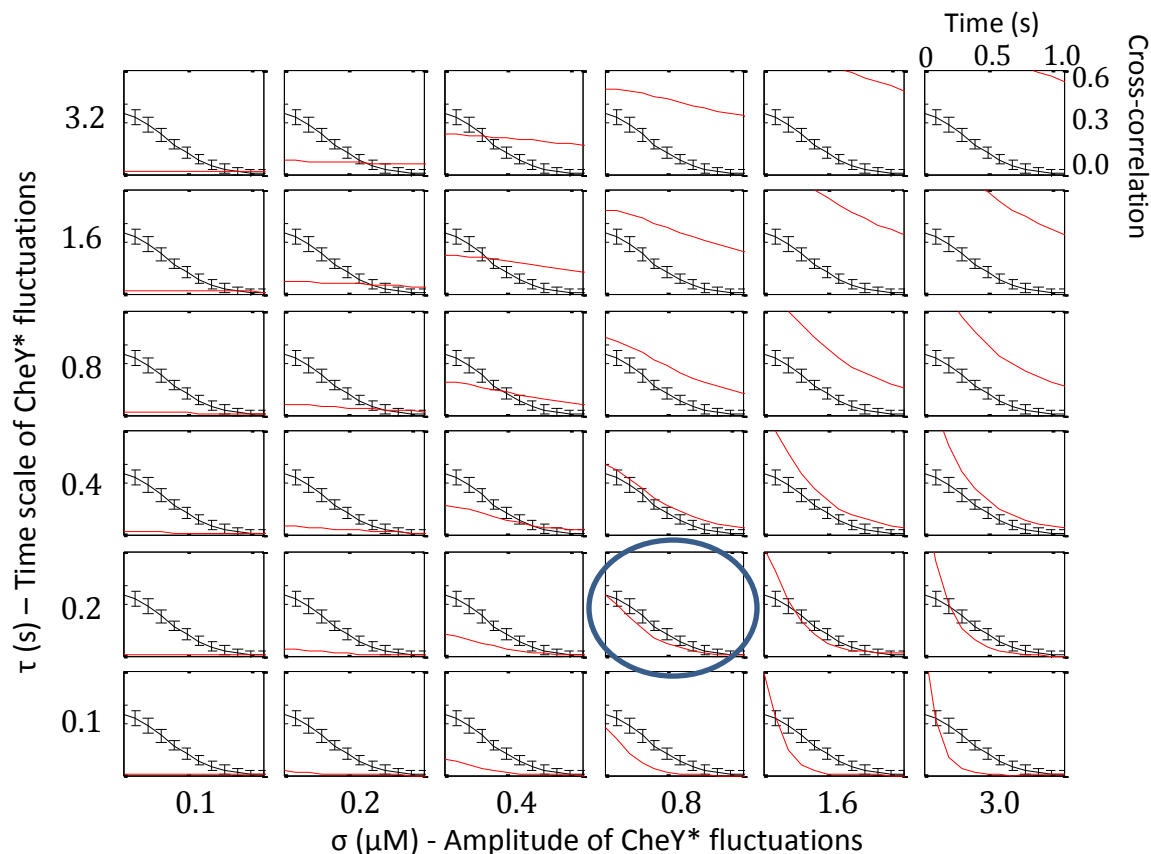


Figure 5.8: Determining CheY-P fluctuations parameter for cross-correlation. Scanning through values for σ and τ to determine the pair of parameters that best reproduce the experimentally observed cross-correlation between flagella. Simulated cross-correlation as a function of σ and τ (red), compared to experimental data (black). The circled panel at $\sigma = 0.8$, $\tau = 0.2$ is the closest match on this figure.

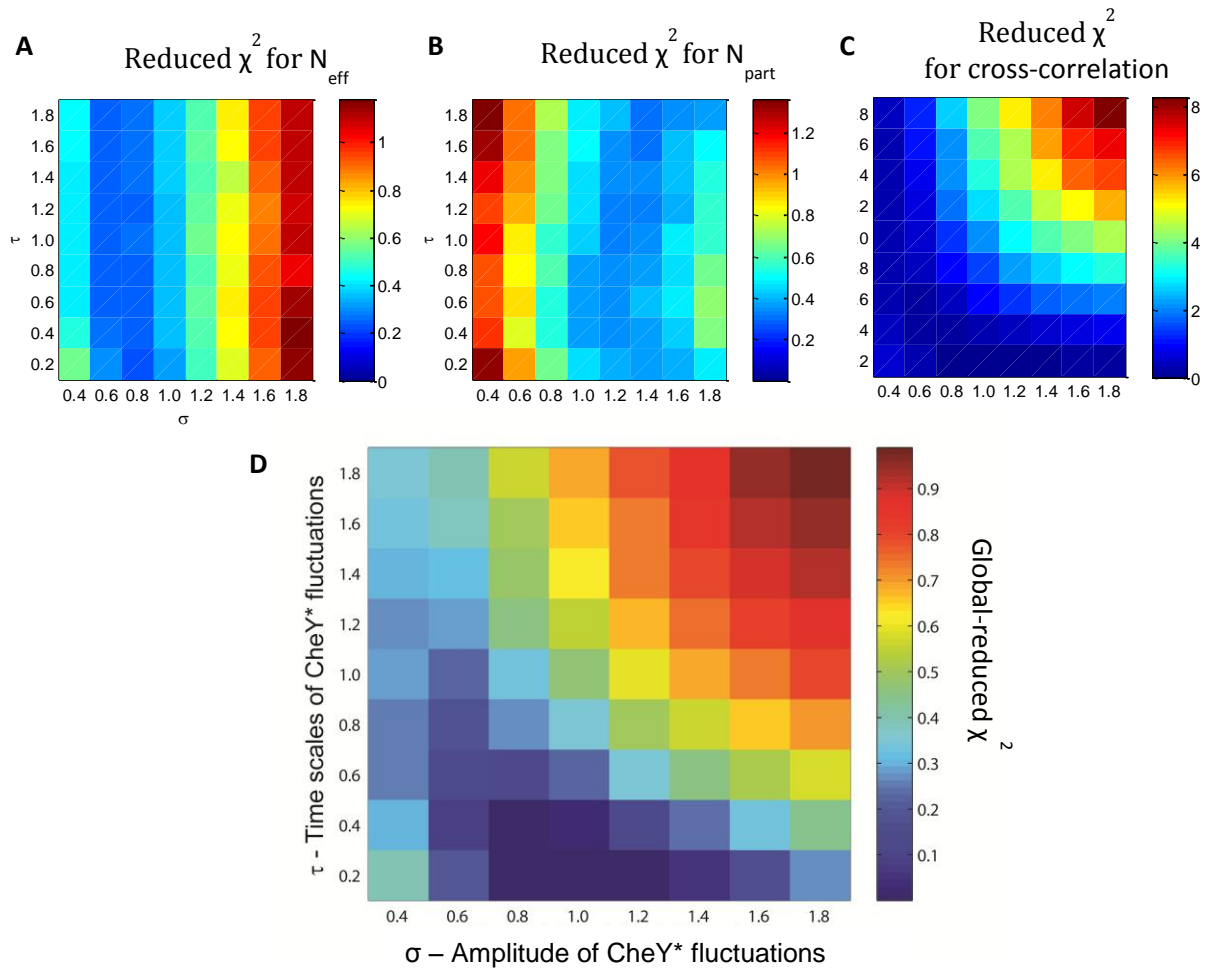


Figure 5.9: Determining CheY-P fluctuations parameters. Reduced- χ^2 was calculated for each variable in **Figure 5.7** by comparing simulated data to experimental data, while scanning through a range of possible values for σ and τ (see **Figure 5.8**). **(A)** Reduced- χ^2 for N_{eff} . **(B)** Reduced- χ^2 for N_{part} . **(C)** Reduced- χ^2 for cross-correlation. **(D)** Global, reduced- χ^2 was calculated by summing the individual χ^2 values from each data set. This was used to determine the amplitude and timescale of CheY-P fluctuations that produced simulations with results that best matched all of the experimental data. The minimum value, which is the best fit, occurred at $\sigma = 1.0 \mu\text{M}^2$ and $\tau = 0.2$ s.

As discussed previously, a well-known feature of the chemotaxis network is the sigmoidal relation between CW bias and CheY-P concentration (**Equation 5.4**) [39, 45]. A consequence of this non-linearity is that the probability of CW rotation is highly sensitive, and can respond dramatically to fluctuations in CheY-P levels, provided their amplitude is sufficiently large. As shown in **Figure 5.6**, when CheY-P concentration is high, the cell experiences a near-100 % probability of CW rotation and multiple motors switch to CW at approximately the same time. In contrast, when CheY-P concentration is low, the probability of any motor rotating CW is essentially zero. This mechanism can explain the elevated number of CW flagella involved in tumbles (**Figure 5.7A**) and correlation between flagella states (**Figure 5.7B**). By contrast, in simulations where CheY-P concentration was held constant, flagellar switching was not as correlated and the majority of tumbles involved only a single CW flagellum (**Figure 5.7A**).

For cells with $N_{flag} > 4$, both strains appear to deviate from the generalized veto model (see **Figure 5.7D**). It is possible that hydrodynamic effects must be taken in consideration in cells with many flagella. Hydrodynamic coupling in the *Hu and Tu* model (see section 5.3 below) leads to a lower N_{eff} , in the direction of the deviation. Alternatively, a mechanism as described by *Sneddon et al.* [111], in which cells with many flagella can run while some of its flagella rotate CW in the *curly-1* state, could lead to a similar deviation (**Figure 5.3**). Finally, it is possible that the apparent deviation is due to systematic experimental error, since it is more difficult to determine visually the state of each flagellum on cells with many flagella.

5.3 Flagellar interactions

The model in this previous section, which invokes short-term fluctuations in CheY-P concentration in wild-type cells, succeeds at reproducing all of my experimental observations. However, this does not rule out the possibility that another model might also be capable of explaining the data. CheY-P fluctuations might not occur at the time-scale and amplitude required to generate correlations in flagella rotational direction. As an alternative, *Hu and Tu* suggest that hydrodynamic interactions between nearby flagella could lead to correlations in rotational direction [114]. In response to the correlations observed by *Terasawa et al.* [108], *Hu and Tu* introduce an interaction term which couples the rotational direction of a pair of motors. The interaction term allows them to reproduce inter-flagellar correlations without invoking fluctuations in CheY-P concentration.

However, my observations of flagella transition rates were in disagreement with the predictions of the *Hu and Tu* model [114]. One consequence of their model is that the flagellar switching rates in a cell with a single flagellum will be different than those in multi-flagellated cells. The model is specifically

formulated for a pair of flagellar motors, but can be expanded for cells with more flagella. In my experiments, the number of flagella per cell did not have a significant effect on the switching rates between CCW and CW states (**Figure 5.10**), nor on the switching rates between different flagellar waveforms (**Chapter 6**). While my observations are in disagreement with the specific model that they construct, it may be possible to construct a similar model that could explain my data. Such a model would need to be constrained such that waveform transition rates do not change with flagella number. An alternative, but similar model could incorporate the effects of different flagellar waveforms or bundle formation on flagellar motor transition rates. It is known that the load on the motor affects switching rate [63, 107] and flagellar waveforms may exert different load on the motor [115]. While I cannot rule out the presence of hydrodynamic interactions between flagella, these must satisfy the strict requirement that switching rates remain independent of flagellar number. In light of these constraints, I believe a mechanism in which chemotaxis network fluctuations engender inter-flagella correlations to be more plausible.

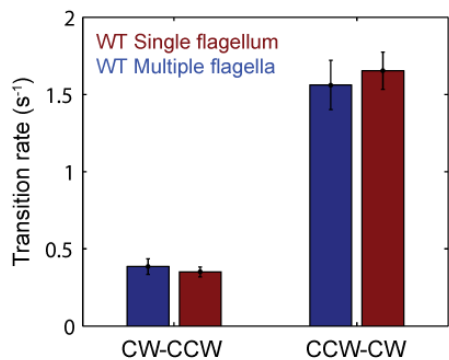


Figure 5.10: Flagellar transition rates vs. number of flagella per cell. Flagella motor transition rates, separated into two groups corresponding to cells with a single flagellum (red) and cells with multiple flagella (blue). Rates for both subpopulations are the same (within the range of error), which disagrees with the *Hu and Tu* model which predicts a significant increase in the rates for multi-flagellated cells. All data from wild-type cells (N = 52 cells). Error bars denote SEM.

5.4 Future Directions

Despite the success of my model in reproducing the data, it is important to acknowledge that there is no direct experimental evidence to-date for the CheY-P fluctuations depicted in **Figure 5.6**. Fluctuations in CheY-P have been inferred from experimental observations of CW bias in tethered-bead assays [62]. However, the fluctuations described in that study are different in their time scale and amplitude from what was required to produce the observed correlations in flagellar rotational direction (**Figure 5.8**). The simulations that I used had larger fluctuations over faster timescales than have been observed in previous studies. Future investigation will be essential in resolving this issue and will likely have to involve direct measurements of CheY-P temporal dynamics in individual cells. Such measurements are challenging, but the development of intra-cellular fluorescence sensors for measuring CheY-P concentration *in vivo* [20, 67] provides a promising approach. In that assay, a Forster

resonance energy transfer (FRET) signal is measured from a pair of fluorescent fusion proteins, CheZ-CFP and CheY-YFP. CheZ is the dephosphatase which removes phosphate groups from CheY-P. CheZ molecules spend more time near phosphorylated CheY, because it takes some time to remove the phosphate [20]. As a result, the FRET signal is roughly proportional to CheY-P concentration.

The CheY-CheX FRET assay is usually performed on populations of cells. The signal from hundreds of cells are integrated by a single photo-multiplier tube to achieve maximum fluorescence sensitivity. This also allows the sample to be illuminated with a faint light source, which reduces photobleaching and facilitates long experiments (>10 minutes). In order to measure real-time fluctuations of CheY-P, it would be necessary to measure the signal from a single cell. Single cell FRET measurements between CheZ-CFP and CheY-YFP have only been done once, but that study focused on spatial, rather than temporal dynamics [68].

It would be even more informative to combine the CheY-CheZ FRET assay with the trap assay, in order to measure CheY-P fluctuations while also measuring the swimming behavior of the cell, and potentially observing flagella. Performing this experiment would be technically challenging, because the fluorescence signal from the trap does not have the high signal-to-noise ratio of TIRF experiments. Nonetheless, a single experiment which could impose chemotaxis stimulus and measure CheY-P concentration, swimming behavior and imaging flagella would provide a wealth of information to address many unresolved questions about bacterial chemotaxis.

5.5 Summary

Several different types of models failed to reproduce the observed behavior of swimming *E. coli* cells. After much searching, we finally found that the veto model, combined with simulations including CheY-P fluctuations, was able to duplicate the observed wild-type behavior, while simulations without fluctuations matched CheY* data. Specifically, using only two free parameters—the amplitude and the characteristic timescale for CheY-P fluctuations (**Table 5.2**)—as fitting parameters, our simulations simultaneously reproduced (i) the relation between flagellar number and flagellar participation in tumbles (**Figure 5.7A**); (ii) temporal correlations between flagella (**Figure 5.7B**); (iii) the effective number of flagella in multi-flagellated wild-type cells (**Figure 5.7C**); and (iv) the degree of deviation from the veto model (**Figure 5.7D**). The model was constrained using transition rates between flagella waveforms that were directly extracted from our experiments (see **Figure 6.3** and **Table 5.2**). In the next chapter, I present additional measurements and observations of trapped cells with fluorescent flagella, including transition rates between flagellar states, and correlations between swimming statistics, flagellar

number, cell length and flagellar rotation rates.

Chapter 6. Detailed observations of flagella activity

Previous chapters described how the number of flagella affected the tumble bias of trapped cells. The same experiments also provided a large amount of data related to other aspects of bacterial swimming. In this chapter I present many of the interesting results which were left out of the previous chapters because they didn't relate directly to the problem of developing a mapping between number of flagella and tumble bias. I begin by discussing the problem of photo-induced flagella cross-linking which was a significant hurdle to acquiring long-term data from swimming cells with labeled flagella. Next, I analyze data related to flagellar waveforms, and derive waveform transition rates which are used in some of the models in **Chapter 5**. Additional swimming statistics such as average run duration, flagella rotation rate and swimming speed are analyzed as a function of flagellar number and cell length. I end with a discussion of some qualitative results from my extensive observations of trapped, swimming cells with labeled flagella.

6.1 Eradicating flagellar cross-linking

Light has been shown to affect bacterial behavior. Some bacteria perform phototaxis and migrate towards light sources. *E. coli* has negative response to blue light, which induces tumbling at high intensities [10, 116]. In other words, *E. coli* phototaxes away from bright sources of blue light. As discussed in previous chapters, near infra-red light leads to the formation of oxygen radicals which can damage and even kill bacteria [2, 69, 91, 117].

In my trapping experiments, cells sometimes stopped swimming shortly after being exposed to fluorescence excitation light (~ 1 s). This was very frustrating, because it prevented long-term studies of cellular behavior. It was also worrying, because it made me wonder how cells that continued swimming might also have been affected by the excitation light. A similar problem was observed previously by *Turner et al.* in the original studies of fluorescently labeled flagella [31]. In that study, when cells with labeled flagella were exposed to high intensity 532-nm light, they stopped swimming within a few seconds.

I wanted to solve this problem to increase throughput and eliminate any concern that the light might be damaging the cells that appeared to continue swimming normally. Several pieces of evidence were useful for diagnosing the problem. The feature was most common in cells with many flagella. The majority of cells with 4 or more flagella stopped swimming within 10 seconds of exposure to excitation light. On the other hand, cells with a single flagellum were completely unaffected. Looking at the fluorescence images of cells that had stopped swimming, it was apparent that the flagella were no longer rotating normally. In some cases the flagella curled into circles.

They usually froze in some shape and stopped moving entirely. It was clear that the excitation light was causing something to go wrong with the flagella.

This problem only occurred when cells with fluorescently labeled flagella were exposed to excitation light (532-nm and 488-nm light had the same effect). Unlabeled cells were unaffected. Labeled cells which were not exposed to excitation laser light were unaffected. At that point, I hypothesized that the flagella were cross-linking, in a way that was mediated by the fluorescent dyes in tandem with the excitation light.

My first hypothesis was that the specific dye might be responsible for the cross-linking. In an attempt to alleviate the problem, I tried labeling flagella with different types of fluorescent dyes. In addition to the AlexaFluor C5-maleimide dye used in previous chapters, I tried a Cy3 maleimide [PA23031, GE Healthcare Lifesciences] and a TAMRA dye [94506, Sigma-Aldrich][118]. Unfortunately I found that flagella labeled with both of those dyes had the same reaction.

Eventually I noticed that on days when the flagella were less brightly labeled, cross-linking seemed to be less common. When they were most bright, the phenomenon occurred more frequently. I performed a series of experiments in which I labeled flagella with various concentrations of dye. When flagella were labeled with a very low concentration of dye, swimming was unaffected by excitation light. When labeled with higher concentrations of dye, the phenomenon returned. This confirmed my hypothesis that the phenomenon that was causing flagella to stop rotating was clearly mediated by an excess of dyes, excited by the fluorescence light.

In conclusion, cross-linking seems to occur when flagella are labeled with an excess of dye. High concentrations of dye create brighter images, but also lead to cross-linking which ruins swimming behavior. I determined an optimal concentration of dye at which flagella were still relatively bright, but cells almost never stopped swimming as a result of exposure to fluorescence excitation light (~1 mg/100 ml, for AlexaFluor532 C₅ maleimide). The idea is to use the maximum amount of dye such that cross-linking does not occur. Using this concentration of dye made cross-linking very uncommon and produced bright images as well.

6.2 Flagella waveforms and transitions

6.2.1 Flagella waveforms

In previous chapters I focused on the rotational state of each flagellum (CW or CCW). However, CW rotating flagella can take on several different waveforms (also called isoforms or polymorphisms). In swimming cells, CCW rotating flagella are always found in the *normal* waveform, but CW rotating flagella have been observed in the *semi-coiled*, *curly-1* and *curly-2*

waveforms [31, 56, 119] (**Figure 6.1**). Other waveforms can also be generated by applying external torque to the motor. A total of 12 distinct waveforms are believed to be possible, but only *normal*, *semi-coiled* and *curly-1* waveforms have been observed in swimming cells.

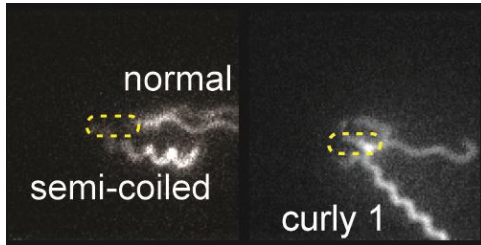


Figure 6.1: Flagella waveforms. Fluorescence images from trapped cells with labeled flagella. On the left is a cell with 3 flagella. Two of them are in the *normal* waveform and the other is in the *semi-coiled* waveform. On the right is a trapped cell with one flagellum in the *curly-1* waveform and a second flagellum which is in the process of transforming into the *normal* waveform.

6.2.2 Sequences of flagella waveforms

The experimental approach described here allows the simultaneous, long-term observation of flagellar activity and swimming behavior in a single cell. By imaging many individual tumbles ($N = 203$ in wild-type cells), we are able to describe in great detail the underlying structure of a tumbling event. For instance, we can follow the sequence of flagellar waveforms that occurs when motors switch from CCW to CW rotation and back to CCW. **Figure 6.2A** shows the distribution of sequences of flagellar waveforms observed during tumbles. The majority of CCW-to-CW switches caused flagella to transition to the *semi-coiled* waveform (77%, 164/213 of all flagellar switching events). Of those flagella, most remained *semi-coiled* until the motor returned to CCW (71%, 117/164), while some instead transitioned to the *curly-1* waveform (29%, 47/164). Some fraction of flagella (22%, 47/213) also skipped the *semi-coiled* waveform altogether and transitioned immediately from CCW to *curly-1*. Strikingly, those flagella never switch to the *semi-coiled* state.

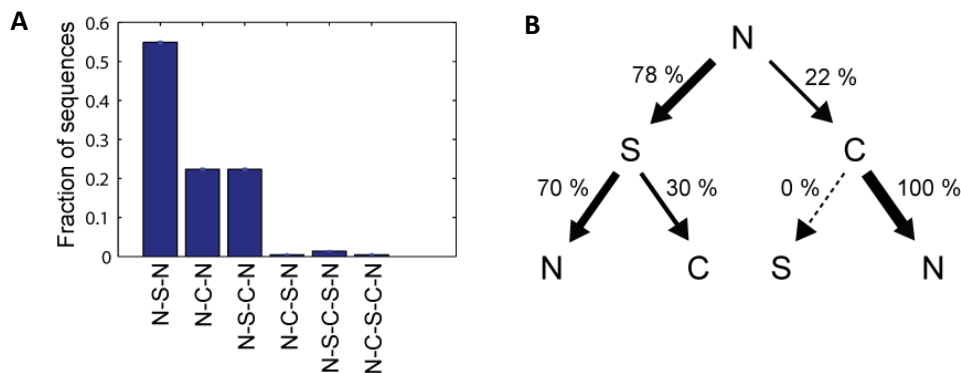


Figure 6.2: Flagella waveform transition sequences. (A) Histogram of the sequence of flagellar waveforms when flagella motor rotation switches from CCW to CW ($N = normal$, $S = semi-coiled$, $C = curly-1$). Note that prior to CW rotation all flagella had the *normal* waveform. (B) Decision tree showing the probability of each sequence of flagellar waveforms when flagella switch from CCW to CW rotation. Arrow thickness is proportional to the probability of a specific transition.

This is the first time that the occurrence of these transition sequences has been quantified. Although we cannot rule out that runs and tumbles in the optical trap are different in some ways than those in free swimming cells [2], the results are in qualitative agreement with previous observations. *Darnton et al.* [56] also observed each of the sequences of events detailed above and described the sequence of states from *normal* to *semi-coiled* to *curly-1* as a “canonical tumble”.

The typical sequence of flagellar states during a tumble—in which *semi-coiled* flagella frequently transition to *curly-1*, but *curly-1* flagella never transition to *semi-coiled* (**Figures 6.2**)—likely occurs in a way that minimizes the elastic energy in the filament. By pulling on flagellar filaments with optical tweezers, *Darnton et al.* [120] demonstrated that load causes flagella to proceed through a sequence of waveforms. Following that work, *Van Albada et al.* [115] proposed a model in which torsional load builds in CW rotating flagella, eventually inducing the waveform to transition to a more relaxed state (e.g., *semi-coiled* to *curly-1*). The absence of transitions from *curly-1* to the less relaxed *semi-coiled* state in my data is consistent with this type of model.

6.2.3 Flagellar waveform transition rates

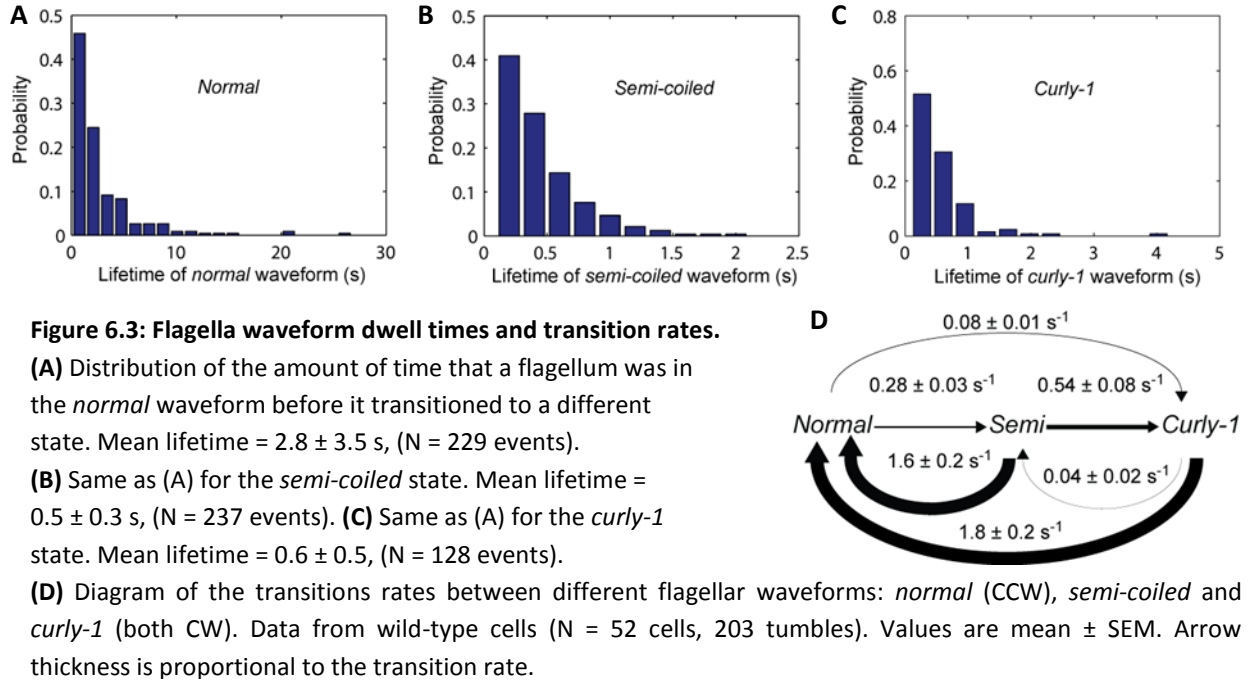
These observations allowed me to calculate transition rates between the three flagellar states. **Figure 6.3** shows the dwell-time distributions for each of these states. Transition rates were calculated by dividing the probability of each transition by the mean duration of the initial state, using **Equations 6.1** and **6.2**. Where P is the probability of the transition, i designates the initial state, f designates the final state, o designates all other states, N is the number of observed transitions, k is the transition rate, and T is the mean dwell time in a given state.

$$P_{i \rightarrow f} = \frac{N_{i \rightarrow f}}{N_{i \rightarrow f} + N_{i \rightarrow o}} \quad (6.1)$$

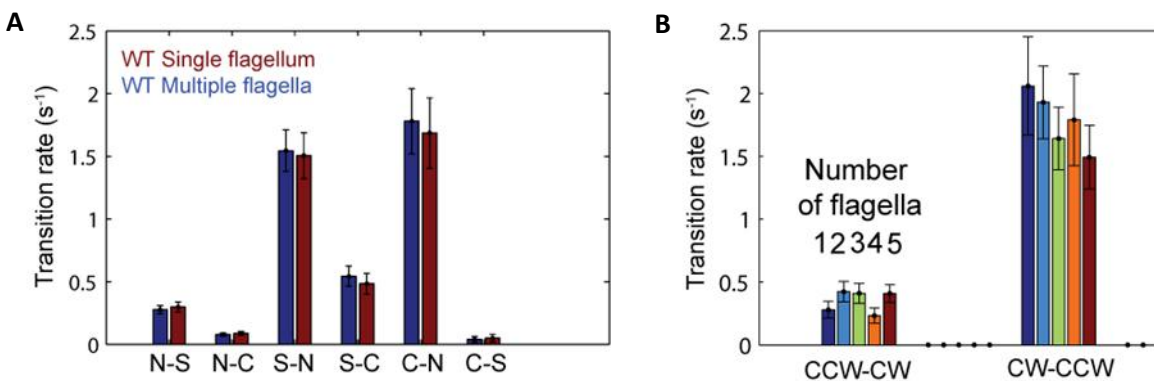
$$k_{i \rightarrow f} = \frac{P_{i \rightarrow f}}{T_i} \quad (6.2)$$

Table 6.1 – Flagella waveform transition rates

Final Initial	<i>Normal</i>	<i>Semi-coiled</i>	<i>Curly-1</i>
<i>Normal</i>		0.28 ± 0.03 s ⁻¹	0.08 ± 0.01 s ⁻¹
<i>Semi-coiled</i>	1.6 ± 0.2 s ⁻¹		0.54 ± 0.08 s ⁻¹
<i>Curly-1</i>	1.8 ± 0.2 s ⁻¹	0.04 ± 0.02 s ⁻¹	



These data are useful for creating realistic models of bacterial swimming. In fact, in **Chapter 5**, I used several of these transition rates as parameters in my models of flagellar activity (**Table 5.2**). I also used the transition rates between *semi-coiled* and *curly-1* waveforms in the Sneddon model which includes information about the specific flagellar waveforms when determining whether a cell is running or tumbling [111]. Comparing the transition rates for cells with different numbers of flagella provides an additional constraint on models that invoke hydrodynamic coupling [114], as discussed in **Chapter 5**. **Figure 6.4A** compares the waveform transition rates for



cells with one or multiple flagella. Transition rates were the same in both populations, which suggests that the presence of other flagella on a cell did not have a significant effect on the average waveform transition rate. **Figure 6.4B** compares motor transition rates (transitions between CW and CCW rotation) for cells with one, two, three, four or five flagella. It appears that the transition rate from CW to CCW rotation decreases as the number of flagella increases. But the trend was not very pronounced, so more data would be required to determine if this is a consistent result.

6.3 Relating flagellar number to other swimming statistics

6.3.1 Run-tumble statistics vs. flagellar number

In previous chapters, I focused on tumble bias as the quantitative measure of cell swimming behavior. Several other parameters are often used to quantify swimming behavior. Run and tumble durations, tumble frequency, and swimming speed are all useful for describing how cells swim [1, 2, 26, 61, 65, 121]. For this analysis, I used long-term (>100 s) swimming data from trapped cells. As described in **Chapter 3**, this data was recorded either before or after fluorescence imaging. (About

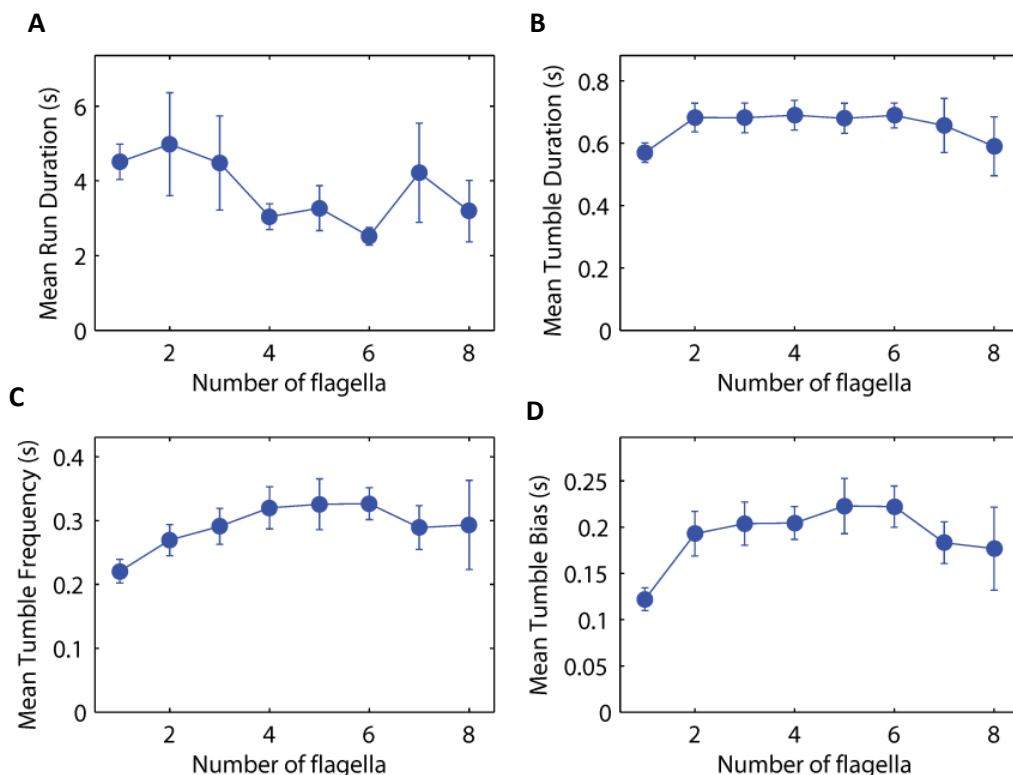


Figure 6.3: Run/Tumble statistics vs. number of flagella. Statistics extracted from trapped cells with long (>100 s) swimming traces ($N = 117$ cells). None of these parameters display significant correlation. (A) Mean run duration vs. number of flagella per cell. (Pearson's $r = -0.12$.) (B) Mean tumble duration. (Pearson's $r = 0.06$.) (C) Mean tumble frequency. (Pearson's $r = 0.19$.) (D) Mean tumble bias. (Pearson's $r = 0.16$.) Error bars are SEM.

2/3rds of this data was recorded prior to fluorescence imaging of the same cell, and the rest was recorded after fluorescence imaging.) Long-term data provides a much more accurate measure of average swimming parameters which have large variance.

Figure 6.5 shows the relationship between number of flagella and several different measures of run-tumble behavior. None of the measurements showed a statistically significant correlation. This further supports the conclusions from previous chapters, that cells have developed a strategy to achieve similar swimming behavior, regardless of how many flagella a particular cell has.

To determine whether or not the observed correlation coefficient was statistically significant, I compared the measured value to the critical value in a lookup table for Pearson's correlation. This was necessary because the probability of observing false correlations in uncorrelated data depends on sample size. For a sample size of 117 (the number of cells observed), the measured correlation must exceed 0.19 to be statistically significant at the $p > 0.05$ confidence level.

6.3.2 Flagella and body rotation rates vs. flagellar number

As described in **Chapter 3**, trapped cells rotate at a rate of about 10 Hz, and their flagella rotate at a rate of about 100 Hz. **Figure 6.6** compares these rates to the number of flagella per cell. There was no correlation between either of these rates and the number of flagella, which was somewhat surprising. One might expect that additional flagella would produce additional torque and cause the cell body to rotate at a faster rate. Instead, much of the additional torque may be dissipated as the different flagella bend around the cell to form a single bundle. Since each flagellum

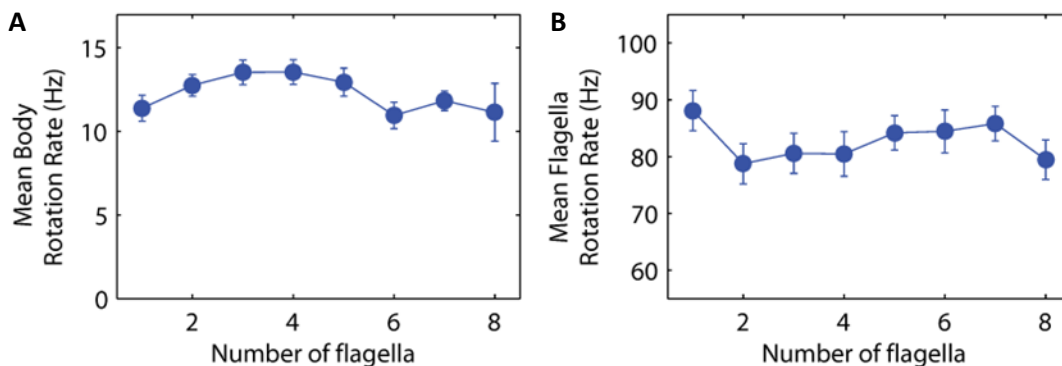


Figure 6.4: Rotation rates vs. number of flagella. (A) Mean body rotation rate vs. number of flagella per cell. (Pearson's $r = -0.06$.) (B) Mean flagella rotation rate vs. number of flagella per cell. (Pearson's $r = 0.02$.) Both rates are very consistent. Apparently the number of flagella on a cell does not affect rotation rates. Error bars are SEM.

is attached to a different location on the cell body, they do not all point out perpendicular to the cell body. Instead, the flagellar hook bends and some of the flagella end up rotating adjacent and parallel to the cell body. It has been proposed that additional flagella do not add much propulsive force because the extra flagella graze the cell body as they rotate, and lose much of their propulsive energy to friction [56].

6.4 Cell length

6.4.1 Cell length and flagellar number

Another critical measure in microbiology is cell size. Cell size is often related to physiological conditions, and can be used to normalize results between individual cells. For rod-shaped bacteria, like *E. coli*, cell size is roughly proportional to cell length. During exponential growth phase a cell continuously elongates while the diameter remains the same. When the length has doubled, the cell divides. Therefore, cell length is often used to relate concentrations and raw numbers of molecules inside the cell. Similarly, since new flagella are produced continuously (**Chapter 2**) I expected the number of flagella to be higher on long cells. **Figure 6.7A** shows the distribution of cell lengths on trapped cells with labeled flagella. Length was measured using a brightfield image of the trapped cell (see **Chapter 3**). The grayscale image was processed in Matlab to enhance contrast. I then manually identified the locations of each end of the cell. The images do not have very high resolution, and there may be systematic measurement error (actual lengths may be somewhat higher or lower than measured). Nonetheless, the relative difference in cell lengths was very pronounced and appears reliable. As expected the longest cells were about twice as long as the shortest cells. The data was well fit by a Poisson distribution. **Figure 6.7B** shows the

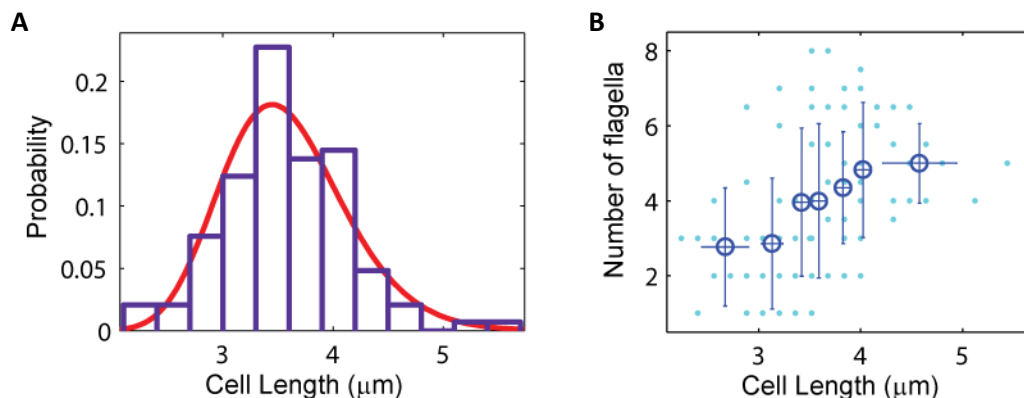


Figure 6.5: Cell length. (A) Cell length distribution, measured from images of trapped cells. Red line is a fit to a Poisson distribution. (B) Cell length vs. Number of flagella per cell. As expected there is significant correlation (Pearson's $r = 0.44$). Dots represent individual cells. Circles show binned data with standard deviation. Each bin contains an equal number of cells. $N = 117$ cells.

relationship between number of flagella and cell length. As expected, flagella number was proportional to cell length. In other words, the concentration of flagella per cell length was roughly constant.

To be sure that I wasn't missing anything, I tried plotting the run-tumble statistics from the previous section (run duration, tumble frequency, etc.) after normalizing flagella number by cell length. Unfortunately there was still no significant correlation in any variables. Similarly, none of the run-tumble statistics were correlated with cell length.

6.4.2 Cell length vs. flagella and body rotation rates

I found that the flagellar rotation rate was correlated with cell length (Pearson's $r = 0.30$, **Figure 6.8**). This was in agreement with a previous study which measured rotation rates of trapped *E. coli* in aerobic conditions [90]. The source of this correlation is not obvious. One might imagine that the rotation rate increases because longer cells have more flagella, which collectively reduce the resistance felt by each individual flagellum. But flagellar number was not correlated with flagellar rotation rates. It seems that the cell length itself somehow leads to a faster flagellar rotation rate. Maybe longer cells are orient more easily along the same axis as the flagellar bundle, thereby decreasing the rotational drag of the cell body? That seems unlikely, since I did not observe a positive correlation between cell body rotation rates and cell length ($r = -0.16$, a slightly negative correlation). However, my result was in disagreement with the previous study which did observe a positive correlation between cell length and body rotation rate [90]. The discrepancy may be due to different trapping geometries. In my dual trap, the cell is held at both ends, which may resist body rotation. In their experiment, cells were held in a single trap along the long-axis of the cell body.

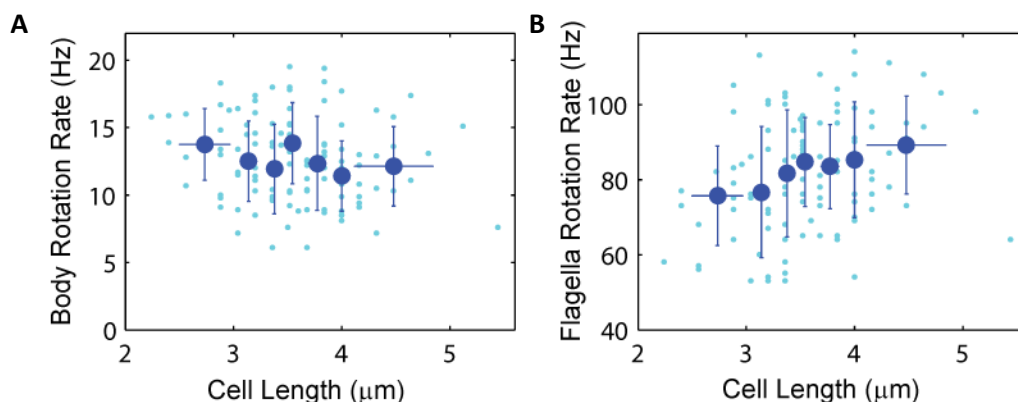


Figure 6.6: Rotation rates vs. cell length. (A) Body rotation rate vs. cell length (Pearson's $r = -0.16$). Dots show data from individual cells, circles with error bars (SD) show binned data (equal bin sizes, $N = 117$ cells). (B) Flagella rotation rate vs. cell length showed statistically significant correlation (Pearson's $r = 0.30$). It appears that flagella rotate slightly faster on longer cells.

That geometry would be less likely to inhibit cell body rotation. If the question is of further interest, it could be easily tested in my instrument by measuring the body rotation rate of a single cell in both geometries.

The rotational frequencies measured by *Chattopadhyay et al.* [90] are a bit higher than mine (**Figure 6.8**). This is most likely due to the fact that the cells were swimming in an anaerobic environment in my experiments. This is a tradeoff. Without Oxygen, cells are less energetic, but continuously swim for tens of minutes. In the presence of Oxygen cells are more energetic, but only swim in the trap for a few seconds before IR induced oxidative damage terminates swimming behavior (see **Chapter 3**). It is also worth noting that the flow rate of the surrounding fluid may affect the body rotation rate. *Chattopadhyay et al.* observed an increase of ~ 2 Hz for every $20 \mu\text{m/s}$ increase in flow speed [90]. My experiments were performed with a flow rate of $30 \mu\text{m/s}$.

6.4.3 Swimming speed and cell length

In free swimming cells, the swimming speed is a critical parameter that governs how efficiently a cell performs chemotaxis. In the trap, it is impossible to measure swimming speed because the cell is immobilized. However, swimming speed can be related to rotational rates of the cell body and flagellar bundle. Using the formalism of the propulsion matrix which developed for rotating flagella by Purcell [33], *Chattopadhyay et al.* investigated the propulsive force and rotational frequencies of a trapped cell subject to a range of flow speeds [90]. The propulsion matrix, also called a resistance matrix, relates force, torque, body rotation rate and drag for a single swimming cell.

Using the results of *Chattopadhyay et al.* we can estimate the effect of cell length on swimming speed [90]. From that paper, swimming speed, $v = B\omega / (A + A_0)$, (where ω = flagellar bundle rotation rate, $A*v$ = viscous drag from the flagella bundle, A_0*v = viscous drag from the cell body, and $B*\omega$ = propulsive force generated by the flagella bundle). Perhaps surprisingly, the flagellar bundle theoretically contributes about half of the total drag of a swimming cell. The only parameter that depends on cell length is the viscous drag from the cell body, which is $A_0 = \frac{4\pi\eta L}{\ln(2L+a)+1/2}$ (where L = cell length, a = cell width, η = fluid viscosity). Treating all other variables as constant, swimming speed is related to cell length by the equation $v \approx 1/(1+L/\ln(2L+1)+1/2)$. Over the range of observed cell lengths (~ 2.5 – $5.5 \mu\text{m}$) the swimming speed decreases by a factor of about 30%. However, as shown in **Figure 6.8**, the flagellar rotation rate is correlated with cell length. Longer cells have faster flagella rotation rates, which increases the swimming speed by up to about 20%. These two effects nearly cancel each other out. Based on these estimates, I expect the

net effect of cell length on swimming speed to be that short cells swim about 10% faster than long cells. This is consistent with my own impressions from watching swimming cells under the microscope. By eye, shorter cells generally appear to swim faster than longer cells.

6.5 Qualitative observations of trapped and swimming cells

Along with the quantitative measurement above, I made many qualitative observations while watching these cells swim. These ideas may be useful for generating future hypotheses and stimulating further investigations.

6.5.1 Runs with CW rotating flagella

It has been proposed that a cell on which all of the flagella are rotating CW might be able to run [36]. It is generally accepted that cells run when all of the flagella rotate CCW and tumble when many rotate CW. The idea of a CW run is based on the thought that if all of the flagella are in the same CW waveform, they might also be able to form a bundle. This is highly unlikely in wild-type cells because it is uncommon for all of the flagella to simultaneously rotate CW for prolonged periods of time. Nonetheless, *Alon et al.* observed that CheY* cells (see **Appendix C.1** for strain info.) induced at to a very high level appeared to run more than cells at an intermediate level [36]. This led them to hypothesize the existence of CW runs.

In my data, I observed a few CheY* cells in which three CW flagella, all in the *curly-1* conformation, formed a loose bundle behind the cell and generated behavior that looked very much like a run. The bundles formed by these flagella were not as tight as the bundles formed by CCW rotating flagella. I never observed this behavior with *semi-coiled* flagella. In cells with a single flagellum, I sometimes observed that the *curly-1* flagellum would orient along the long-axis of the cell body, in front of the cell (180 degrees from the orientation of the same flagellum in the CCW *normal* state.) In other words, the flagellum moved to the upstream side of the cell, pointing into the direction of the oncoming fluid. By contrast, bundles always formed on the down-stream side of the trapped cell. There is a large amount of literature on the hydrodynamics of flagella rotation and interactions.[34, 35, 122-124] In a particularly novel study, *Kim et al.* created a macroscopic structure to mimic the rotation of 2 nearby flagella, and showed the hydrodynamics lead to bundling [35]. The existence of runs generated by CW rotating flagella may be of interest to this community.

6.5.2 Flagella and surface attachment

Cells with flagella are much more likely to attach to or swim near the surface of a

microfluidic chamber. When I grow cells without flagella, they are much less likely to aggregate on the surface of my glass and silica chambers. Swimming cells are known to swim in circles next to the surface [36, 125] and have been shown to swim on the right hand-side when traversing chambers with split channels [126]. In my experiments I have found that runny cells are more likely to remain near the surface than tumbling cells. This may be because tumbles give the cell a chance to break away from the surface. It also seems that cells with less flagella are more likely to remain near the surface. Although, I have not tried to quantify these effects.

6.6 Future Directions

6.6.1 Collect additional data to verify correlations between swimming variables

There remain many open questions related to flagellar propulsion. Some of the results in this chapter may serve as starting points for future studies. A few variables exhibited correlation which was not statistically significant, (based on the sample size) but the observed trends might still be real. For example, the transition rate from CW→CCW rotation appeared to decrease in cells with greater numbers of flagella (**Figure 6.4B**), and tumble frequency appeared to increase with flagellar number (**Figure 6.5C**). Collecting more data would allow us to determine if these effects are real, or just due to chance. We could also use a mutant strain that expresses a greater number of flagella than wild-type cells to see if these effects are more pronounced in cells with many flagella.

There was a discrepancy between my results and those of *Chattopadhyay et al.* regarding the relationship between cell length and body rotation rate (**Figure 6.8A**) [90]. It is possible that I did not observe the correlation that they saw because of differences in trapping geometry. This could be tested by measuring the rotation rate of a single cell in both trapping geometries. First, measure its body rotation rate in a single trap, and then turn on the second trap and measure the rotation rate when held by two traps.

6.6.2 Examine flagella length and bundle tightness

The correlation between flagellar rotation rate and cell length was in agreement with the previous study [90], but the source of this correlation is unknown. It could be due to hydrodynamic coupling effects, in which the rotation of one flagellum reduces the drag experienced by other nearby flagella. Trap experiments could be performed in fluid media of different viscosity to test this effect, similar to a previous study with labeled flagella on free swimming cells [56]. Alternatively, the effect may be related to bundle formation or some other poorly studied feature. It would be interesting to re-analyze the existing data to extract flagellar lengths, and to characterize the

tightness of the flagellar bundles on different cells. On some cells, the flagellar bundle appeared very tight. On others, even while running the flagella appeared to be further apart within a loose bundle. Bundle tightness could affect many factors, including swimming speed. Loose bundles create more drag and would probably make cells swim slower.

6.6.3 Investigate runs with all *curly-1* (CW) flagella

I observed cells that appeared to be running while all of their flagella were rotating CW in the *curly-1* waveform. This poses a fundamental question: Why have *E. coli* evolved to rotate their flagella CCW most of the time? In other words, why do cells run with flagella in the *normal* waveform? A likely explanation is that flagella in the *normal* waveform form better bundles and/or provide more propulsive force than flagella in other waveforms. To test this, we could perform more experiments with inducible CheY* cells. In cells with high concentrations of CheY*, flagella should all spend most of the time rotating CW, often in the *curly-1* waveform. We could then determine how commonly bundles are formed when all flagella are in the *curly-1* waveform. We could also measure the propulsive force generated by *curly-1* bundles, by measuring the deflection of the cell along the direction of motion (along the X direction, see **Chapter 3**). The propulsive force could be compared to cells with *normal* bundles, and to the forces measured by *Chattopadhyay et al.* [90].

6.7 Summary

The new E Fleezers instrument described in **Chapter 3** allowed me to count flagellar number, measure cell length, and simultaneously measure long-term statistics related to swimming behavior. In this chapter I have provided several of the new results, both quantitative and qualitative, that have been revealed by the use of this new tool. Several measures related to run-tumble behavior corroborate the conclusions of **Chapter 4**, that cells have developed a mechanism to achieve similar swimming behavior regardless of the number of flagella per cell. The data from these experiments was very rich, and this chapter provided a survey of the types of information that can be gleaned from fluorescence videos and run-tumble statistics. The next chapter will discuss results from a complementary set of experiments using the 2-D swimming assay.

Chapter 7. Two-dimensional swimming

The previous chapters focused on data acquired using the new E Fleezers instrument. This chapter presents results from a complementary assay in which free swimming cells were tracked as they moved in two dimensions. I first describe how the assay works. I then present results related to the degree of angular change during tumbles. Next I present results from chemotaxis adaptation experiments, including a receptor mutant strain which does not sense aspartate. Finally, I present results from a flagella dilution experiment which investigates the behavior of populations of cells with different average numbers of flagella per cell.

7.1 Background

Many different types of assays have been developed to study the model system of bacterial chemotaxis. Swimming cells have been tracked in three dimensions [26, 58, 59] and two dimension [1, 36, 60, 61]. The activity of individual flagella has been monitored by measuring the rotation of a bead attached to a flagellum [39, 46, 62, 63], or by watching a cell rotate relative to a flagellum that was attached to a surface [64, 65]. More recently, assays have been developed to monitor the interactions of signaling proteins inside the cell [17, 66-68]. Each of these assays provides a different set of information that can be used to better understand the complicated process that is bacterial chemotaxis.

I frequently performed the 2D swimming assay to test newly constructed strains or as a control for the trap assay (protocol in **Appendix B.5**). The basic idea is to record videos of cells swimming inside a thin chamber (~10 μm) and then trace the trajectories of each cell to analyze their behavior. The chamber is kept thin so that cells remain in a single focal plane which can be imaged by a commercial, phase contrast microscope. The 2D assay is complementary to trap assay. It provides some measurements that the trap cannot, and others that can be compared to trap results. For example, both assays provide run-tumble statistics, but only the 2D assay can measure swimming speed or the angular change of direction during a tumble.

A significant advantage of the 2D assay, compared to the trap assay, is that a large amount of data can be collected rapidly. Tens of cells can be monitored simultaneously, and several movies can be recorded from a single chamber, without any additional steps in between movies. By comparison, each cell in the trap must be carefully trapped, moved and aligned before data can be collected from that cell. In a typical 2D experiment, hundreds of cells can be monitored, compared to ~10 cells in the trap assay. This high throughput makes the 2D assay a perfect test-bed for new mutant strains and different experimental conditions, including different growth media, swimming media, inducer concentrations and fluorescence dye concentrations.

In the context of my thesis, the biggest down-side is that it is impossible to count flagella on the individual swimming cells that are tracked in the 2D assay, so results are only relevant for a population of cells. Additionally, cells swim out of the field of view, so each cell is usually only tracked for about 30 seconds.

7.2 Wild-type 2D assay results

7.2.1 General results

Movies of cells swimming in a 2D chamber were recorded and then analyzed in Matlab (**Figure 7.1**). I wrote a series of Matlab programs to identify cells, determine their trajectories, and calculate various swimming parameters, including speed and tumble frequency. This began with image processing which was used to identify individual cells in each frame of a movie. Next, each individual cell was tracked over time by comparing the location of a cell in one frame to the location of cells in the next frame. The trajectory of a single cell contained a sequence of locations in two-dimensional space. The linear speed and angular speed of the cell was calculated from the spatial information. Finally, the run/tumble state of the swimming cell was determined using the swimming speed. Specifically, a cell was identified as tumbling whenever its linear speed dropped below a threshold and the angular speed rose above a threshold (**Figure 7.2**). Physically speaking, this corresponded to times when the cell had slowed down and was changing its direction, which is the basic definition of a tumble. This algorithm is based on the algorithm described in *Alon et al.* [36].

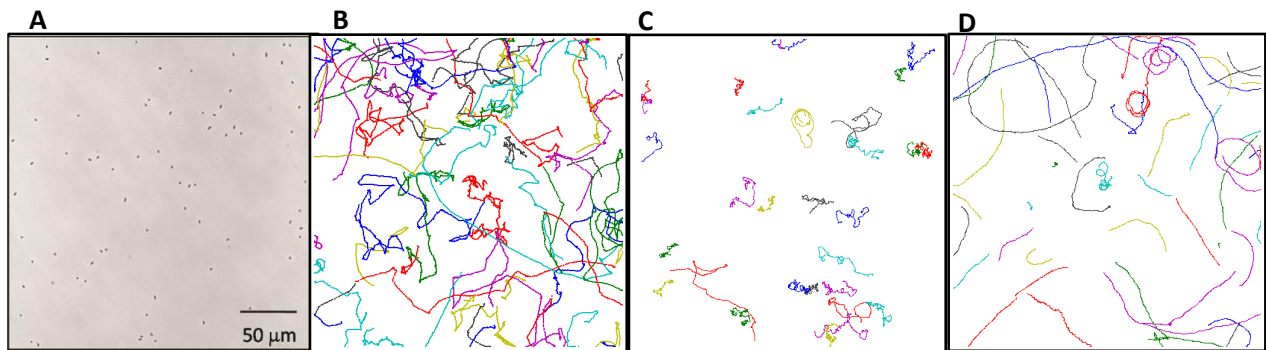


Figure 7.1: Watching cells swim in two dimensions. (A) A single frame of raw swimming data. Typical movies lasted 30 seconds and contained 900 such frames. **(B)** Wild-type cell trajectories as determined using my Matlab code. Statistics including swimming speed and tumble frequency were calculated from these trajectories. **(C)** Trajectories from tumbling cells. CheY* strain induced with 100 μM IPTG to over-express CheY*. Cells tumbled continuously. **(D)** Trajectories from runny cells. CheY* strain induced with 1 μM IPTG express very little CheY*. Cells ran continuously.

From the sequence of run-tumble states, I calculated the same types of swimming parameters that were analyzed in previous chapters when studying trapped cells. Statistics such as tumble frequency, run duration, tumble duration, tumble bias and average swimming speed were calculated. In the 2D assay, the tumble frequency was a more reliable measure than tumble bias. This is because the tumble frequency was not sensitive to the specific thresholds or algorithms used to identify runs and tumbles. In other words, it is fairly easy to identify whether or not a tumble occurred. On the other hand, tumble bias was a less reliable measure. It was very sensitive to the threshold values in speed which were used to identify tumbles. The end of a tumble is a somewhat ambiguous event, because the flagellar bundle slowly coalesces and the linear speed gradually increases following a tumble event.

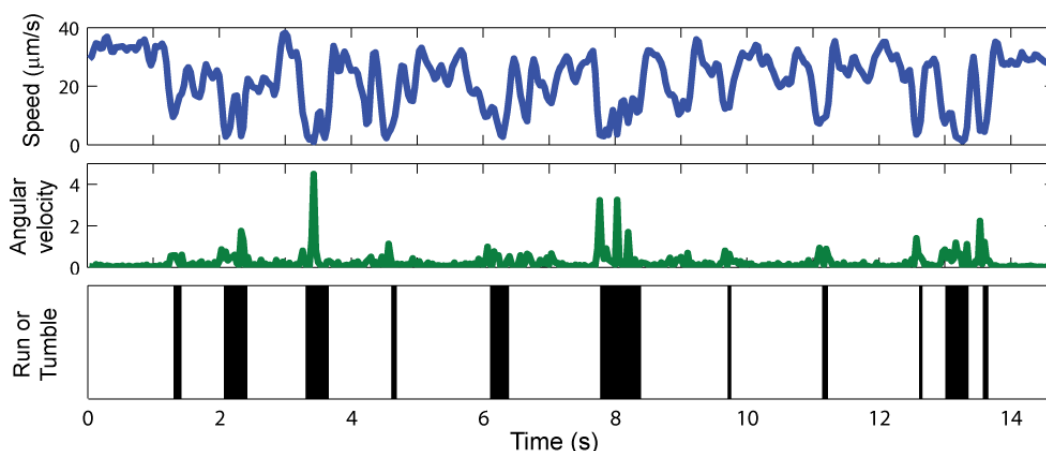


Figure 7.2: Extracting statistics from 2D swimming trajectories. Swimming speed (top, blue) and angular velocity (middle, green) were calculated for each cell, using the cell's location over time. Tumbles were identified when swimming speed drops below a threshold and angular velocity increases above a threshold (bottom, tumbles = black, runs = white). Run-tumble statistics were calculated from this binary signal.

The assay was very useful for identifying and characterizing swimming mutants. For example, runner and tumbler mutants were easily distinguished from wild-type cells by viewing their trajectories (**Figure 7.1B-D**). At a quantitative level, the 2D assay was used to characterize the tumble frequency of the inducible CheY* mutant strain as a function of the inducer which promotes production of the CheY* protein which increases the probability of tumbling (see **Figure 4.2**). I have also used the 2D assay to characterize the tumble frequency of a CheY-YFP mutant (strain CR41, **Appendix C.1**). In that strain, I found that even without inducer, the cells were much more tumbly than wild-type cells. This led me to create a series of new mutant strains in order to create a CheY-YFP strain whose range of inducible tumble frequencies spanned the range of values observed in wild-type cells (PM94).

7.2.2 Angle change during tumbles

A unique measurement that can only be provided by cell-tracking assays is the angular change in direction during a tumble (which I call “tumble angles”). When a cell tumbles, it reorients and then begins running in a new direction. The change in direction is random, but the distribution is not uniform. **Figure 7.3A** shows the distribution of Tumble Angles from a population of wild-type cells. The distribution is not uniform. Cells are more likely to continue running in the same general direction than to change direction by more than 90°. 180° changes in direction are very uncommon. This is consistent with previous results from a 3D tracking assay which found a distribution peaked at about 60 degrees [26].

This distribution of tumble angles acted as a useful control for our first study of trapped swimming cells [2]. In that study, we found that the flagellar bundle could form on either side of the trapped cell (in the absence of external fluid flow.) The bundle switched sides about once out of every 6 tumbles, or about 18% of the time. For free swimming cells, a bundle switching sides would correspond to a tumble in which the tumble angle was greater than 90 degrees. The trap result was in excellent agreement with the 2D assay. The fraction of tumbles that resulted in a tumble angle greater than 90 degrees was also 18%. (**Figure 7.3A**, right of red dashed line).

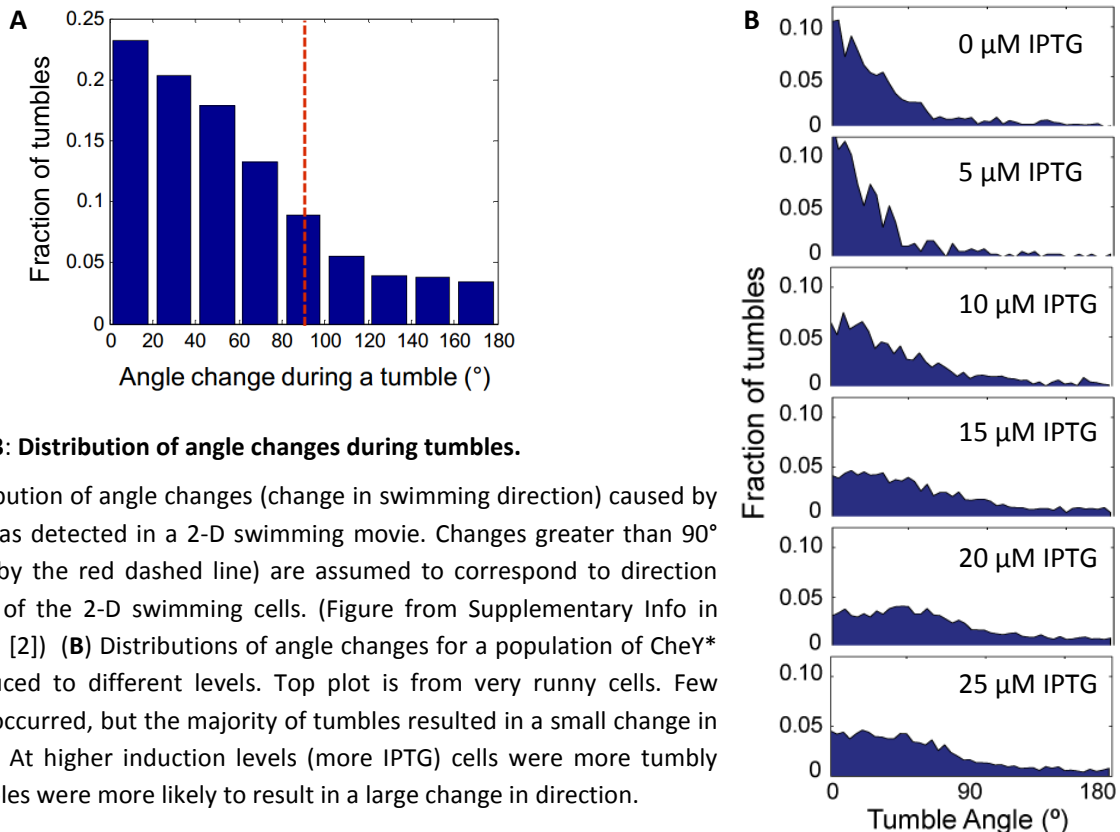


Figure 7.3: Distribution of angle changes during tumbles.

(A) Distribution of angle changes (change in swimming direction) caused by tumbles, as detected in a 2-D swimming movie. Changes greater than 90° (marked by the red dashed line) are assumed to correspond to direction reversals of the 2-D swimming cells. (Figure from Supplementary Info in *Min et al.* [2]) (B) Distributions of angle changes for a population of CheY* cells induced to different levels. Top plot is from very runny cells. Few tumbles occurred, but the majority of tumbles resulted in a small change in direction. At higher induction levels (more IPTG) cells were more tumbly and tumbles were more likely to result in a large change in direction.

I also measured the tumble angle change for CheY* mutant cells induced at different concentrations (**Figure 7.3B**). In cells with a higher induction level, and therefore a higher concentration of CheY*, tumbles were more common, as expected. Additionally, I found that the average tumble angle was larger in the more tumbling cells. In other words, when these cells tumbled, they more likely to resume running in a very different direction from their initial trajectory. This makes sense, given that these tumbles probably involve more CW rotating flagella and also lasted longer.

7.3 Chemotaxis adaptation

Our second paper utilizing the bacterial trapping assay investigated chemotaxis adaptation [15]. This is the phenomenon whereby a cell that has been exposed to a large, sudden change in environment eventually becomes accustomed to the new condition and resumes normal run-tumble behavior. Immediately after being exposed to a large increase in aspartate concentration (an attractant for *E. coli*) cells entered a prolonged run. The duration of this run increased at higher concentrations of attractant [15]. But eventually the cells adapted to the new environment and began tumbling again. Adaptation is a crucial and ubiquitous feature in all organisms that respond to their environment.

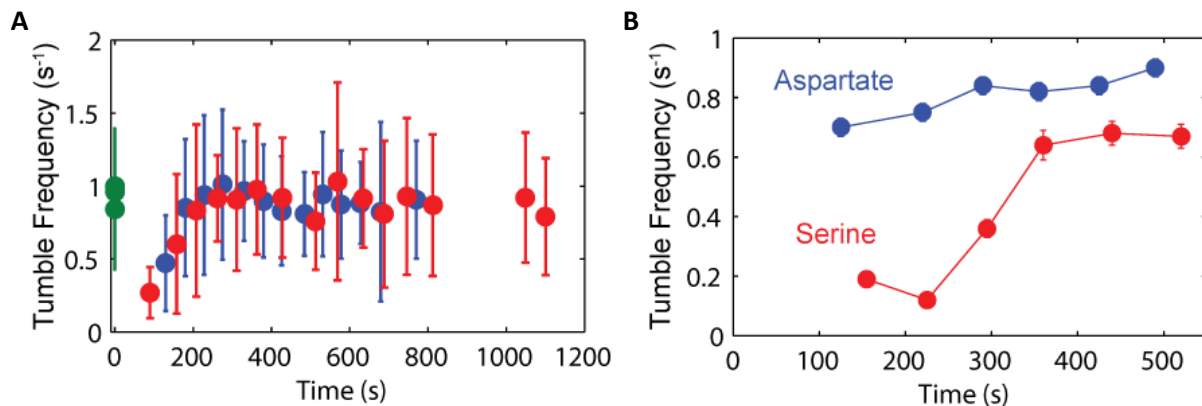


Figure 7.4: Chemotaxis adaptation in 2D swimming movies. (A) Chemotaxis adaptation of wild-type cells to aspartate (100 μM). Prior to stimulus, the tumble frequency was about 1 tumble per second (green). Two repeats showed the same adaptation time, ~200 s (red and blue). Each data point is the mean tumble frequency from a population of cells in a 30-s 2D swimming movie. Error bars are standard deviation between cells. (B) Chemotaxis adaptation responses of Δ Tar mutant strain. When exposed to Serine (100 μM) cells initially run, and eventually adapt to the new environment (red). When exposed to aspartate (100 μM) cells do not respond. Tumble behavior remains approximately unchanged (blue). For strain info see **Appendix C.1**.

Once again, we used the 2D assay as a control for the trap assay. **Figure 7.4A** shows the adaptation response of wild-type cells to a 100 μM aspartate stimulus (strain RP437, **Appendix C.1**, protocol in **Appendix B.7**). Adaptation takes about 200-seconds. The assay was very useful for testing mutant strains, especially when trying to develop a new strain to study the effect of a particular gene or

protein. For example, we were interested in testing a mutant strain in which the Tar receptor, which senses aspartate, was deleted (strain RP2361, **Appendix C.1**). To verify that the receptors had successfully been removed, we performed adaptation with two different stimulants. As a positive control, we exposed these cells to serine, and saw that they adapted as expected (**Figure 7.4B**). When exposed to aspartate, cells continued tumbling at approximately the same rate that they had prior to stimulus. This confirmed that the cells were not sensitive to aspartate.

7.4 Flagella dilution experiments

To complement the trap experiments investigating cells with different numbers of flagella per cell (**Chapter 4-6**), I designed a flagella-dilution experiment. The idea was to grow separate populations of wild-type cells with different average numbers of flagella per cell. These could then be tested in the 2D assay to see how swimming speed and tumble frequency were affected by flagellar number.

To understand the assay requires a brief description about how flagella are constructed. During exponential growth phase, bacteria continually produce new flagella. Under typical growth conditions for swimming cells, each cell doubles in length and divides into two daughter cells every 45 minutes. To maintain a consistent density of flagella per cell, this means that the number of flagella must double every 45 minutes. To explain such rapid growth a model was proposed in which cells begin producing 16 new flagella each generation [77]. Flagella are constructed from the bottom up. The entire process is tightly regulated [47, 82, 83]. It takes about two generations to construct the flagellar motor [77]. Once the motor is constructed, flagellin (FliC) is pumped through the motor and attaches to the distal end of the new flagellum [30]. Growth continues with subsequent flagellin molecules flowing through the existing flagellum and attaching to the distal end of the flagellum. In this way, new flagella are continually constructed and existing flagella continually grow.

7.4.1 Producing populations of cells with different numbers of flagella

To obtain populations of cells with different mean numbers flagella per cell I used a strain in which flagella production was controlled by an inducible promoter. Our collaborator, Chris Rao (UIUC), created a strain in which the master regulator for all chemotaxis machinery (*flhDC*) is under the control of a tetracycline promoter (MG1655TPOP, see **Appendix C.1**). In the presence of anhydrous-tetracycline (aTc), these cells grow flagella and produce all of the chemotaxis and flagellar motor proteins. Without aTc, cells stop producing flagella. A detailed protocol is provided in **Appendix B.7**. Briefly, cells were grown under normal conditions, with aTc to promote flagella production, and harvested at mid-exponential growth phase. Cells were then washed and resuspended in growth medium without aTc. As

a result cells stopped producing flagella. Each time a cell divided, the existing flagella were split between the two daughter cells, decreasing the average number of flagella per cell (**Figure 7.5A**). To verify this, cells were labeled with a fluorescent dye, following the protocol used in [127] (**Appendix B.1**). Flagella were also counted using electron microscopy (**Chapter 2, Figure 7.6**). The result was a set of populations with different mean numbers of flagella per cell (**Figures 7.5C and 7.6**).

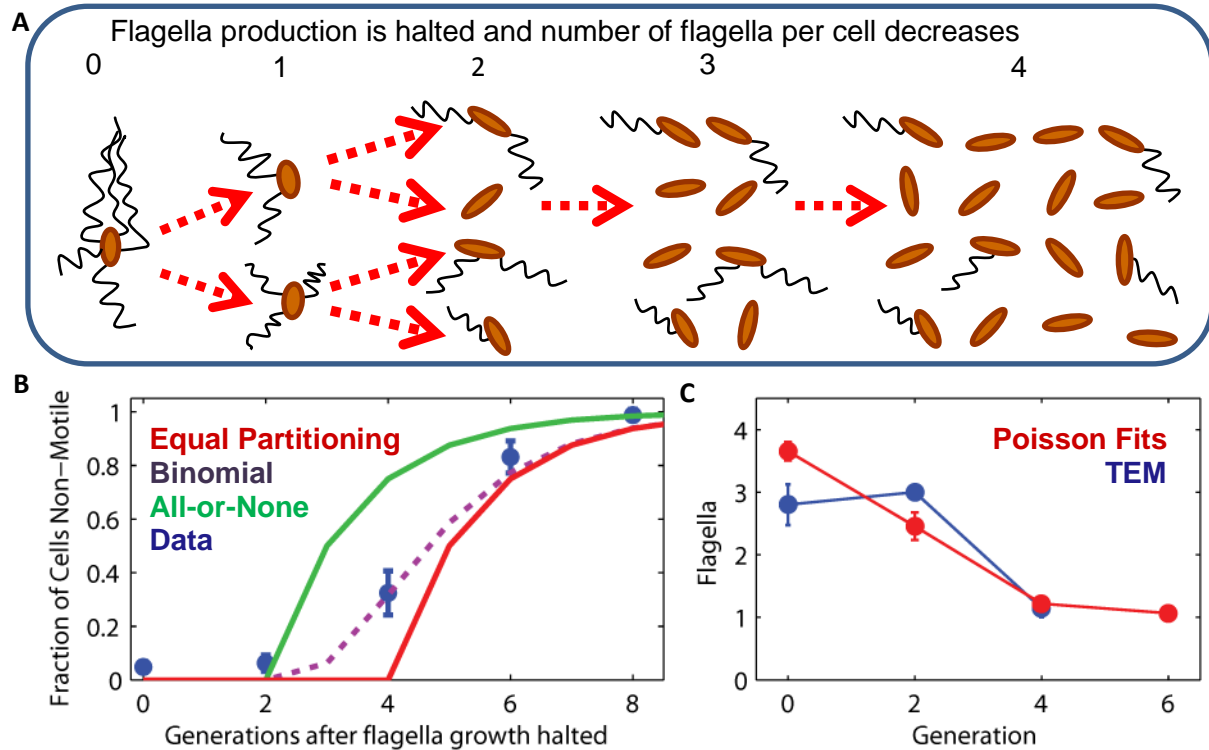


Figure 7.5: Producing cells with different numbers of flagella. (A) Flagella production was halted at generation zero. The average number of flagella per cell is halved every generation, as cells divide. (B) Experimental evidence for flagella dilution. As a fixed number of flagella are split between increasing numbers of cells, there emerges a large fraction of cells that no longer swim because they have no flagella. Data from 2-D swimming movies (blue) agrees with predictions from theoretical model of binomial partitioning of flagella between daughter cells (purple dashed line). Note that there is a two-generation delay before flagella start diluting, because those flagellar motors had already been produced and it takes some time for fliC production to completely stop. (C) Average number of flagella on swimming cells (excluding cells with zero flagella), determined by counting from electron microscopy images (blue) and using the fraction of cells non-motile in (B) while assuming a Poisson distribution (red). See **Figure 7.6** for distributions.

Unfortunately, after performing these experiments, I realized a problem with the experimental design. I wanted to study the isolated effect of flagella number. But the dilution protocol stopped production of all chemotaxis and flagellar motor proteins, not just flagella. Therefore, there were many other changing factors which might also have affected the behavior of cells in the experiment. Because there are a large number of chemotaxis and motor proteins, the effects of decreasing the concentration

of all of these proteins is not obvious. Therefore, I present the results from this assay with the caveat that they should be repeated using a different strain in which flagella production is decoupled from the rest of the chemotaxis and flagellar machinery.

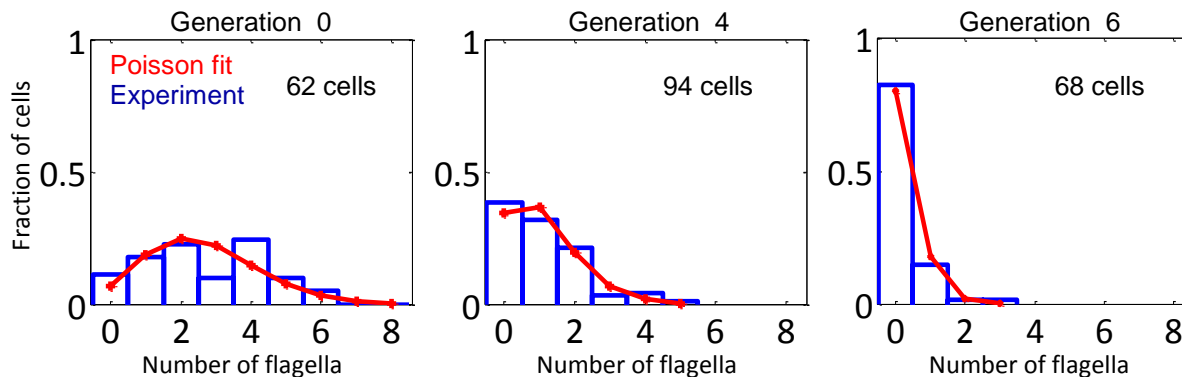


Figure 7.6: Counting flagella at different generations after flagella production halted. (A) Cells that have been grown continuously in the presence of aTc inducer, so flagella have been growing continuously. Flagella distribution is similar to that of wild-type cells (Chapter 2). (B) Distribution from a population of cells 2 generations after flagella production has been halted (4 generations after removal of aTc). Cells have fewer flagella on average. (C) After 4 generations, the majority of cells have zero flagella. The majority of remaining swimming cells have only 1 flagellum.

7.4.2 Effect of flagella number on swimming parameters

I have determined the dependence of several swimming parameters on flagella number by combining this dilution method and the 2D assay. Swimming speed appears to increase slightly with the number of flagella (Figure 7.7A). It makes intuitive sense that additional flagella would cause cells to swim faster, because they provide additional propulsive force. Cells with an average of 4 flagella swam about twice as fast as cells with only one flagellum. So doubling the number of flagella increased speed,

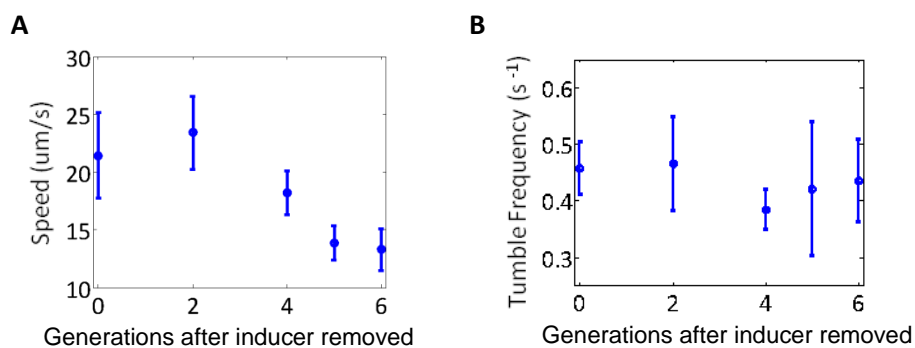


Figure 7.7: Swimming parameters as a function of flagella number. (A) Average swimming speed in different populations of cells. Later generations have less flagella (see Figure 7.6). Swimming speed decreases in populations with a lower average number of flagella per cell. (B) Average tumble frequency. Similar to the trap assay tumble frequency does not appear to depend on the number of flagella per cell.

but did not quite double the propulsive force. This is in qualitative agreement with previous works which suggested that additional flagella did not result in a significant increase in torque generated by the flagellar bundle [127, 128].

On the other hand, tumble frequency appeared uncorrelated with flagella number (**Figure 7.7B**). This is in agreement with my results from the trap assay in **Chapter 4** and **Chapter 6**. In **Chapter 6**, I found that the tumble frequency had a small, statistically insignificant correlation with flagella number. The evidence from the 2D assay corroborates evidence from the trap. As mentioned above, this data is somewhat suspect because of the experimental design, so results should not be viewed as conclusive.

7.5 Future Directions

7.5.1 2D dilution experiment with strain HCB1660

The 2D dilution experiment offers a great way to look at the effects of flagellar number at the population level, and provides some measurements that cannot be made in the trap, such as swimming speed. As discussed above, the current iteration of the protocol used a strain in which all chemotaxis and flagellar proteins were shut off together. So it is impossible to determine if the observed features are the result of differences in flagellar number, or if they are due to other changes in the chemotaxis network. This can be fixed by repeating the experiment with a different strain; one in which flagella production is decoupled from the rest of the chemotaxis network. Fortunately we already have a strain in which flagella production can be controlled without affecting any of the other chemotaxis genes. Strain HCB1660, the strain which was used in **Chapters 2** and **4-6**, and referred to as “wild-type for chemotaxis”, expresses *FliC*^{S219C} from a plasmid. The native *fliC* gene is deleted, so flagella production is controlled by the concentration of inducer in the growth media (**Appendix C.2**). The protocol for the dilution can be followed exactly using strain HCB1660, using arabinose instead of aTc as the inducer for flagella production. The results from the strain will be conclusive because chemotaxis proteins will be unaffected throughout the experiment; the only changing parameter will be the average number of flagella per cell.

7.5.2 Step-down chemotaxis adaptation with CheB mutant

Chemotaxis adaptation experiments in the trap revealed that step-down adaptation is much faster than step-up adaptation [15]. Step-up adaptation to 1 mM aspartate took several minutes, while step-down adaptation from 1 mM to zero aspartate took only about fifteen seconds. It is believed that step-down adaptation is faster because the chemotaxis network has an additional feedback loop which

accelerates the rate of adaptation to negative stimuli [129]. Adaptation is governed by the methylation and demethylation of chemotaxis receptors by a pair of proteins called CheR and CheB. CheR adds methyl groups and CheB removes them. When cells experience a large negative stimulus, CheB gets phosphorylated, which increases its activity by a factor of about 70 [130]. In chemotaxis models, fast step-down adaptation is attributed to this phosphorylation of CheB. However, the chemotaxis network in *E. coli* has frequently proven to have multiple, unexpected and redundant levels of adaptation and control [109, 131]. Therefore, it is important to quantify the effects of CheB phosphorylation, and determine whether or not it is entirely capable of explaining the observed rates of step-down adaptation.

Experiments have not been done to measure the effect of CheB phosphorylation on chemotaxis adaptation. We could use the 2D assay and the trap assay to measure step-down adaptation in a strain expressing a mutant CheB which cannot be phosphorylated. Strain PM10 has a mutation which prevents it from being phosphorylated [129] (**Appendix C.1**). Based on current models, we would expect that step-down adaptation times would be much longer in this strain than they were in the wild-type strain. In our previous studies, step-down adaptation occurred too quickly to be observed in the 2D adaptation assay. If the CheB mutant successfully slows down the rate of adaptation, we should be able to see the adaptation response in the 2D assay. Either way, we can observe adaptation at the single-cell level, with higher temporal resolution in the trap assay, following the protocol in *Min et al.* [15].

7.6 Summary

In this chapter I described the 2D assay which served as a complementary assay for assessing the swimming behavior of bacterial strains which were studied in the optical trap. I showed that the average tumble angle is larger in tumbling cells, and that wild-type cells change direction by more than 90 degrees in about 1 out of every 6 tumbles. I presented chemotaxis adaptation results from wild-type cells and a Δ Tar mutant exposed to aspartate and serine stimuli. As expected the Δ Tar mutant responded to serine but was unaffected by the addition of aspartate. Finally, I described the flagella-dilution protocol which I developed to study populations of cells with different numbers of flagella. The preliminary results matched those from the trap assay, in that the tumble frequency was apparently unaffected by flagellar number. However, future studies should be conducted with a strain in which flagellin production is decoupled from the chemotaxis machinery, to confirm that these results are entirely due to changes in flagellar number.

References

1. Alon, U., et al., *Robustness in bacterial chemotaxis*. Nature, 1999. **397**(6715): p. 168-171.
2. Min, T.L., et al., *High-resolution, long-term characterization of bacterial motility using optical tweezers*. Nat Methods, 2009. **6**(11): p. 831-5.
3. Comstock, M.J., T. Ha, and Y.R. Chemla, *Ultra-high-resolution optical trap with single-fluorophore sensitivity*. Nat Methods, 2011. **8**(4): p. 335-40.
4. Berg, H.C., *E. coli in motion*. Biological and medical physics series. 2004, New York: Springer. xi, 133 p., [1] col. plate.
5. Adler, J., *A method for measuring chemotaxis and use of the method to determine optimum conditions for chemotaxis by Escherichia coli*. J Gen Microbiol, 1973. **74**: p. 77-91.
6. Adler, J. and B. Templeton, *The effect of environmental conditions on the motility of Escherichia coli*. J Gen Microbiol, 1967. **46**(2): p. 175-84.
7. Adler, J., *Chemotaxis in bacteria*. Science, 1966. **153**(737): p. 708-16.
8. Adler, J., *Effect of amino acids and oxygen on chemotaxis in Escherichia coli*. J Bacteriol, 1966. **92**: p. 121-9.
9. Tisa, L.S., J.J. Sekelsky, and J. Adler, *Effects of organic antagonists of Ca(2+), Na(+), and K(+) on chemotaxis and motility of escherichia coli*. J Bacteriol, 2000. **182**: p. 4856-61.
10. Yang, H., H. Inokuchi, and J. Adler, *Phototaxis away from blue light by an Escherichia coli mutant accumulating protoporphyrin IX*. Proc Natl Acad Sci U S A, 1995. **92**(16): p. 7332-6.
11. Li, C. and J. Adler, *Escherichia coli shows two types of behavioral responses to osmotic upshift*. J Bacteriol, 1993. **175**: p. 2564-7.
12. Adler, J., G.L. Hazelbauer, and M.M. Dahl, *Chemotaxis toward sugars in Escherichia coli*. J Bacteriol, 1973. **115**: p. 824-47.
13. Mesibov, R. and J. Adler, *Chemotaxis toward amino acids in Escherichia coli*. J Bacteriol, 1972. **112**: p. 315-26.
14. Alon, U., *An introduction to systems biology : design principles of biological circuits*. Chapman & Hall/CRC mathematical and computational biology series. 2007, Boca Raton, FL: Chapman & Hall/CRC. xvi, 301 p., [4] p. of plates.
15. Min, T.L., et al., *Chemotactic adaptation kinetics of individual Escherichia coli cells*. Proc Natl Acad Sci U S A, 2012. **109**: p. 9869-74.
16. Park, H., et al., *Interdependence of behavioural variability and response to small stimuli in bacteria*. Nature, 2010. **468**(7325): p. 819-23.
17. Shimizu, T.S., Y. Tu, and H.C. Berg, *A modular gradient-sensing network for chemotaxis in Escherichia coli revealed by responses to time-varying stimuli*. Mol Syst Biol, 2010. **6**: p. 382.
18. Kalinin, Y.V., et al., *Logarithmic sensing in Escherichia coli bacterial chemotaxis*. Biophys J, 2009. **96**: p. 2439-48.
19. Wadhams, G.H. and J.P. Armitage, *Making sense of it all: bacterial chemotaxis*. Nat Rev Mol Cell Biol, 2004. **5**(12): p. 1024-37.
20. Sourjik, V. and H.C. Berg, *Receptor sensitivity in bacterial chemotaxis*. Proc Natl Acad Sci U S A, 2002. **99**(1): p. 123-7.
21. Jasuja, R., et al., *Chemotactic responses of Escherichia coli to small jumps of photoreleased L-aspartate*. Biophys J, 1999. **76**(3): p. 1706-19.
22. Neidhardt, F.C., *Escherichia coli and Salmonella: Cellular and Molecular Biology, 2nd Edition*. 1996: ASM Press; 2 edition (May 1996). 2822.
23. Lutz, R. and H. Bujard, *Independent and Tight Regulation of Transcriptional Units in Escherichia Coli Via the LacR/O, the TetR/O and AraC/I1-I2 Regulatory Elements*. Nucl. Acids Res., 1997. **25**(6): p. 1203-1210.

24. Keseler, I.M., et al., *EcoCyc: fusing model organism databases with systems biology*. Nucleic Acids Res, 2013. **41**(Database issue): p. D605-12.
25. Zhou, J. and K.E. Rudd, *EcoGene 3.0*. Nucleic Acids Res, 2013. **41**(Database issue): p. D613-24.
26. Berg, H.C. and D.A. Brown, *Chemotaxis in Escherichia coli analysed by three-dimensional tracking*. Nature, 1972. **239**: p. 500-4.
27. Khan, S. and R.M. Macnab, *The steady-state counterclockwise/clockwise ratio of bacterial flagellar motors is regulated by protonmotive force*. J Mol Biol, 1980. **138**: p. 563-97.
28. Gabel, C.V. and H.C. Berg, *The speed of the flagellar rotary motor of Escherichia coli varies linearly with protonmotive force*. Proc Natl Acad Sci U S A, 2003. **100**(15): p. 8748-51.
29. Mears, P.J., et al., *Escherichia coli swimming is robust against variations in flagellar number*. Elife, 2014. **3**: p. e01916.
30. Turner, L., A.S. Stern, and H.C. Berg, *Growth of flagellar filaments of Escherichia coli is independent of filament length*. J Bacteriol, 2012. **194**(10): p. 2437-42.
31. Turner, L., W.S. Ryu, and H.C. Berg, *Real-time imaging of fluorescent flagellar filaments*. J Bacteriol, 2000. **182**(10): p. 2793-801.
32. Macnab, R.M., *Examination of bacterial flagellation by dark-field microscopy*. J Clin Microbiol, 1976. **4**: p. 258-65.
33. Purcell, E.M., *The efficiency of propulsion by a rotating flagellum*. Proc Natl Acad Sci U S A, 1997. **94**(21): p. 11307-11.
34. Purcell, E.M., *Life at Low Reynolds-Number*. American Journal of Physics, 1977. **45**(1): p. 3-11.
35. Kim, M., et al., *A macroscopic scale model of bacterial flagellar bundling*. Proc Natl Acad Sci U S A, 2003. **100**(26): p. 15481-5.
36. Alon, U., et al., *Response regulator output in bacterial chemotaxis*. EMBO J, 1998. **17**(15): p. 4238-48.
37. Segall, J.E., S.M. Block, and H.C. Berg, *Temporal comparisons in bacterial chemotaxis*. Proc Natl Acad Sci U S A, 1986. **83**(23): p. 8987-91.
38. Sourjik, V. and H.C. Berg, *Binding of the Escherichia coli response regulator CheY to its target measured in vivo by fluorescence resonance energy transfer*. Proc Natl Acad Sci U S A, 2002. **99**(20): p. 12669-74.
39. Cluzel, P., M. Surette, and S. Leibler, *An ultrasensitive bacterial motor revealed by monitoring signaling proteins in single cells*. Science, 2000. **287**(5458): p. 1652-1655.
40. Emonet, T., et al., *AgentCell: a digital single-cell assay for bacterial chemotaxis*. Bioinformatics, 2005. **21**(11): p. 2714-2721.
41. Emonet, T. and P. Cluzel, *Relationship between cellular response and behavioral variability in bacterial chemotaxis*. Proceedings of the National Academy of Sciences of the United States of America, 2008. **105**(9): p. 3304-3309.
42. Andrews, B.W., T.M. Yi, and P.A. Iglesias, *Optimal noise filtering in the chemotactic response of Escherichia coli*. PLoS Comput Biol, 2006. **2**: p. e154.
43. Tu, Y., T.S. Shimizu, and H.C. Berg, *Modeling the chemotactic response of Escherichia coli to time-varying stimuli*. Proc Natl Acad Sci U S A, 2008. **105**(39): p. 14855-60.
44. Vladimirov, N., et al., *Dependence of bacterial chemotaxis on gradient shape and adaptation rate*. PLoS Comput Biol, 2008. **4**(12): p. e1000242.
45. Yuan, J. and H.C. Berg, *Ultrasensitivity of an adaptive bacterial motor*. J Mol Biol, 2013. **425**(10): p. 1760-4.
46. Korobkova, E.A., et al., *Hidden stochastic nature of a single bacterial motor*. Phys Rev Lett, 2006. **96**(5): p. 058105.
47. Kalir, S., et al., *Ordering genes in a flagella pathway by analysis of expression kinetics from living bacteria*. Science, 2001. **292**: p. 2080-3.

48. Saini, S., et al., *FliZ Is a posttranslational activator of FlhD4C2-dependent flagellar gene expression*. J Bacteriol, 2008. **190**(14): p. 4979-88.
49. Smith, T.G. and T.R. Hoover, *Deciphering bacterial flagellar gene regulatory networks in the genomic era*. Adv Appl Microbiol, 2009. **67**: p. 257-95.
50. Kalir, S., S. Mangan, and U. Alon, *A coherent feed-forward loop with a SUM input function prolongs flagella expression in Escherichia coli*. Mol Syst Biol, 2006. **1**: p. 2005 0006.
51. Suzuki, H., K. Yonekura, and K. Namba, *Structure of the rotor of the bacterial flagellar motor revealed by electron cryomicroscopy and single-particle image analysis*. J Mol Biol, 2004. **337**(1): p. 105-13.
52. Ryu, W.S., R.M. Berry, and H.C. Berg, *Torque-generating units of the flagellar motor of Escherichia coli have a high duty ratio*. Nature, 2000. **403**: p. 444-7.
53. Arkhipov, A., et al., *Coarse-grained molecular dynamics simulations of a rotating bacterial flagellum*. Biophys J, 2006. **91**: p. 4589-97.
54. Yonekura, K., S. Maki-Yonekura, and K. Namba, *Complete atomic model of the bacterial flagellar filament by electron cryomicroscopy*. Nature, 2003. **424**(6949): p. 643-50.
55. Samatey, F.A., et al., *Structure of the bacterial flagellar hook and implication for the molecular universal joint mechanism*. Nature, 2004. **431**(7012): p. 1062-8.
56. Darnton, N.C., et al., *On torque and tumbling in swimming Escherichia coli*. Journal of Bacteriology, 2007. **189**(5): p. 1756-1764.
57. Cohen-Ben-Lulu, G.N., et al., *The bacterial flagellar switch complex is getting more complex*. EMBO J, 2008. **27**: p. 1134-44.
58. Vigeant, M.A. and R.M. Ford, *Interactions between motile Escherichia coli and glass in media with various ionic strengths, as observed with a three-dimensional-tracking microscope*. Appl Environ Microbiol, 1997. **63**(9): p. 3474-9.
59. Frymier, P.D., et al., *Three-dimensional tracking of motile bacteria near a solid planar surface*. Proc Natl Acad Sci U S A, 1995. **92**(13): p. 6195-9.
60. Amsler, C.D., *Use of computer-assisted motion analysis for quantitative measurements of swimming behavior in peritrichously flagellated bacteria*. Anal Biochem, 1996. **235**(1): p. 20-5.
61. Staropoli, J.F. and U. Alon, *Computerized analysis of chemotaxis at different stages of bacterial growth*. Biophysical Journal, 2000. **78**(1): p. 513-519.
62. Korobkova, E., et al., *From molecular noise to behavioural variability in a single bacterium*. Nature, 2004. **428**(6982): p. 574-578.
63. Fahrner, K.A., W.S. Ryu, and H.C. Berg, *Biomechanics: bacterial flagellar switching under load*. Nature, 2003. **423**(6943): p. 938.
64. Berg, H.C., et al., *Computerized Video Analysis of Tethered Bacteria*. Review of Scientific Instruments, 1987. **58**: p. 418-423.
65. Block, S.M., J.E. Segall, and H.C. Berg, *Impulse Responses in Bacterial Chemotaxis*. Cell, 1982. **31**(1): p. 215-226.
66. Kentner, D. and V. Sourjik, *Dynamic map of protein interactions in the Escherichia coli chemotaxis pathway*. Mol Syst Biol, 2009. **5**: p. 238.
67. Sourjik, V., et al., *In vivo measurement by FRET of pathway activity in bacterial chemotaxis*. Methods Enzymol, 2007. **423**: p. 365-91.
68. Vaknin, A. and H.C. Berg, *Single-cell FRET imaging of phosphatase activity in the Escherichia coli chemotaxis system*. Proceedings of the National Academy of Sciences of the United States of America, 2004. **101**(49): p. 17072-17077.
69. Ashkin, A., J.M. Dziedzic, and T. Yamane, *Optical Trapping and Manipulation of Single Cells Using Infrared-Laser Beams*. Nature, 1987. **330**(6150): p. 769-771.
70. Ashkin, A., et al., *Observation of a single-beam gradient force optical trap for dielectric particles*.

- Opt Lett, 1986. **11**(5): p. 288.
71. Horner, F., et al., *Full 3D translational and rotational optical control of multiple rod-shaped bacteria*. Journal of Biophotonics, 2010. **3**: p. 468-475.
 72. Leitz, G., et al., *Stress response in Caenorhabditis elegans caused by optical tweezers: wavelength, power, and time dependence*. Biophys J, 2002. **82**(4): p. 2224-31.
 73. Xiao, J., et al., *Imaging Gene Expression in Living Cells at the Single-Molecule Level in Single Molecule Techniques A Laboratory Manual*, P.Selvin, T.J. Ha, Editor. 2008, Cold Spring Harbor, N.Y.: Cold Spring Harbor Laboratory Press. vii, 507 p.
 74. Yildiz, A., et al., *Myosin V walks hand-over-hand: single fluorophore imaging with 1.5-nm localization*. Science, 2003. **300**(5628): p. 2061-5.
 75. Golding, I., et al., *Real-time kinetics of gene activity in individual bacteria*. Cell, 2005. **123**(6): p. 1025-36.
 76. Joo, C. and T. Ha, *Single-Molecule FRET with Total Internal Reflection Microscopy, in Single-Molecule Techniques: A Laboratory Manual*, P. Selvin, T.J. Ha, Editor. 2008, Cold Spring Harbor, N.Y.: Cold Spring Harbor Laboratory Press. vii, 507 p.
 77. Aizawa, S.I. and T. Kubori, *Bacterial flagellation and cell division*. Genes Cells, 1999. **3**: p. 625-34.
 78. Kudo, S., Y. Magariyama, and S. Aizawa, *Abrupt changes in flagellar rotation observed by laser dark-field microscopy*. Nature, 1990. **346**: p. 677-80.
 79. Magariyama, Y., et al., *Simultaneous measurement of bacterial flagellar rotation rate and swimming speed*. Biophys J, 1995. **69**: p. 2154-62.
 80. Hesse, W.R. and M.J. Kim, *Visualization of flagellar interactions on bacterial carpets*. J Microsc, 2009. **233**: p. 302-8.
 81. Berg, H.C., *The rotary motor of bacterial flagella*. Annu Rev Biochem, 2003. **72**: p. 19-54.
 82. Macnab, R.M., *How bacteria assemble flagella*. Annu Rev Microbiol, 2003. **57**: p. 77-100.
 83. Aldridge, P. and K.T. Hughes, *Regulation of flagellar assembly*. Curr Opin Microbiol, 2002. **5**: p. 160-5.
 84. Parkinson, J.S. and S.E. Houts, *Isolation and behavior of Escherichia coli deletion mutants lacking chemotaxis functions*. J Bacteriol, 1982. **151**(1): p. 106-13.
 85. Saini, S., et al., *FlhZ Induces a Kinetic Switch in Flagellar Gene Expression*. Journal of Bacteriology, 2010. **192**(24): p. 6477-6481.
 86. Kalir, S. and U. Alon, *Using a quantitative blueprint to reprogram the dynamics of the flagella gene network*. Cell, 2004. **117**: p. 713-20.
 87. Ashkin, A. and J.M. Dziedzic, *Optical trapping and manipulation of viruses and bacteria*. Science, 1987. **235**(4795): p. 1517-20.
 88. Koshland, D.E., Jr., *A response regulator model in a simple sensory system*. Science, 1977. **196**(4294): p. 1055-63.
 89. Rowe, A.D., et al., *Rapid rotation of micron and submicron dielectric particles measured using optical tweezers*. Journal of Modern Optics, 2003. **50**(10): p. 1539-1554.
 90. Chattopadhyay, S., et al., *Swimming efficiency of bacterium Escherichia coli*. Proceedings of the National Academy of Sciences of the United States of America, 2006. **103**(37): p. 13712-13717.
 91. Neuman, K.C., et al., *Characterization of photodamage to Escherichia coli in optical traps*. Biophysical Journal, 1999. **77**(5): p. 2856-2863.
 92. Rasmussen, M.B., L.B. Oddershede, and H. Siegmundfeldt, *Optical tweezers cause physiological damage to Escherichia coli and Listeria bacteria*. Appl Environ Microbiol, 2008. **74**(8): p. 2441-6.
 93. Matthaus, F., M. Jagodic, and J. Dobnikar, *E. coli Superdiffusion and Chemotaxis-Search Strategy, Precision, and Motility*. Biophysical Journal, 2009. **97**(4): p. 946-957.
 94. Silverman, M. and M. Simon, *Flagellar rotation and the mechanism of bacterial motility*. Nature, 1974. **249**(452): p. 73-4.

95. Larsen, S.H., et al., *Change in Direction of Flagellar Rotation Is Basis of Chemotactic Response in Escherichia-Coli*. Nature, 1974. **249**: p. 74-77.
96. Lang, M.J., et al., *Simultaneous, coincident optical trapping and single-molecule fluorescence*. Nat Methods, 2005. **1**: p. 133-9.
97. Gittes, F. and C.F. Schmidt, *Interference model for back-focal-plane displacement detection in optical tweezers*. Opt Lett, 1998. **23**(1): p. 7-9.
98. Moffitt, J.R., et al., *Differential detection of dual traps improves the spatial resolution of optical tweezers*. Proceedings of the National Academy of Sciences of the United States of America, 2006. **103**(24): p. 9006-9011.
99. Brau, R.R., et al., *Interlaced optical force-fluorescence measurements for single molecule biophysics*. Biophys J, 2006. **91**(3): p. 1069-77.
100. Schulmeister, S., et al., *Protein exchange dynamics at chemoreceptor clusters in Escherichia coli*. Proc Natl Acad Sci U S A, 2008. **105**(17): p. 6403-8.
101. Wu, K., et al., *Attractant binding induces distinct structural changes to the polar and lateral signaling clusters in Bacillus subtilis chemotaxis*. J Biol Chem, 2011. **286**(4): p. 2587-95.
102. Ishihara, A., et al., *Coordination of Flagella on Filamentous Cells of Escherichia-Coli*. Journal of Bacteriology, 1983. **155**(1): p. 228-237.
103. Bray, D., M.D. Levin, and K. Lipkow, *The chemotactic behavior of computer-based surrogate bacteria*. Curr Biol, 2007. **17**: p. 12-9.
104. Jiang, L.L., O.Y. Qi, and Y.H. Tu, *Quantitative Modeling of Escherichia coli Chemotactic Motion in Environments Varying in Space and Time*. Plos Computational Biology, 2010. **6**(4).
105. Flores, M., et al., *Signaling noise enhances chemotactic drift of E. coli*. Phys Rev Lett, 2012. **109**: p. 148101.
106. Turner, L., et al., *Visualization of Flagella during bacterial Swarming*. J Bacteriol, 2010. **192**: p. 3259-67.
107. Yuan, J., K.A. Fahrner, and H.C. Berg, *Switching of the bacterial flagellar motor near zero load*. J Mol Biol, 2009. **390**(3): p. 394-400.
108. Terasawa, S., et al., *Coordinated Reversal of Flagellar Motors on a Single Escherichia coli Cell*. Biophys J, 2011. **100**(9): p. 2193-200.
109. Vladimirov, N., D. Lebiedz, and V. Sourjik, *Predicted Auxiliary Navigation Mechanism of Peritrichously Flagellated Chemotactic Bacteria*. Plos Computational Biology, 2010. **6**(3).
110. Spiro, P.A., J.S. Parkinson, and H.G. Othmer, *A model of excitation and adaptation in bacterial chemotaxis*. Proc Natl Acad Sci U S A, 1997. **94**(14): p. 7263-8.
111. Sneddon, M.W., W. Pontius, and T. Emonet, *Stochastic coordination of multiple actuators reduces latency and improves chemotactic response in bacteria*. Proc Natl Acad Sci U S A, 2012. **109**: p. 805-10.
112. Bai, F., et al., *Conformational spread as a mechanism for cooperativity in the bacterial flagellar switch*. Science, 2010. **327**(5966): p. 685-9.
113. Bevington, P.R. and D.K. Robinson, *Data reduction and error analysis for the physical sciences*. 3rd ed. 2003, Boston: McGraw-Hill, xi, 320 p.
114. Hu, B. and Y.H. Tu, *Coordinated Switching of Bacterial Flagellar Motors: Evidence for Direct Motor-Motor Coupling?* Physical Review Letters, 2013. **110**(15).
115. van Albada, S.B., S. Tănase-Nicola, and P.R. ten Wolde, *The switching dynamics of the bacterial flagellar motor*. Mol Syst Biol, 2009. **5**: p. 316.
116. Wright, S., et al., *Differential activation of Escherichia coli chemoreceptors by blue-light stimuli*. J Bacteriol, 2006. **188**: p. 3962-71.
117. Mohanty, S.K., M. Sharma, and P.K. Gupta, *Generation of ROS in cells on exposure to CW and pulsed near-infrared laser tweezers*. Photochem Photobiol Sci, 2006. **5**: p. 134-9.

118. Leslie, B., *Ben Leslie provided helpful advice on potential photo-chemistry issues that might be occurring and suggested trying these dyes.*
119. Macnab, R.M. and M.K. Ornston, *Normal-to-curly flagellar transitions and their role in bacterial tumbling. Stabilization of an alternative quaternary structure by mechanical force.* J Mol Biol, 1977. **112**: p. 1-30.
120. Darnton, N.C. and H.C. Berg, *Force-extension measurements on bacterial flagella: triggering polymorphic transformations.* Biophys J, 2007. **92**(6): p. 2230–2236.
121. Berg, H.C. and P.M. Tedesco, *Transient response to chemotactic stimuli in Escherichia coli.* Proc Natl Acad Sci U S A, 1975. **72**(8): p. 3235-9.
122. Chattopadhyay, S. and X.L. Wu, *The effect of long-range hydrodynamic interaction on the swimming of a single bacterium.* Biophys J, 2009. **96**: p. 2023-8.
123. Lighthill, J., *Helical distributions of stokeslets.* Journal of Engineering Mathematics, 1996. **30**: p. 35-78.
124. Lauga, E. and T.R. Powers, *The hydrodynamics of swimming microorganisms.* Reports on Progress in Physics, 2009. **72**: p. -.
125. Lauga, E., et al., *Swimming in circles: Motion of bacteria near solid boundaries.* Biophysical Journal, 2006. **90**: p. 400-412.
126. DiLuzio, W.R., et al., *Escherichia coli swim on the right-hand side.* Nature, 2005. **435**: p. 1271-1274.
127. Darnton, N.C., et al., *On torque and tumbling in swimming Escherichia coli.* J Bacteriol, 2007. **189**(5): p. 1756-64.
128. Chattopadhyay, S. and X.L. Wu, *The effect of long-range hydrodynamic interaction on the swimming of a single bacterium.* Biophys J, 2009. **96**(5): p. 2023-8.
129. Schulmeister, S., K. Grosse, and V. Sourjik, *Effects of receptor modification and temperature on dynamics of sensory complexes in Escherichia coli chemotaxis.* BMC Microbiol, 2011. **11**: p. 222.
130. Anand, G.S., P.N. Goudreau, and A.M. Stock, *Activation of methylesterase CheB: evidence of a dual role for the regulatory domain.* Biochemistry, 1998. **37**(40): p. 14038-47.
131. Yuan, J., et al., *Adaptation at the output of the chemotaxis signalling pathway.* Nature, 2012. **484**: p. 233-6.
132. Sambrook, J. and D.W. Russell, *Molecular cloning : a laboratory manual.* 3rd ed. 2001, Cold Spring Harbor, N.Y.: Cold Spring Harbor Laboratory Press.

Glossary

AOD	Acousto-optic deflector, device for deflecting laser beam in a controlled manner
AOM	Acousto-optic modulator, essentially the same as an AOD
Arabinose	A sugar, used as an inducer to control flagellin production in strain HCB1660
aTc	Anhydrous tetra-cycline, a common inducer
CCD	Charge-couple device, a type of camera
CheA	Histidine kinase, chemotaxis protein which adds phosphate to CheY
CheY	The response regulator protein, When phosphorylated (CheY-P) it binds to the flagellar motor and increases the probability of CW rotation. Wild-type cells have ~17,000 CheY proteins per cell [36]
CheY*	CheY ^{D13K} . Also used as a short-hand name for the strain which expresses this protein. CheY protein with a point mutation which makes it effectively permanently phosphorylated
CheZ	Protein which removes phosphate from CheY-P
Chemotaxis	The self-directed movement of cells up concentration gradients of attractants, including amino acids, oxygen and temperature.
Culture	A population of cells grown from a single colony, and presumed to be genetically identical.
CB	CW rotational bias, a variable
EMCCD	Electron-multiplying charge-coupled device (Camera with high quantum efficiency)
Epi-fluorescence	Microscopy technique. Dyes are attached to the object of interest (e.g. proteins, flagella), and excited by a specific wavelength of light. The backwards emitted light is then collected by a camera
η	Deviation from veto model, a variable
FliC	Flagellin, the protein that makes up the entire flagella filament: Copy number ~20,000 per flagellum [4]
Inducer	A chemical which promotes transcription of a particular gene. (e.g. aTc, IPTG)
IPTG	Isopropyl-B-D-thiogalactopyranoside, a chemical inducer used to control production of some genes from plasmids
MB	Motility buffer, a fluid buffer used during flagella labeling
N_{cw}	Number of flagella that rotate CW during a tumble, a variable fit to data
N_{eff}	Effective number of flagella per cell, a variable fit to data
N_{flag}	Number of flagella per cell
Promoter	Region of DNA before a gene which controls whether or not the gene is transcribed

QPD	Quadrant photo-diode, detector used to monitor laser beam location and focus
RF	Radio-frequency electronic signal, used to control deflection of laser beam in acousto-optic devices
SD	Standard deviation, a statistical measure
SEM	Standard error in the mean, a statistical measure
TB	Tumble bias, a variable
TB	Tryptone broth, a fluid medium used to grow cell cultures
TEM	Transmission electron microscopy, technique used here to visualize flagella
TMB	Trap motility buffer, a fluid buffer for trapping and swimming experiments

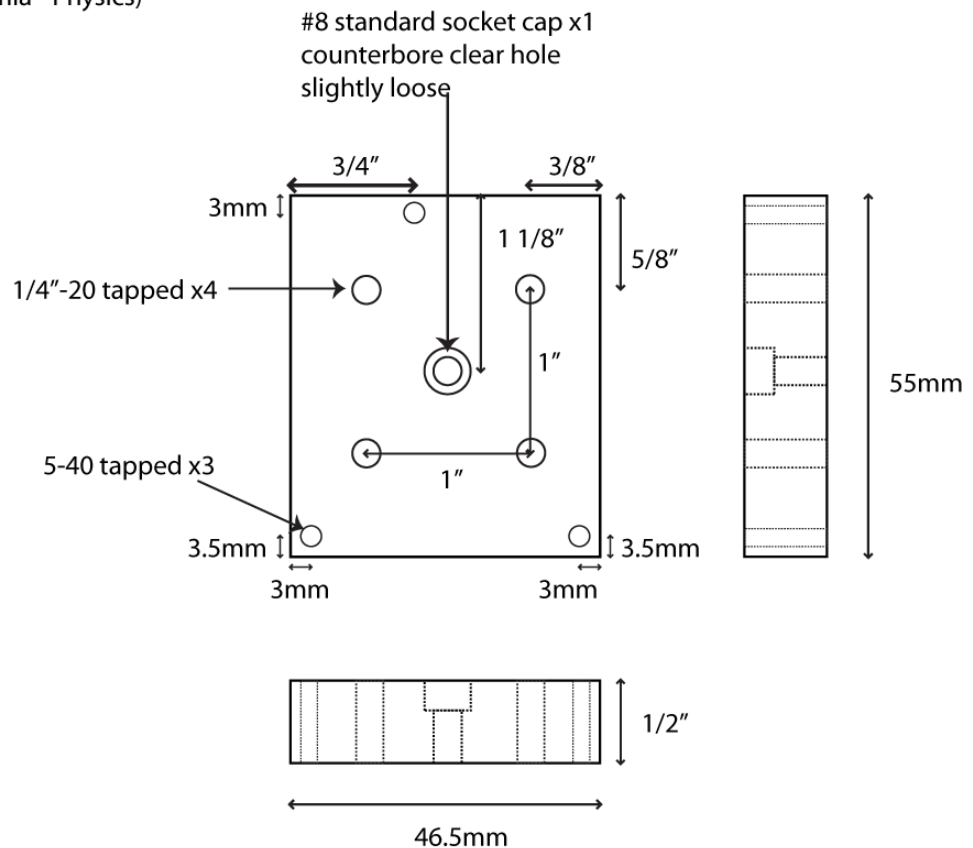
Appendix A. Instrumentation

This appendix includes detailed information about various aspects of the E Fleezers instrument whose design was described in **Chapter 3**. The purpose and function of most of the components are described in **Chapter 3**. Additionally *Comstock et al.* contains a large amount of relevant information about the trap design. This appendix contains information that is specific to the E Fleezers and is not published anywhere else.

A.1 Custom mount for acousto-optic deflector

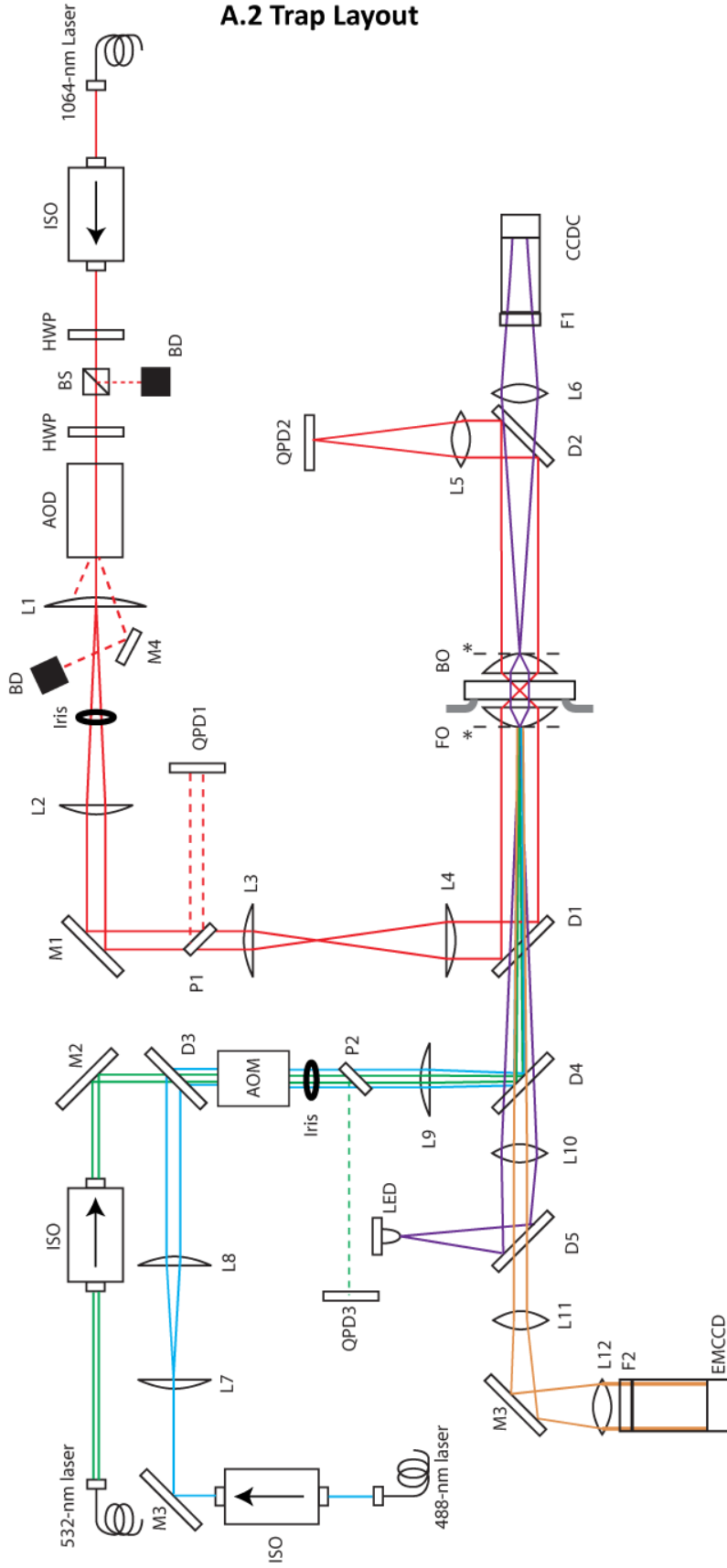
This mount attaches to the acousto-optic deflector (*AA Optoelectronics*) and to the Newport 5-axis stage which is used to fine tune the alignment of AOD. Mounts were constructed by the machinists at the UIUC ECE machine shop.

AOD mount to New Focus xyz stage, v4
 Patrick Mears (Yann Chemla - Physics)
 128 Loomis Lab
 847-254-7192
 pmears2@illinois.edu



make 1 piece
 aluminum

E Fleezers Instrument Layout



A.2 Trap Layout

- ISO - Optical Isolator
- HWP - Half-wave Plate
- BD - Beam Dump
- BS - Polarized Beam Splitter
- AOD - 2-axis Acousto-Optic Deflector
- AOM - Acousto-Optic Modulator
- FO - Front Objective
- BO - Back Objective
- P - Pickoff mirror
- L - Lens
- M - Mirror
- D - Dichroic Mirror
- QPD - Quadrant Photodiode Detector
- CCDC - Charge-Coupled Device Camera
- EMCCD - Electron Multiplying CCD camera

A.3 Optical components

This table contains a list of all of the optical components used in the E Fleezers instrument (lenses, mirrors, lasers, etc.).

Label	Part number	Company	Description
HWP	WPMH05M-1064	Thorlabs	Half-wave plate
Iso	10-3-1064-VHP	OFR (Thorlabs)	Optical isolators (specific for each wavelength)
BS	10BC16PC.9	Newport	Polarizing beam splitter
BD	ABD-075NP	Kentek	Beam dump
AOD	DTD-276HD6	IntraAction	Acousto-optic deflector
L1	KPX184AR.33	Newport	IR Lens, 88.3 mm focal length
M4	BB05-E03	Thorlabs	IR mirror, discards undeflected beam after AOD
Iris	KBX070AR.33	Newport	Iris, blocks off-center beams
L2	KPX103AR.33	Newport	IR Lens, 175 mm focal length
M1	BB1-E03	Thorlabs	IR mirror
P1	10Q20NC.3	Newport	IR Pickoff mirror, AKA beam sampler
QPD (1,2,3)	10-067	Pacific Silicon Se	nsor Quadrant-photo diodes
L3	KPX088AR.33	Newport	IR lens, 75.6 mm focal length
L4	KPX112AR.33	Newport	IR lens, 300 mm focal length
D1, D2	SWP-45-RU1064-TUVIS-PW-1012-C	CVI Laser	Dichroic mirror (reflects IR, passes visible)
FO, BO	Plan Apo VC 60x WI	Nikon	Objectives (1.2 N.A., water immersion)
L5	KBX070AR.33	Newport	IR biconvex lens, 150 mm focal length
L6	PAC064AR.14	Newport	Visible, achromatic doublet lens, 200 mm focal length
F1	FES0900		Filter (blocks 1064-nm IR light)
CCDC	WAT-502B	Watec	Charge-coupled device camera, for brightfield imaging
M2	10D20BD.1	Newport	Visible mirror
M3	10Z20ER.1	Newport	Visible mirror (wider spectrum down to 450 nm)
D3	-	-	Dichroic mirror, longpass (reflects 488nm, passes 532nm light)
L7	KPX082AR.14	Newport	Visible lens, 50 mm focal length
L8	KPX094AR.14	Newport	Visible lens, 100 mm focal length
AOM		IntraAction	Acousto-optic modulator
P2	n/a	n/a	Visible pickoff mirror (microscope slide)
L9	KPX115AR.14	Newport	Visible lens, 400 mm focal length
D4	Di01-R532-25x36	Semrock	Dichroic mirror (when using 532nm) Reflects 532, passes all other
D4 alternate	ZT488DCRB	Chroma	Dichroic mirror (when using 488nm) Reflects 488, passes all other
L10	KPX106AR.14		Visible lens, 200 mm focal length
D5	ZT488rdc	Chroma	Dichroic mirror, longpass (passes emission, reflects brightfield illumination below 500nm)
LED	ZT488dcrb	Chroma	Light-emitting diode, provide illumination for bright-field imaging
L11	BAC23AR.14	Newport	Visible lens, achromatic concave doublet, -30 focal length
M3	10D20BD.1	Newport	Visible mirror
L12	PAC058AR.14	Newport	Visible achromatic doublet lens, 150 mm focal length
F2	ZET532NF	Chroma	Filter on EMCCD (when using 532nm), notch blocks 520-545nm
F2 alternate	ZET488NF	Chroma	Filter on EMCCD (when using 488nm), notch blocks 475-500nm

A.4 FPGA breakout box wiring assignments

This table contains the channel and pin number for each signal passing through the breakout boxes that connect the FPGA to the instrument. Channel numbers are used to assign channels inside the LabVIEW Host code. DIO channels are Digital Input/Output signals. Most DIO channels are digital output signals to the FPGA synthesizers which generate the RF signal used to control laser beam deflection in the acousto-optic devices. AI channels are Analog Inputs, which are all signals from the QPDs measuring trap and other laser beam power and deflection.

Connector 1 (DIO)			Connector 0 (MIO)		
DIO		Pin #	AI		Pin #
0	Data BD1 (07)	35	0	IR QPD Y	68-34
1	Data BD1 (06)	36	1	IR QPD X	66-32
2	Data BD1 (05)	37	2	IR QPD SUM	65-31
3	Data BD1 (04)	38	3	QPD FB SUM	63-29
4	Data BD1 (03)	39	4	QPD FB Y	62-28
5	Data BD1 (02)	40	5	Green FB SUM	60-26
6	Data BD1 (01)	41	6	Green FB X	59-25
7	Data BD1 (00)	42	7	QPD FB X	57-23
8	*Address (05)	43			
9	*Address (04)	44			
			DIO		
10	*Address (03)	45	0	Data BD3 (07)	36
11	*Address (02)	46	1	Data BD3 (06)	37
12	*Address (01)	47	2	Data BD3 (05)	38
13	*Address (00)	48	3	Data BD3 (04)	39
14	Writing debug signal	49	4	Data BD3 (03)	40
15	*RF WR signal	50	5	Data BD3 (02)	41
16	*RF RD signal	51	6	Data BD3 (01)	42
17	*RF PMODE signal	52	7	Data BD3 (00)	43
18	RF OSK BD1	53	8		10
19	RF Reset BD1	54	9	Flip Mount	44
20	Data BD2 (07)	55	10		11
21	Data BD2 (06)	56	11		45
22	Data BD2 (05)	57	12		12
23	Data BD2 (04)	58	13		46
24	Data BD2 (03)	59	14		13
25	Data BD2 (02)	60	15		47
26	Data BD2 (01)	61			
27	Data BD2 (00)	62			
28	RF OSK BD2	29			
29	RF Reset BD2	63			
30	*RF update clock signal	30			
31	AI timing signal	64			
32	RF WR BD3	31			
33	RF OSK BD3	65			
34	FSK for 532nm AOM	32			
35	Green FB AI timing	66			
36	*FSK signal (BD1 & BD2)	33			
37	RF Reset BD3	67			
38	BD3 update clock	34			
39		68	* Shared channel for multiple boards		

Appendix B. Protocols

This appendix contains many of the protocols which were used to conduct experiments for my thesis project.

B.1 Flagella labeling protocol

This is the protocol for growing *E. coli* cells and labeling their flagella with fluorescent dyes. The general process was described in **Chapter 2**. The strain HCB1660 (strain info in **Appendix C.1**) expresses flagella with a mutation that allows them to be labeled specifically with maleimide functionalized dyes. The dye used most often was AlexaFluor 532 C₅ maleimide (*A-10255*; *Life Technologies*.)

1. Prepare over-night culture using HCB1660 strain. Include 1µl cm antibiotic.

- a. Pipette 1 ml TB (Tryptone Broth) in a labeled round bottom Falcon tube.
- b. Pipette 1 µl Chloramphenicol into the tube.
- c. Touch a single *E. coli* colony on an agar plate with an autoclaved pipette tip.
- d. Place the tip in the round bottom tube with TB.
- e. Incubate test tube into a shaker at 30° C, 265 RPM for 14-18 hours.
- f. Wrap the agar plate in parafilm and return it to the 4 °C refrigerator.

2. Dilute, measure OD₆₀₀ and incubate again with inducer

- a. Remove the over-night (ON) round bottom tube from shaker.
- b. Dilute 5-fold into TB. (Remove 200µl and add to 800µl TB in a cuvette).
- c. Check OD₆₀₀ (Optical Density at 600nm wavelength) with spectrophotometer.
 - i. Turn on spectrophotometer.
 - ii. Blank spectrophotometer with TB.
 - iii. Read sample and record the measured OD in log book.
- d. Dilute that sample another 20-fold in 12-ml TB in a 125-ml flask.
 - i. Add 12 µl of 10% arabinose (final concentration = 0.025%, 667µM) to induce flagella production
- e. Incubate in shaker at 30° C, 265 RPM for ~4.5 hours

3. Harvest and wash cells

- a. Measure OD. It should be around 0.5-0.6. If lower, wait longer.
- b. Centrifuge 10 ml cells in a round-bottom tube at 1300xg for 10 min @ room temp.

- c. Resuspend gently in 1-ml MB. *Do not pipette up and down to mix.* Gently swirl by hand. This may take 5-10 minutes. Resuspending violently can cause flagella to break.
- d. Centrifuge again in round-bottom tube at 1300xg for 10 min @ room temp.
- e. Resuspend gently in 500 µl MB.

4. Label cells

- a. If not already done, dissolve dry dye in H₂O. For AlexaFluor 532 C₅ maleimide, dissolve 1mg of dye in 300µl H₂O. Vortex for 1 min. Then make several aliquots and store in -20C.
- b. (*Alternative*) If labeling non-specifically, use NHS-ester functionalized dye. (Note this will label the cell body in addition to the flagella.) First dissolve Cy3-NHS ester dye in 500 µl H₂O+25 µl of NaHCO₃. Then use 25 µl of this solution in the next step (instead of 2 µl.)
- c. Mix 2 µl maleimide functionalized dye (in H₂O) with 500 µl of cells in MB, in a 1.5 ml Eppendorf tube. Pipette up and down, very slowly with a wide-orifice tip, a few times to mix. *(Note the concentration of dye needed will vary for each diluted vial of dye. Excess dye will lead to flagella cross-linking when illuminated in the trap. Insufficient dye will yield dimmer flagella which photobleach more rapidly.)
 MB (Motility Buffer) = 10 mM KPO₄ (pH 7.0), 70 mM NaCl and 0.1 mM EDTA
- d. Cover tube with aluminum foil to keep dyes in the dark.
- e. Put tube on rotator for 90 minutes. (Part way through, pipette up and down very gently a couple times with a wide-orifice tip to make sure the solution is well mixed.)

5. Wash labeled cells

- a. Centrifuge in round-bottom tube at 1300xg for 10 min @ room temp.
- b. Resuspend gently in 1-ml MB.

6. Prepare cells for trapping

- a. If trapping, dilute 1:20 in 1-ml TMB + 2 µl gloxy. Label this tube "Cells"
- b. Also, prepare a blank solution of 1-ml TMB + 2 µl gloxy. Label this tube "Blank"

B.2 Bacterial trapping protocol

This is the protocol for trapping bacteria in the E Fleezers. It also contains instructions for imaging flagella and applying a chemotaxis stimulus. The instrument was described in **Chapter 3** and the experiments were described in **Chapters 2** and **4**. This outline can be used as a reference when trapping cells.

1. Prepare over-night incubation (the night before)

- a. Pipette 1 ml TB (Tryptone Broth) in a labeled round bottom Falcon tube.
- b. Touch a single *E. coli* colony on an agar plate with an autoclaved toothpick.
- c. Place the toothpick in the round bottom tube with TB.
- d. Incubate test tube into a shaker at 30° C, 265 RPM for 14-18 hours
- e. Wrap the agar plate in parafilm and return it to the refrigerator.

2. Dilute, measure OD600 and incubate again

- a. Remove the over-night (ON) round bottom tube from shaker.
- b. Dilute 10-fold into TB. (Remove 100µl and add to 900µl TB in a cuvette).
- c. Check OD₆₀₀ (Optical Density at 600nm wavelength) with spectrophotometer.
 - i. Turn on spectrophotometer.
 - ii. Blank spectrophotometer with TB.
 - iii. Read sample and record the measured OD in log book.
- d. Dilute that sample another 10-fold in 1-ml TB in a fresh round-bottom Falcon tube.
- e. Incubate in shaker at 30° C, 265 RPM for ~4.5 hours.
- f.

3. Prepare samples

- a. Dilute the over-day culture 1:10 into 1 ml Trap Motility Buffer (TMB) + methionine + 2 µl gloxy in a micro-centrifuge tube, label "Cell"
- b. Prepare a second micro-centrifuge tube with 1 ml TMB + methionine + 2 µl gloxy, label "Blank"
- c. Prepare a third micro-centrifuge tube with 1 ml TMB + methionine + 2 µl gloxy + attractant/repellent of choice, label "Stim"

4. Set up sample chamber

- a. Fill chamber with H₂O
 - i. Attach 10-ml syringes with H₂O to each inlet
 - ii. Have outlets draining into a container labeled "Bacteria"
 - iii. Push in H₂O to fill chamber, be careful to avoid or remove bubbles

If bubbles cannot be removed, flow in air to clear the chamber and repeat.
THIS STEP IS VERY IMPORTANT! IF THERE ARE BUBBLES IN THE
CHAMBER, CELLS WILL NOT SWIM WELL.

- b. Put chamber in place
 - i. Unwind front objective to provide maximum space between objectives
 - ii. Screw metal cylinder post into the chamber holder
 - iii. Very carefully place chamber between objectives
 - iv. Move front objective back into place
 - v. Drop water from a syringe onto chamber/objective interface for water immersion
 - vi. Be sure that outlets from the chamber lead to a beaker, not the trap bench
 - vii. Do not fix chamber in place yet

5. Turn on trapping equipment

- a. Turn on the hallway laser warning light. (Switch near door)

b. *PUT ON GOGGLES!!!**

THE 5-W infra-red laser is invisible and can blind you!!!

- c. Turn on Spectra-Physics Power Supply
 - i. Turn Key to ON/1
 - ii. Wait for display to read "Current Mode ready"
- d. Power on RF amplifiers and then the RF synthesizer board
- e. Turn on Newport Universal Motion Controller
 - Switch on back of device
- f. Power on the white LED which illuminates the sample chamber
- g. Turn on Harvard Apparatus syringe pump controller
 - Switch on back of device
- h. Open LabVIEW software on the trap computer
 - i. Open "Ecoli Trap Project" on the desktop
 - ii. Open "Ecoli Trap (Host)_2.1.vi"
 - iii. Open "LaserControl.vi"
 - 1. Run "Laser Control" (click white arrow in top left corner)
 - 2. Switch on the Diode
 - 3. Be sure goggles are on!!!

- Turn current up to ~18 A.
- i. Run Ecoli Trap (Host)_2.1.vi (click white arrow in top left corner)

6. Get oriented inside the trapping chamber

- a. Adjust position of CCD camera so that it's ~200 mm away from the focusing lens
- b. Joystick should be active when you first turn on the Newport motion controller.
If Joystick is not active, press "Menu" -> "Run Program" -> "Run" on the controller
- c. Move the chamber with joystick and try to find the point of interest (depends on the particular experiment) inside the chamber
*When moving in Z-axis, be careful not to hit objectives. Move slowly
- d. Move to the center of the chamber in Z-direction (~50 μm away from either surface)
- e. Set this as zero position on Newport controller
Press "Menu" -> "Reset Position" -> "Clear" for each axis

7. Prepare trapping LASER

- a. Using joystick, navigate to a FOV with no objects, just H₂O
- b. Focus LASER
 - i. Take IR filter out (flipping mount) and add neutral density filters onto the lens tube attached to the CCD camera (This allows viewing the IR trapping beam)
 - ii. Look at the CCD image on monitor. Adjust objective position until trap is nearly in focus
 - iii. Check for sample chamber tilt by defocusing the trapping beam and adjusting until the diffraction rings appear symmetric (Temporarily turn down brightfield illumination by closing the brightfield light-source iris)
 - iv. Adjust the front objective to get the trapping beam in focus
 - v. If trap is not at the center of the field of view, adjust the tube lens so that the trap appears near the center
 - vi. Take out the neutral density filters, and flip IR filter back on

8. Flow cells into chamber

- a. Remove H₂O syringes from inlets
- b. Check for and remove bubbles at all stages. (Use a syringe needle to remove bubbles if necessary)
- c. Fill 1-ml Hamilton syringes with ~0.6 ml of the contents of the three sample micro-centrifuge tubes

- d. Attach 1-ml syringes to inlets
- e. Place syringes on the syringe pump and fix them in place
- f. On Harvard Apparatus pump controller, flow cells into chamber
 - i. Press 'Set', then 'Diameter', then type '4.61' (mm), then press 'Enter'
 - ii. Press 'Set', then 'Infuse rate', then type '1000' ($\mu\text{l/hr}$), then press 'Enter'
 - iii. Set\Target Volume, 0.1 ml
 - iv. Select Mode\Volume Mode
 - v. Press 'Run'
 - vi. Wait about 10 minute for cells to flow into chamber
 - vii. When the 0.1 ml target volume has been dispensed, change the flow rate to $25 \mu\text{l/hr}$, and keep it at that throughout the experiment

9. Trap cell

- a. Make sure the trap is on
- b. Locate a cell (usually found near boundaries of the flow chamber)
- c. Move the chamber so that a cell gets trapped
- d. Move the CCD camera backwards on its rail so that the trapped cell is in focus and appears white (it is easier to see the cell this way)
- e. Using Mouse Control (hold down the mouse scroll wheel), manipulate the second trap to align the trapped cell horizontally in x-axis

10. Acquire Data

- a. Once a cell is aligned between 2 traps and appears to be swimming well, start recording:
- b. To save data, click 'Save Data' near the upper right hand side of the LabVIEW host code.

ALWAYS WATCH THE CELL WHEN COLLECTING DATA TO BE SURE THAT NOTHING STRANGE HAS HAPPENED (e.g. other cell swam into trap, etc.)

11. Applying stimuli (optional)

- a. In order to apply a stimulus, the cell will be moved from one channel in the sample chamber into a different channel which contains a different concentration of chemoeffector. The cell should be moved at $100 \mu\text{m/s}$, in one smooth motion. Use the joystick to move the cell from the center of one channel to the center of the channel above or below, which should be $\sim 1\mu\text{m}$. This should take ~ 10 seconds.
- b. Watch the QPD signal. The behavioral response should be noticeable by eye.

- c. Continue recording data until at least 50 seconds after the cell appears to have returned to its steady-state swimming behavior.

12. Process data offline using Matlab

B.3 Trap fluorescence imaging protocol

This protocol describes how to configure the E Fleezers instrument and collect fluorescence images in the trap. An important note is that the current setup allows for illumination with either 532-nm or 488-nm light. Switching between excitation modes involved switching the dichroic mirror which is used to direct excitation light towards the sample.

Briefly, a summary of the protocol: Make sure that the fluorescence excitation dichroic mirror and the emission filter on the EMCCD camera are correct for the wavelength of the laser used (see **Appendix A.2** and **Appendix A.3**). Turn on the lasers and the oscilloscope. Open Andor Solis (software) and set parameters in “set up acquisition”. Set interlacing using LabVIEW code and while viewing signals on the oscilloscope. Trap a cell and record images.

1. Configure EMCCD camera software to record images

- a. In “set up acquisition”, change the name of the saving file in spooling and disable spooling (auto-saving) (saving should be disabled while setting up so that films do not accidentally get saved to existing files)
- b. Adjust exposure time, EM gain, etc. if necessary

Flagella imaging:

Exposure = 30 μ s

EM gain = 100

Triggering = External

CheY-YFP imaging:

Exposure = 1000 μ s

EM gain = 100

Triggering = External

2. Configure parameters in the Labview program “Ecoli Trap (Host).2.1.vi”

- a. In the “EMCCD” tab adjust the timing of EMCCD camera exposure duration and intervals. (Exposure + wait time) must be a multiple of trap cycle time (2400) and one such that the frame rate of EMCCD is lower than that in “set up acquisition”
- b. In the “Green laser” tab, adjust the timing of the fluorescence excitation pulse. Full cycle count of green laser = (exposure + wait time) of EMCCD

3. Set-up oscilloscope to monitor interlacing timing

- a. Turn on the traps

- b. Click on video in Solis, and then go to Labview to turn on Green laser interlacing and EMCCD
- c. On the oscilloscope, make sure that green laser signal (signal 2) is on when trap signal (signal 3) is off. If not, adjust the phase of the green laser.
- d. (*488nm only*) Increase the number of green laser signals until they cover the span where the camera signal (signal 1) is on. Then adjust the phase of the EMCCD so that the green laser signals and the EMCCD signals overlap. *again, only -phase
- e. (*532nm only*) Shift the phase of the EMCCD camera exposure so that it is synchronous with the 532nm excitation pulse.

4. Adjust the excitation beam location

(Only necessary if the dichroic mirror has been changed since the last experiment)

1. Put on a filter on the Watec brightfield camera to block excitation light
2. Adjust the nobs on the dichroic mirror so that the laser is focused on the cell (where the trap is focused)

5. Record data

- a. Trap and align cell
- b. Turn off white LED
- c. Click “video” in Andor Solis
- d. Turn on “save QPD and EMCCD and Green laser”
- e. Stop “save QPD and EMCCD and Green laser” (in Andor Solis, do not save the last image)
- f. Change saving file name in “set up acquisition” (to avoid saving over previous movie)

6. Prepare for next cell

- a. Turn off traps (Turning off traps before turning on white LED can avoid white LED messing up trap signals?)
- b. Turn on white LED
- c. Turn traps back on

B.4 Flagella imaging electron microscopy protocol

This protocol was designed for counting flagella on JEM 2100 “cryo” electron microscope in UIUC Materials Research Lab. The hardest part of imaging flagella in the electron microscope is the sample preparation step. Samples are very sensitive and many samples result in broken flagella or poor images. It requires some patience to get a good sample on which flagella are kept intact. Many of the steps in the protocol were introduced to increase the chances of getting a good sample. For example, use wide orifice pipette tips to avoid shearing of flagella. And use glutaraldehyde or another chemical to fix cells before placing the sample in the microscope. This seems to prevent flagella from breaking, presumably because they are not moving when the sample is introduced to vacuum.

Supplies list when going to the electron microscopy facility: Glutaraldehyde, tweezers, pipettes and tips, microfuge tubes with cell cultures, KimWipes, ddH₂O, PBS, petri dish, parafilm, carbo-coated grids, waste bag, USB thumb drive

(Thanks to Dr. Madeleine Leisner for advice on the sample preparation protocol)

Growing cells

0. (Previous day) Start 1-ml over-night (ON) culture in shaker @ 30°C, 265 RPM.
1. Check ON OD and start 100-fold diluted Culture in TB + 10ng/ml (f.v) aTc. (10 ml total).
Wait ~4.5 hours.
2. Measure OD, make 1 slide to check that cells are swimming.
3. Don't centrifuge cells unless they need to be concentrated. (Protect flagella) Centrifuge in round-bottom tubes

To concentrate, centrifuge 5 min @ 2000xg. Resuspend in PBS.

Preparing sample on grid

1. Fix cells. Gently mix 46 ul cells in PBS + 4ul glutaraldehyde (25% stock) in Eppendorf tube.
Wait 1 min.
** Glutaraldehyde is dangerous.* Put all containers that touch it in the sharps box. Put waste in an container for Formaldehyde, etc.
2. Put grid on parafilm (shiny side up) on a petri-dish.
3. Pipette 5 µl of fixed cells onto carbon-coated grid. Wait ~2 min.
4. Remove excess fluid from the TOP with KimWipe.
5. Wash twice with 5 µl distilled water. Wait ~45 seconds each time before blotting.
6. Wait ~10 min after blotting To be sure the sample is dry.

7. Place grid in EM holder with tweezers.

Use JEM @ 200 kV.

Take 1 sec. exposures.

Additional notes

*Do not stain. Flagella are visible without stain, and stain goo appears all over sample, making it harder to see.

*Do not use holey grids. Cells and flagella hang over edge, so flagella break and cannot be counted.

*Always resuspend cells in PBS or some minimal medium. Rich media like TB, contain amino acids which appear to clump up around cells forming crystal looking clumps that make flagella very hard to see.

*Always blot from top of grid (same side as liquid). Blotting from other side tears apart grid.

*Glutaraldehyde seems to help prevent flagella from breaking off of cells. Possibly because cells flagella stop moving and don't get broken during evaporation.

B.5 2D swimming protocol

The 2D swimming assay and several results from the assay are presented in **Chapter 7** and the protocol is provided in the Methods section of *Min et al.* [2]. This protocol describes how to perform the experiment. In general the assay involves depositing a drop of fluid containing cells in solution onto a microscope slide. A coverslip is then placed on top of the droplet, forming a sandwich with the fluid in between the coverslip and slide. Cells are then observed swimming in 2-dimensions using a microscope. Later, offline, movies of the swimming cells are analyzed using Matlab code to determine when cells are running and tumbling.

Like all swimming assays, there are some common technical hurdles. The most common source of frustration comes from cells sticking to the surface of the chamber. Sticking is made less common by sonicated slides in 1 M KOH, and coating the surface with detergents or BSA. I also found that cells in a rich medium, such as the Tryptone Broth, were less likely to stick to the surface. Another common problem was to presence of large air bubbles in the chamber. Their occurrence became less common with practice, but to some extent seemed unavoidable. Finally, since the fluid in which the cells swim is not exchanged or replenished, a chamber can only be used for a limited time (tens of minutes) before cells begin to deplete the available nutrients and Oxygen.

One limit of the current algorithm is that it does not distinguish two cells whose paths cross. So any time that two cells swim past each other, both trajectories are terminated. Additionally, the algorithm is not perfect at identifying tumbles. The user should be careful to compare some the automated results from Matlab against manually analyzed results from a few “typical” cells.

1. Grow cells

Grow cells in the same manner as all other experiments.

2. Wash Slides

- a. If not already done, sonicate slides and coverslips in KOH (1M)
- b. Rinse slides and coverslips with distilled water
- c. Dry slides using presuurized air and dabbing the edges on a Kim wipe
- d. Store slides and coverslips for later use

3. Harvest cells

- a. Harvest the cells and read the OD. It should be $\sim 0.50 \pm 0.1$. If below 0.4, return sample to shaker and wait longer. If over 0.6, the sample may be overgrown and results are unreliable.
- b. Dilute the sample 1:4 into a solution of TB. (Other solutions can be used depending on the experiment being performed. I found that TB reduced the occurrence of cells

sticking to the chamber surface.)

4. Perform chemotaxis experiment

- a. Turn on the microscope and software.
- b. Pipette 5 μ l of the mixed sample onto a slide.
- c. Gently put coverslip on top of sample. (Try to avoid forming bubbles)
- d. Seal edges with Epoxy.
- e. Put sample on the microscope.
- f. Turn off lights in the room.
- g. Look at cells in MetaMorph and focus on a good section. (No stuck cells, no junk, no air bubbles)
- h. Record a 30 second movie.
- i. Save the movie with a descriptive name

5. Analyze data using custom Matlab software

B.6 2D chemotaxis adaptation protocol

This is the protocol for performing chemotaxis adaptation experiments using the 2D protocol. It basically involves mixing two solutions, one containing the cells and the other containing the chemotaxis stimulant, and then performing the 2D assay with the mixed solution. Timing is critical for this experiment. Once the samples are combined, the cells experience the stimulus. Therefore it is best to prepare everything, including the microscope and software before applying a stimulus. I usually performed the experiment with the help of a second person, and applied the stimulus in the microscope room, to minimize the time from stimulus to observation.

1. Prepare sample solutions

- a. Pipette 750 μ l TMB + 2 μ l Methionine (50mM solution) into a 1.5-ml Eppendorf microcentrifuge tube. Label as "Sample 1".
- b. Pipette 1000 μ l TMB + 2 μ l Methionine (50mM solution) + 8 μ l Aspartic Acid (50mM solution) into a 1.5-ml Eppendorf microcentrifuge tube. Label "AA"
- c. Pipette 1000 μ l TMB + 2 μ l Methionine (50mM solution) + 8 μ l Serine (50mM solution) into a 1.5-ml Eppendorf microcentrifuge tube. Label "Ser"

2. Wash slides

- a. If not already done, sonicate slides and coverslips in KOH (1M)
- b. Rinse slides and coverslips, store in containers.

3. Harvest cells

- a. Harvest the cells and read the OD. Same as regular 2D protocol
- b. Pipette 250 μ l of the cell culture into the microcentrifuge tube labeled "Sample 1." This is now $\frac{1}{4}$ cells $\frac{3}{4}$ TMB.

4. Prepare to perform chemotaxis experiment

- a. Turn on the microscope and Metamorph.
- b. Using a test sample, get cells in focus, record a short movie of swimming cells, and save the movie with a very descriptive name. EG 100614_RP437_100uMSerine_test.
- c. Bring supplies into the microscope room:
 - i. Slides and coverslips
 - ii. P1000 pipettor and tips
 - iii. P10 pipettor and tips
 - iv. Epoxy and aluminum foil
 - v. Sample 1, AA, Ser tubes, and a few empty Eppendorf tubes.

vi. Stop watch or timer

5. Stimulate cells and record swimming

(This is best done with 2 people. The faster the better, as cells begin responding immediately)

- a. Mix some fresh Epoxy on a piece of aluminum foil using a pipette tip (Person A)
- b. Pipette 200 μ l of cells into an empty Eppendorf tube. (Person B)
- c. Pipette 200 μ l of AA or Ser solution in the same Eppendorf tube. Swirl with the tip to mix gently for \sim 10 seconds. (Person B)
- d. Start stop watch! (Person A)
- e. Pipette 5.0 μ l of the mixed sample onto a slide. (Person A)
- f. Gently put coverslip on top of sample. (Person A)
- g. Seal edges with Epoxy. (Person A)
- h. Put sample on the microscope. (Person A)
- i. Turn off lights in the room. (Person B)
- j. Look at cells in MetaMorph and focus on a good section. (No stuck cells, no junk)
- k. Record a 30 second movie.
- l. Save the movie with a descriptive name, including the time since cells were stimulated. (Use stop watch. Use the time $\frac{1}{2}$ way through recording the movie)
- m. Close the movie, and record a new one on the same sample. Save. Repeat...
- n. After about 15 minutes, cell should be fully adapted. Stop recording movies.

B.7 Flagella dilution protocol (with optional labeling)

This is the protocol for the flagella dilution experiment which was described in **Chapter 7**. The purpose of the experiment is to create populations of cells with different average numbers of flagella per cell. This is done by growing cells with inducible flagella, and then stopping flagella production and resuming cell growth. As cells grow and divide, the future generations will split the existing flagella, and therefore have less flagella per cell. The protocol contains an optional section for labeling flagella during the experiment, so they can be viewed and counted. The labeling protocol is basically identical to the protocol in **Appendix B.1**.

The protocol was originally performed with a strain in which all chemotaxis and swimming machinery was shut off when induction stopped. In the future, it should be done using strain HCB1660 (**Appendix C.1**) in order to control flagella production separately from other swimming and chemotaxis genes.

Supplies

- Wide orifice pipette tips
- Slides (Gold Seal micro slides, Cat No. 3010)
- Coverslips (Fisherbrand microscope cover glass, 12-541-B 22x22-1)
- Epoxy (5 Minute® Epoxy)
- 1x 14-ml round-bottom Falcon tubes
- 5x 125-ml beveled graduated cylinder
- 1.5 ml centrifuge tubes

Reagents

- TB
- Cm
- Arabinose
- KOH

Things to do before starting

- Sonicate and rinse slides and coverslips. Store in a container in air. Need 12 each day.
- Create 1mM IPTG stock for the day. Store in 4^o C fridge.

Procedure

1. Prepare over night incubation in 1ml TB + 1 μ l cm (34 mg/ml). Shake at 265 RPM, 30°C.
2. Measure over-night OD (dilute 1:5 in TB, OD should be ~ 0.4), dilute 1:100 in a graduated cylinder with arabinose (0.25% to induce FliC* production). 265 RPM, 30°C.
11.4-ml TB + 30 μ l arabinose (10% stock) + 600 μ l ON x 0.2
3. Prepare slides, motility media and dilution media. Put dilution medium in flasks in incubator to preheat to 30°C.
If not already done, sonicate slides in 1M KOH, rinse and blow dry.
Coat slides with BSA.
Dilution and motility media are TB.

4. Prepare a test slide to get microscope settings and focus correct. Use ON culture.
5. After ~4.4 hours, check OD. Once $OD = 0.50 \pm 0.05$, wash 11-ml cells by centrifugation at 1300g for 10 min in a round bottom Falcon tube at room temperature. (Recall, each sample should be staggered by ~20 min.)
6. Gently resuspend in 11-ml dilution medium (TB, no arabinose). Measure and record OD.
7. Add dilution medium to flask to make 12-ml dilution culture. Place in shaker.
4 samples: Gen 1 = 6 mL cells/6 mL TB, Gen 2 = 3 ml cells/9 mL TB,
Gen 3 = 1.5 mL cells/10.5 mL TB.
8. Prepare slide of Generation 0 for observing. Dilute 1:4 in motility medium. Pipette 5 μ l onto slide, gently place coverslip, and then seal edges with Epoxy. Record at least 3 movies at different locations on each sample.
9. Repeat previous step for each dilution when OD reaches the original resuspended level. Take more movies at later generations. (~ 5 at Gen 3, ~6 at Gen 4, ~8 at Gen 5)
10. Label cells from Gen 2 (sample 3).
 - a. When sample has reached correct OD (see previous step), follow normal labeling protocol.
 - b. Also, make 2D swimming movies while cells centrifuge.
 - i. Centrifuge 10-ml, 10 min, 1300g, room temp and resuspend in 1-ml MB
 - ii. Centrifuge again, resuspend in 0.5-ml MB.
 - iii. Label with 2 μ l of dye in 1.5 ml tube for 90 minutes, wrapping in foil, rotating.

B.8 Cloning a gene into a different plasmid protocol

This protocol outlines the general strategy that I used for performing molecular cloning to create new plasmids. In most cases I had one plasmid which contained a gene or other sequence of DNA that I wanted to move into a different plasmid. The reason for moving the gene was usually related to how many copies of the protein encoded by that gene were expressed in a cell. For example, if a plasmid was producing too much protein I could move it to a plasmid with a lower copy number or a tighter promoter. However, there could many other reasons for cloning genes.

The protocol takes several days, and it is very common for steps to fail, which requires repeating that step or going back a few steps. Do not be discouraged, but be sure to carefully plan everything before beginning a new cloning project. It is better to spend extra time planning than to get half-way through and realize that the proposed cloning strategy won't work, or that you are using the wrong restriction enzymes. Plan everything and order all of the necessary primers for colony PCR and sequencing as early as possible. Label everything, and keep all intermediate plates and DNA samples until the entire cloning project is complete.

Most of the individual steps involved in the process are standard protocols which can be found in commercial kits (e.g. Miniprep kits from *Qiagen* contain instructions for doing minipreps to extract plasmid DNA from cells). Other protocols were taken from the extremely useful Molecular Cloning manual by Sambrook and Russell [132]. The appendix of this manual is an extremely useful resource for all kinds of molecular cloning and biology protocols.

Supplies

- Initial plasmid (or strain containing plasmid)
- Target plasmid (or strain containing plasmid)
- Primers for sequencing and potentially amplifying GOI
- Restriction enzymes & NEBuffers
- Miniprep kit
- Gel extraction materials
- Competent cells/transformation buffers
- Appropriate antibiotics
- LB plates with antibiotics

Definitions

- GOI = Gene of interest, the gene to be cloned
- Initial plasmid = Plasmid containing the GOI
- Target plasmid = The plasmid into which the GOI will be inserted
- RE = Restriction enzyme (endonuclease)

Preparation

1. Determine where to obtain GOI and target plasmid
2. Determine which restriction enzymes to cut with & which NEBuffer to use with those RE
3. If no compatible cut sites exist in the plasmids, design primers to PCR amplify the gene and add cuts sites on the end of the gene. (Be sure to make the reverse-compliment of the reverse primer, and add ggg after the cut site, so the RE can bind to the DNA and cut it)

Protocol

1. Extract plasmids

- a. Grow culture of strains containing plasmids
- b. Mini-prep to get plasmids (Initial and target)
I used the *Qiagen* Miniprep kit, but other commercial kits are available

2. PCR amplify the GOI to add restriction enzyme cut sites (Optional)

- a. IF the gene was not flanked by RE sites compatible with the target plasmid, design primers to PCR amplify the gene and add cut sites.
- b. PCR the initial plasmid using these primers
- c. Run PCR cleanup to get clean

3. Digest donor and acceptor plasmids using the chosen restriction enzymes

- a. RE's were almost always purchased from New England Biolabs.
- b. New England Biolabs has a very useful website. Consult it when choosing which enzymes and buffers to use during digestions.
<https://www.neb.com/tools-and-resources/interactive-tools/double-digest-finder>

4. Run gel and purify GOI and digested target plasmid

- a. Run gel with a ladder for reference and with control, undigested plasmid
- b. While looking at the gel on a UV illuminator, cut out the GOI and digested plasmid bands
- c. Purify the GOI and digested target plasmid

5. Ligate GOI into target plasmid

6. Transform competent cells with ligated product

- a. There are many ways to acquire competent cells and do transformations
- b. I usually used the protocol in **Appendix B.9**
- c. Select for transformants on antibiotic plates

7. Colony PCR

Colony PCR is a quick method to screen for transformants that contain the correct new plasmid containing the GOI.

- a. Get primers for the flanks of the insert region (~100bp upstream from RE sites)
- b. Perform PCR on several colonies and re-streak those colonies on another plate

c. Run gel to see which colonies contained plasmids with the insert

8. Miniprep colonies that contained the insert

If everything has gone correctly, this should be your new plasmid.

9. Transform the final strain with the new plasmid

Be sure to make a permanent -80°C stock of any new strains. Even if the cloning did not go as planned and the plasmid does not behave as expected, it is better to save the plasmid inside a strain than to lose it forever.

10. Sequence the new plasmid (optional)

To verify that the sequence appears as expected and to check for mutations or other problems that may have occurred. I usually sent plasmids to a company called *ACGT Inc.* to be sequenced. The UIUC Biology Storeroom has a box where samples can be conveniently deposited any day of the week. Sequencing can be ordered online and results usually take 2 days to arrive via email.

11. Test the new strain to verify that it behaves as expected

B.9 One-step preparation and transformation of competent cells

Based on *Current Protocols in Molecular Biology*.

Based on the protocol optimized by “Tommy” Lok-hang So, Golding Lab

Materials

LB containing 20mM (0.36%) glucose (900 μ L per transformation)

1 \times TSS (100 μ L per transformation)

1. Dilute sterile (autoclaved) PEG 3350 to 10% (w/v) in LB containing 50mM MgCl₂.
2. Add DMSO to 5% (v/v).
3. Adjust to pH 6.5.

4mL	50% PEG
3350	
1mL	DMSO
15mL	LB +

Preparations needed

- Pre-cool centrifuge to 4°C.
- Prepare ice-water bath.
- Prepare labeled ice-cold tubes (15-ml Corning centrifuge tubes for harvesting cells, 14-ml round-bottom Falcon tubes for each transformation and corresponding negative control).
- Cool TSS and water on ice.
- Warm selection plates.

Protocol

1. Dilute overnight culture 1:100 into LB. Incubate at 37°C until OD₆₀₀ is about 0.3 to 0.4.
[~1mL of culture per transformation + ~1mL of culture for negative control]
[MGZ1: ~ 1hr; DH5 α PRO: ~ 2hr]
2. Pellet cells by centrifugation at 1000g, 4°C for 10min in ice-cold Corning tubes. Discard supernatant and resuspend cells at 1/10 of original volume in 1 \times TSS. Mix gently on ice for ~2min. [Resuspend cells quickly to avoid pipetting up and down several times: Break up the pellet in 1-3 pipette squirts]
3. Add 100 μ L competent cells and plasmid DNA to an ice-cold Falcon tube. Mix gently on ice for ~3 min.
[high-copy plasmid miniprep: ~ 2 μ L, negative control: same amount of water (or PBS) instead of plasmid]
4. Incubate 30min at 4°C.
5. Add 900 μ L LB containing 20mM glucose and incubate by shaking for 30min at 37°C to allow expression of the antibiotic resistance gene. [label the plates!]
6. Select transformants on appropriate antibiotic agar plates: Pipette ~200 μ L culture on a plate, flame a glass spreader, spread cells, place in 37°C incubator over night.

Appendix C. Bacterial strains and plasmids

This appendix includes detailed information about every bacterial strain and DNA plasmid that was used in this thesis.

C.1 Strains

All strains are *E. coli*, derived from the RP437 “wild-type” strain, unless noted otherwise. Three strains were used most commonly throughout my thesis project:

HCB1660 has the *fliC* deleted, and contains a plasmid which expresses a mutant version of the FliC protein (FliC^{S219C}), which facilitates specific labeling of the flagella with maleimide functionalized dyes [106]. Production of FliC^{S219C} in this strain is induced by arabinose, so flagella are only made when cells are grown in the presence of arabinose.

PM87 has two deletions; genes *cheB cheY cheZ* (which are located together on a single operon) and *fliC* have been deleted. Strain PM87 contains two plasmids. Plasmid pMS164 expressed a mutant version of CheY which I refer to as CheY*[36]. CheY* is constitutively active, so it functions as if it were permanently phosphorylated. Plasmid pPM5 expresses the same FliC^{S219C} mutant protein which facilitates specific labeling of flagella in the HCB1660 strain. It was necessary to construct pPM5 because plasmid pBAD33-*fliC*^{S219C} was not compatible with plasmid pMS164. Production of CheY* is induced by IPTG (see **Figure 4.2**).

RP437 is the standard wild-type strain used in *E. coli* swimming and chemotaxis studies [4]. This strain was used in our initial tests with the trap assay, labeling protocols and all chemotaxis experiments.

Strain	Genotype	Plasmid(s)	Comments	Source
RP437	-	None	Wild-type for chemotaxis	Chris Rao [84]
HCB1660	<i>fliC</i> ::Tn5 (Kan ^R)	pBAD33- <i>fliC</i> ^{S219C}	“wild type” for chemotaxis, maleimide labelable <i>fliC</i> *	Howard Berg [106]
PM87	<i>cheBYZ</i> ::FRT, <i>fliC</i> ::Tn5 (Kan ^R)	pMS164 and pPM5	“CheY*”	Patrick Mears & Santosh Koirala [29]
PS2001	Δ <i>cheBcheYcheZ</i> (Kan ^R)	pMS164 (Cm ^R)	IPTG inducible CheY*	Philippe Cluzel [36]
PM41	- (RP437)	pDK58 (Amp ^R)	Tar-YFP	Patrick Mears
LC923	Δ (<i>P_{flhDC}</i>)::tetRA, Δ <i>cheYcheZ</i> ::FRT	None	aTc inducible flagella, <i>cheYcheZ</i> deletion	Lon Chubiz, Chris Rao

PM1	$\Delta(P_flhDC)::tetRA$, $\Delta cheYcheZ::FRT$	pMS164 (Cm ^R)	aTc inducible flagella and chemotaxis genes, IPTG inducible cheY ^{D13K}	Patrick Mears
MG1655TPOP	$\Delta(P_flhDC)::tetRA$	None	aTc inducible flagella	Chris Rao
PM94	<i>cheBYZ::FRT</i> , <i>fliC::Tn5</i> (Kan ^R)	pPM9 (Cm ^R), pPM5 (Amp ^R)	CheY-YFP and FliC*	Patrick Mears
RP4972	$\Delta cheB$	None	CheB knockout	Victor Sourjik [133]
PM10	$\Delta cheB$	pVS97 (cm ^R)	CheB ^{D56E} mutant under arabinose induction	Patrick Mears
RP2361	<i>Δtar</i>	None	Deleted aspartate receptors	John S. Parkinson
SK109	<i>cheBYZ::Cm</i>	None	Intermediate strain while cloning	Santosh Koirala [29]
SK110	<i>cheBYZ::FRT</i>	None	Intermediate strain while cloning	Santosh Koirala [29]
SK112	<i>cheBYZ::FRT</i> , <i>fliC::Tn5</i> (Kan ^R)	None	Precursor to PM87, without the plasmids	Santosh Koirala [29]

C.2 Plasmids

Plasmids are short, circular segments of DNA (a few thousand base pairs). Plasmids are a common tool for expressing specific proteins at controlled concentrations in bacterial cells. For a guide on using plasmids see the Molecular Cloning Handbook by Sambrook and Russell [132]. When working with plasmids, it is important to be aware of several characteristics. In addition to the gene which encodes for the protein-of-interest (POI) which will be expressed by the plasmid, there are several parts to a plasmid which regulate how it functions:

The promoter is a section of DNA, located upstream of the POI, which is used to control the expression level of the POI. Promoters are regulated by the concentration of a specific inducer chemical inside the cell. Common inducers include IPTG, arabinose, tetracycline. Generally, in the absence of an inducer, cells will produce almost none of the POI. Higher concentrations of inducer lead to higher concentrations of the POI.

Every plasmid has at least one Origin of replication, which controls how many copies of a plasmid exist in a cell. There exist different types or Origins, ranging from low-copy plasmids which exist in just 1-5 copies per cell, to high copy Origins which result in hundreds of copies of a plasmid in a single cell.

Plasmids usually contain a gene encoding for resistance to a specific antibiotic. This allows

the researcher to select for cells that contain the plasmid, by growing cells in the presence of that antibiotic. Any cells that do not contain the plasmid will die, leaving a population of cells that all contain the plasmid. Another essential aspect of a plasmid is the promoter which is used to control expression of the protein-of-interest.

Plasmid	Details	Comments	Source
pBAD33- <i>fliC</i> ^{S219C}	<i>fliC</i> ^{S219C} under P _{araBAD} promoter, Cm ^R , p15a origin	Expresses mutant version of FliC for fluorescent labeling	Howard Berg [106]
pPM5	<i>fliC</i> ^{S219C} under P _{araBAD} promoter, Amp ^R , colE1 origin	Expresses mutant version of FliC for fluorescent labeling	Patrick Mears [29]
pPM7	<i>cheY-YFP</i> under P _{Trc} promoter, Cm ^R , pSC101 origin, contains <i>lacI_q</i>	Changed RBS from pPM6 to reduce protein expression. Made from pVS18, successfully reduced expression, so it can be controlled by IPTG.	Patrick Mears
pPM9	<i>cheY-YFP</i> under P _{Lac} promoter, Cm ^R , pSC101 origin, contains <i>lacI_q</i>	CheY-YFP from pVS18. This plasmid has reduced expression, so it can be controlled by IPTG.	Patrick Mears
pMS164	<i>cheY</i> ^{D13K} under P _{lacOP} promoter, Cm ^R , pSC101 origin	Expresses constitutively active version of CheY	Philippe Cluzel [36]
pDK58	<i>Tar-YFP</i> under IPTG, Amp ^R	Expresses YFP labeled aspartate receptors. Receptors are not functional. Needs to be used in strain with the wild-type receptors.	Victor Sourjik [134]
pVS18	<i>cheY-YFP</i> under P _{trc} , promoter, Amp ^R , pBR322 origin	Over-expresses CheY-YFP, even when uninduced with IPTG	Chris Rao [135]
pVS97	<i>cheB</i> ^{D56E} under arabinose promoter, Cm ^R , pAYC origin	Expresses CheB ^{D56E} , with point mutation that prevents it from being phosphorylated	Victor Sourjik
pDK46	-	Helper plasmid for cloning	[136]
pKD3	-	Template for Cm ^R cassette	[136]
pCP20	-	Helper plasmid for cloning	[137]

Note: The plasmid from Howard Berg's lab expressing the FliC mutant protein was labeled as *fliC*^{S217C}, but after sequencing twice, it appeared that the actual mutation was *fliC*^{S219C}.

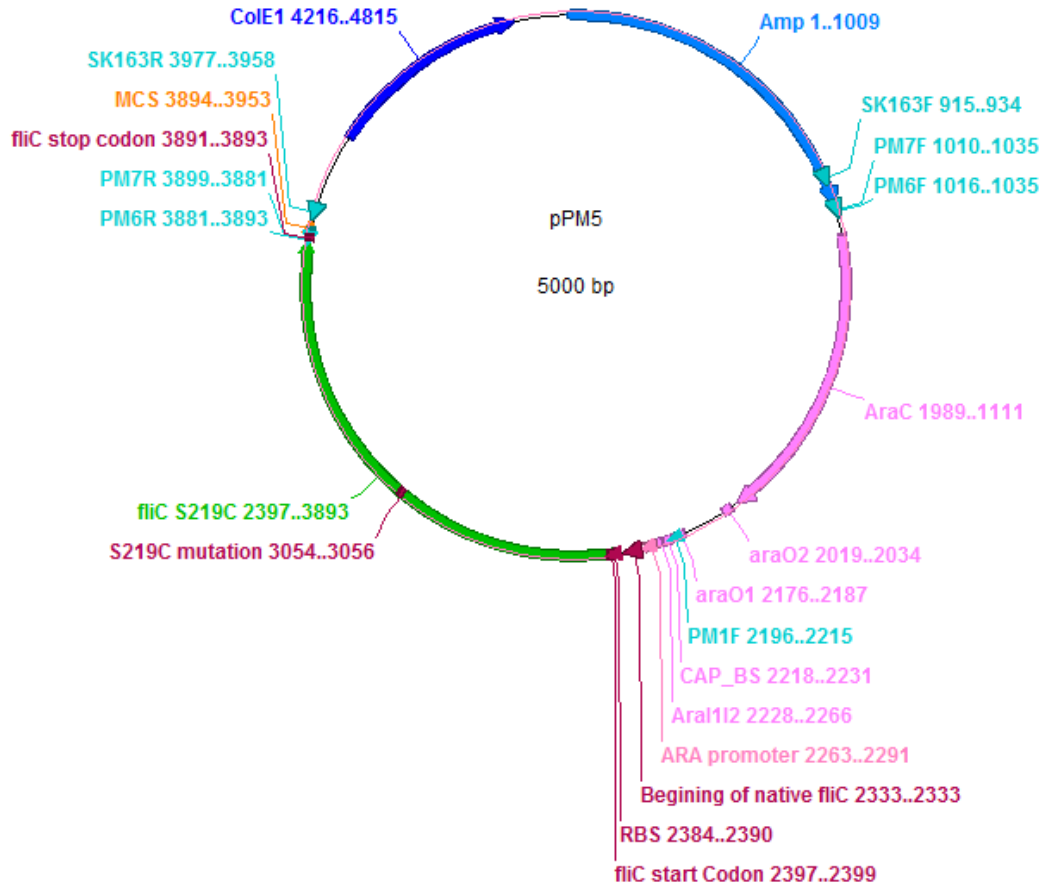
Note: The plasmid pPM9 was created from pVS18 to express CheY-YFP at a concentration similar to that of wild-type cells. The expression level from pVS18 was too high; even in the absence of

inducer, cells produced much more CheY-YFP than is present in a normal cell, and as a result the cells tumbled continuously. pPM9 was created by changing the promoter and origin to reduce the plasmid copy number and the tightness of control by the promoter. Separately, I modified the plasmid to create pPM6,7,8, in which I modified the Ribosome Binding Site. The RBS controls how frequently a protein is translated from an mRNA by ribosomes in the cell. By reducing the affinity of RBS, I was able to construct a plasmid which expresses an inducible range of CheY-YFP which spans the range of behaviors. In the absence of inducer, cells just run. As the concentration of inducer is increased, cells become brighter under YFP fluorescence excitation light and tumble more often.

C.3 Plasmid pPM5 sequence and map

Below is map showing the location of all of the important features of the plasmid pPM5, which I created to be used in together with plasmid pMS164 (CheY* plasmid). The origin of replication, antibiotic resistance and promoter were all chosen to be compatible with pMS164. They use different types of Origins of replication (pSC101 and ColE1), are resistant to different antibiotics (Chloramphenicol and Ampicillin), and have promoters which are induced by different inducers (IPTG and arabinose). pPM5 was created via molecular cloning techniques (see **Appendix B.8**). It was constructed by inserting *fliC*^{S219C} and the promoter from pPM1 into the plasmid pZE11-MCS [23]. The pZE11 plasmid was created by Lutz and Bujard created a series of modular plasmids which are very convenient for creating new plasmids with given set of characteristics [23].

In green is the *fliC*^{S219C} gene, which expressing the protein-of-interest. In blue is a section labeled ColE1, the origin of replication. The section labeled Amp is the gene conferring antibiotic resistance to ampicillin. In pink are sections related to the arabinose promoter, AraC is a protein involved in regulation of the arabinose promoter. Important features of the *fliC* gene, such as the ribosome binding site and start codon are labeled in maroon. In orange is the multiple cloning site, which a short sequence of DNA containing several different sequences which can be cut by commercially available restriction enzymes. In cyan are the locations of sequences for which I have DNA primers which were used for sequences and cloning.



Sequence of plasmid pPM5

GTAAACTTGGTCTGACAGTTACCAATGCTTAATCAGTGAGGCACCTATCTCAGCGATCTGTCTATTTTCGTTTCATCCATAGTTGCCT
 GACTCCCCGTCGTGTAGATAACTACGATACGGGAGGGCTTACCATCTGGCCCCAGTGCTGCAATGATACCGCGAGACCCACGCTCA
 CCGGCTCCAGATTTATCAGCAATAAACAGCCAGCCGGAAGGGCCGAGCGCAGAAGTGGTCCGCAACTTTATCCGCCCTCCATCCA
 GTCTATTAATTGTTGCCGGGAAGCTAGAGTAAGTAGTTCGCCAGTTAATAGTTTTGCGCAACGTTGTTGCCATTGCTACAGGCATCG
 TGGTGTACAGCTCGTCGTTTGGTATGGCTTCATTCAGCTCCGGTTCCTAACGATCAAGGCGAGTTACATGATCCCCATGTTGTGC
 AAAAAAGCGGTTAGCTCCTTCGGTCTCCGATCGTTGTGCAAGTAAGTTGGCCGAGTGTTATCACTCATGGTTATGGCAGCACT
 GCATAATTCTCTTACTGTGCATGCCATCCGTAAGATGCTTTTCTGTGACTGGTGAGTACTCAACCAAGTCATTCTGAGAATAGTGTA
 TCGGCGGACCGAGTTGCTCCTTGCCCGCGTCAATACGGGATAATACCGCGCCACATAGCAGAACTTTAAAGTGCTCATCATTGGA
 AAACGTTCTTCGGGGCGAAAACCTCAAGGATCTTACCCTGTTGAGATCCAGTTCGATGTAACCCACTCGTGACCCCAACTGATC
 TTCAGCATCTTTTACTTTTACCAGCGTTTCTGGGTGAGCAAAAACAGGAAGGCAAAATGCCGCAAAAAGGGAATAAGGGCGACAC
 GGAAATGTTGAATACTCATACTCTTCTTTTCAATATTATTGAAGCATTATCAGGGTATTGTCTCATGAGCGGATACATATTT
 GAATGTATTTAGAAAAATAAACAAATAGGGGTTCCGCGCACATTTCCCCGAAAAGTGCCACCTGACGTCATCGATGCATAATGTGC
 CTGTCAAATGGACGAAGCAGGGATTCTGCAAACCTATGCTACTCCGTCAAGCCGTC AATTGTCTGATTCGTTACCAATTATGACA
 ACTTGACGGCTACATCATTCACTTTTCTTCAACCCGGCACGGAACCTCGCTCGGGCTGGCCCCGGTGCATTTTTTAAATACCCGC
 GAGAAATAGAGTTGATCGTCAAACCAACATTGCGACCGACGGTGGCGATAGGCATCCGGGTGGTGTCAAAGCAGCTTCGCTG
 GCTGATACGTTGGTCTCGCGCCAGCTTAAGACGCTAATCCCTAACTGCTGGCGGAAAAGATGTGACAGACCGACGGCGACAAGC
 AAACATGCTGTGCGACGCTGGCGATATCAAAATTGCTGTCTGCCAGGTGATCGCTGATGTACTGACAAGCCTCGCGTACCCGATTA
 TCCATCGGTGGATGGAGCGACTCGTTAATCGCTTCCATGCGCCGAGTAACAATTGCTCAAGCAGATTTATCGCCAGCAGCTCCGA

ATAGCGCCCTTCCCCTTGCCCGGCGTTAATGATTTGCCCAAACAGGTCGCTGAAATGCGGCTGGTGCGCTTCATCCGGGCGAAAGA
ACCCCGTATTGGCAAATATTGACGGCCAGTTAAGCCATTCATGCCAGTAGGCGCGGACGAAAGTAAACCCACTGGTGATACCAT
TCGCGAGCCTCCGGATGACGACCGTAGTGATGAATCTCTCCTGGCGGGAACAGCAAAATATCACCCGGTCGGCAAACAAATTCTCG
TCCCTGATTTTTTACCACCCCTGACCGCGAATGGTGAGATTGAGAAATAAACCTTTCATTCCCAGCGGTGGTCGATAAAAAAAT
CGAGATAACCGTTGGCCTCAATCGGCGTTAAACCCGCCACCAGATGGGCATTAACAGATATCCCGGCAGCAGGGGATCATTTTTGC
GCTTCAGCCATACTTTTCATACTCCC GCCATT CAGAGAAGAAACCAATTGTCCATATTGCATCAGACATTGCCGTCACTGCGTCTT
TTACTGGCTCTTCTCGCTAACCAAACCGGTAACCCCGCTTATTAAGCATTCTGTAAACAAAGCGGGACCAAAGCCATGACAAAA
CGCGTAACAAAAGTGTCTATAATCACGGCAGAAAAGTCCACATTGATTATTTGCACGGCGTCACACTTTGCTATGCCATAGCATT
TTATCCATAAGATTAGCGGATCTACCTGACGCTTTTTATCGCAACTCTCTACTGTTTCTCCATACCCGTTTTTTTTGGGCTAGCGA
ATTTCGAGCTCCGATTGAGCCGACGGGTGAAACCAATACGTAATCAACGACTTGCAATATAGGATAACGAATCATGGCACAAGTC
ATTAATACCAACAGCCTCTCGCTGATCACTCAAAAATAATATCAACAAGAACCAGTCTGCGCTGTCGAGTTCTATCGAGCGTCTGTC
TTCTGGCTTGCGTATTAACAGCGGAAGGATGACGCAGCGGGTCAGGCGATTGCTAACCGTTTACCTCTAACATTAAGGCCTGA
CTCAGCGGCCCCGTAACGCCAACGACGGTATCTCCGTTGCGCAGACCACCGAAGGCGCGCTGTCCGAAATCAACAACAACCTTACAG
CGTGTGCGTGAACGACGGTACAGGCCACTACCGGTACTAACTCTGAGTCTGATCTGTCTTCTATCCAGGACGAAATTAATCCCG
TCTGGATGAAATTGACCGCGTATCTGGTCAGACCCAGTTCAACGGCGTGAACGTGCTGGCAAAAAATGGCTCCATGAAATCCAGG
TTGGCGCAAATGATAACCAGACTATCACTATCGATCTGAAGCAGATTGATGCTAAAACCTTTGGCCTTGATGGTTTTAGCGTTAAA
AATAACGATACAGTTACCACTAGTGCTCCAGTAACTGCTTTTTGGTGTACCACCACAAACAATATTAACCTTACTGGAATTACCT
TTCTACGGAAGCAGCCACTGATACTGGCGAACTAACCCAGCTTGCAATTGAGGGTGTATACTGATAATGGTAATGATTACTATG
CGAAAATCACCGGTGGTGATAACGATGGGAAGTATTACGCAGTAAACGTTGCTAATGATGGTACAGTGACAATGGCGACTGGAGCA
ACGGCAAATGCAACTGTAACGATGCAAAATACTACTAAAGCTACAACATCACTTCAGGCGGTACACCTGTTTCCAGATTGATAATAC
TGCAGGTTCCGCAACTGCCAACCTTGGTGTGTTAGCTTAGTAAAACGAGGATCCAAGGTAATGATACCGATACATATGCGC
TTAAAGATACAAATGGCAATCTTTACGCTGCGGATGTGAATGAACTACTGGTGTGTTTTCTGTTAAAACATTTACCTATACTGAC
TCTTCCGGTGCCGCCAGTTCTCCAACCGCGGTCAAACCTGGGCGGAGATGATGGCAAAACAGAAGTGGTCGATATTGATGGTAAAC
ATACGATTCTGCCGATTTAAATGGCGGTAATCTGCAAAACAGGTTTACTGCTGGTGGTGAGGCTCTGACTGCTGTTGCAAAATGGTA
AAACCACGGATCCGCTGAAAGCGCTGGACGATGCTATCGCATCTGTAGACAAATCCGTTCTTCCCTCGGTGCGGTGCAAAACCGT
CTGGATTCCGCGGTTACCAACCTGAACAACACCCTACCAACCTGCTGTAAGCGCAGTCCCGTATTCAGGACGCCGACTATGCGAC
CGAAGTGTCCAATATGTGCAAGCGCAGATCATCCAGCAGGCCGTAACCTCCGTTGTTGGCAAAAGCTAACCCAGGTACCGCAGCAGG
TTCTGTCTCTGCTGCAGGGTTAAGTCGACGGTATCGATAAGCTTGATATCGAATTCCTGCAGCCCGGGGATCCCATGGTACGCGT
GCTAGAGGCATCAAATAAAACGAAAGGCTCAGTCGAAAGACTGGGCTTTTCTGTTTATCTGTTGTTTGTGCGGTGAACGCTCTCCTG
AGTAGACAAATCCGCCGCCCTAGACCTAGGGCGTTCCGGCTGCGGCGAGCGGTATCAGCTCACTCAAAGCGGTAATACGGTTATC
CACAGAATCAGGGGATAACGCAGGAAAGAACATGTGAGCAAAAGGCCAGCAAAAGGCCAGGAACCGTAAAAAGGCCGCGTTGCTGG
CGTTTTTCCATAGGCTCCGCCCCCTGACGAGCATCACAAAAATCGACGCTCAAGTCAGAGGTGGCGAAACCCGACAGGACTATAA
AGATACCAGGCGTTTTCCCCTGGAAGCTCCCTCGTGCCTCTCCTGTTCCGACCCTGCCGCTTACCCGGATACCTGTCCGCCTTTCT
CCCTTCGGGAAGCGTGGCGCTTTCTCAATGCTCACGCTGTAGGTATCTCAGTTCGGTGTAGGTGCTTCGCTCCAAGCTGGGCTGTG
TGCACGAACCCCCGTTTCCAGCCGACCGCTGCGCCTTATCCGTAACCTATCGTCTTGAGTCCAACCCGGTAAGACACGACTTATCG
CCACTGGCAGCAGCCACTGGTAACAGGATTAGCAGAGCGAGGTATGTAGGCGGTGCTACAGAGTTCTTGAAGTGGTGGCCTAACTA
CGGCTACACTAGAAGGACAGTATTTGGTATCTGCGCTCTGCTGAAGCCAGTTACCTTCGGAAAAAGATTGGTAGCTCTTGATCCG
GCAACAAAACACCCTGGTAGCGGTGGTTTTTTTTGTTTGAAGCAGCAGATTACGCGCAGAAAAAAGGATCTCAAGAAGATCCT
TTGATCTTTTCTACGGGTCTGACGCTCAGTGAACGAAAACCTACGTTAAGGATTTTGGTCATGACTAGTGCTTGGATTCTCAC
CAATAAAAAACGCCGGCGCAACCCGAGCGTTCTGAACAAATCCAGATGGAGTTCTGAGGTCACTACTGGATCTATCAACAGGAGT
CCAAGCGAGCTC

C.4 DNA Primers

This is a list of all of the primers that I used while working on my thesis project. Most were used for cloning or sequencing to confirm the results of cloning experiments.

Primer	Comments	Sequence
PM1F	Before fliC gene Reverse, from pPM1,sequencing primer from the SacI end	attattttgcacggcgtcaca
PM1R	After fliC gene Forward, from pPM1,sequencing primer from the HindIII end	TTCGGCATGGGGTCAGGTGG
PM2F	(AKA P Mears seq primer cheY front) Inside cheY gene, near the end, Forward	CAGTGGCTATGTGGTGAAGC
PM2R	(AKA P Mears seq primer cheY back) Inside cheY gene, near the front, Reverse	GCTCTTTTCAGCAGGTTACGC
PM3F	(AKA P mears seq primer pHSG576)On pHSG576, Forward. Trying to sequence pMS164	CGAATCAAAGCTGCCGACAA
PM6F	PBAD promoter Forward, from pPM1, Sall	ggg gtcgac ATCGATGCATAATGTGCCTG
PM6R	fliC gene Reverse, from pPM1, XbaI	GAC TCTAGA TTAACCCTGCAGC
PM7F	PBAD promoter Forward, from pPM1, AatII	ggg gacgtc ATCGATGCATAATGTGCCTG
PM7R	fliC gene Reverse from pPM1, Sall	ggg gtcgac TTAACCCTGCAGC
PM8F	Before PLtetO promoter Forward, from protet.E, SphI	ggg gcatgc GTGAAAGTTGGAACCTCTT
PM8R	Before TL3 terminator Forward, from protet.E-tetR, XmaI	ggg cccggg CAGCATAACCTTTTTCCGGCG
PM9R	After TL3 terminator Forward from protet.E-tetR, XmaI	ggg cccggg CGGTATCAGCTCACTCAAAG
PM10F	lacI near end Forward, from pMS164	GTTGGTGC GGATATCTCGGT
PM10R	lacI near front Reverse, from pMS164	GCATACTCTGCGACATCGTA
PM11R	Before TL3 terminator (or maybe PLtetO) promoter Reverse, from protet.E, SphI or XmaI	ggg cccggg CGCCGGAAAAAGGTTATGCTG
PM12R	Before TL3 terminator Reverse, from protet.E-tetR, XmaI	ggg cccggg CTTTGAGTGAGCTGATACCG
PM14R	fliC gene Reverse from pPM1, XmaI	ggg cccggg TTA TTAACCCTGCAGC
PM15F	before cheY, Forward, from pMS164 guess (Ecoli genome)	GTGCCGGACAGGCGATACGT
PM15R	after cheY, Reverse from pMS164 guess (Ecoli genome)	AGCTTGCATCATAGTCGCATCC
PM16R	Similar to PM8F, reverse compliment, from pMS164 guess	cgtaagaggtccaactttcacc
PM17F	Before lacI, Forward, from pVS18, AatII	ggg GACGTC CGAAGCGGCATGCATTTACG

PM17R	After cheY-YFP, Reverse, from pVS18, BamHI	ata ggatcc CTCATGAGCGGATACATATTTGAATG
PM18F	pProtet.E check Forward, inside CmR near end	CAACGGTGGTATATCCAGTG
PM18R		
PM19F	Before cheY-YFP, Forward, from pVS18, XbaI	ggg TCTAGA CACACAGGAAACAGACCATG
PM19R	After cheY-YFP, Reverse, from pVS18, check primer (cut upstream with HindIII)	CTCATGAGCGGATACATATTTGAATG
PM20F	Before cheY-YFP, Forward, from pVS18, BamHI	ggg ggatcc CACACAGGAAACAGACCATG
SK162F	proTetE tetR Check Forward	GTGAAAGTTGGAACCTCTTACG
SK162R	proTetE tetR Check Reverse	TCACCTTACTTTTATCTAATCTAGAC
SK163F	pZE11 Check Forward	AGGGTTATTGTCTCATGAGC
SK163R	pZE11 tetR Check Reverse	GTTTTATTTGATGCCTCTAG
SK164F	pAH143/153 Check Forward	TTGTCGGTGAACGCTCTCCT
SK164R	pAH143/153 Check Reverse	AGGATGCGTCATCGCCATTA
SK140F	<i>cheBYZ</i> deletion forward	TGCGTGGTCAGACGGTGTATGCGCTAAGTAAGGATTAACG GTGTAGGCTGGAGCTGCTTC
SK140R	<i>cheBYZ</i> deletion reverse	GCCTGATATGACGTGGTCACGCCACATCAGGCAATACAAA CATATGAATATCCTCCTTAG
SK141F	<i>cheBYZ</i> deletion check forward	CCTTAAACCCGACGGATTGC
SK141R	<i>cheBYZ</i> deletion check reverse	TTGCTGCCACACATCAAGC
SK163F	pZE11 sequencing forward	AGGGTTATTGTCTCATGAGC
SK163R	pZE11 sequencing reverse	GTTTTATTTGATGCCTCTAG

Appendix D. Models

This appendix contains analytical derivations of the veto model and unanimous model, which were used in **Figure 5.1**

D.1: Veto model – Analytical derivation

The veto model assumes that all flagella must be rotating counter-clockwise (CCW) for the cell to run. Any flagellum can “veto” the run by rotating clockwise (CW), which causes the cell to tumble (see **Figure 1A**). To describe the veto model mathematically, we write the expression for the run bias (the fraction of time that a cell spends running) as a function of the CCW bias (the fraction of time that each flagellum spends rotating CCW). Assuming that the CCW bias is fixed in time, one obtains:

$$Run\ bias = \frac{Time\ ALL\ motors\ CCW}{Total\ time} \quad (D.1)$$

$$Run\ bias = (CCW\ bias)^{N_{flag}} \quad (D.2)$$

Where N_{flag} is the number of flagella. We can write the tumble bias (TB) as a function of the run bias, and the CW bias (CB) as a function of CCW bias:

$$TB = 1 - Run\ Bias \quad (D.3)$$

$$CB = 1 - CCW\ Bias \quad (D.4)$$

We then use these relations to solve for the tumble bias as a function of CW bias and the number of flagella:

$$TB = 1 - (1 - CB)^{N_{flag}} \quad (D.5)$$

D.2: Unanimous model – Analytical derivation

The unanimous model is basically the opposite of the veto model. The unanimous model posits that the cell is running unless every flagellum is rotating CW. Assuming that the CW bias is fixed in time, one obtains:

$$Tumble\ bias = \frac{Time\ ALL\ motors\ CW}{Total\ time} \quad (D.6)$$

$$TB = (CW\ bias)^{N_{flag}} \quad (D.7)$$